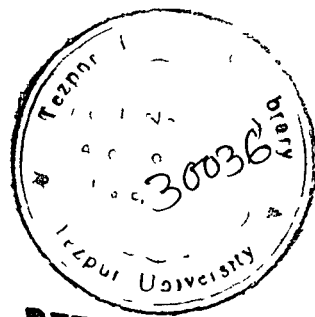



CENTRAL LIBRARY
TEZPUR UNIVERSITY
Accession No T 62
Date 22/02/13



REFERENCE BOOK
NOT TO BE ISSUED
TEZPUR UNIVERSITY

Tezpur University Library



30036

**SOLUTION OF CERTAIN TWO-DIMENSIONAL INVERSE
PROBLEMS IN POTENTIAL THEORY AND THEIR
APPLICATION IN EXPLORATION GEOPHYSICS**

**A
thesis submitted in partial fulfillment
for the award of degree of
Doctor of Philosophy**

By

**Pallabee Choudhury
Regn. No. 098 of 1998**

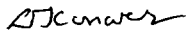
**In
The School of Energy, Environment and Natural Resources
Department of Energy
Tezpur University
Napaam – 784 028
Assam, India**

JULY 2005

333.79
CHO

CERTIFICATE

This is to certify that the matter embodied in the thesis entitled “**Solution of Certain two-dimensional Inverse Problems in Potential Theory and their Application in Exploration Geophysics**” submitted by **Ms. Pallabee Choudhury** for the award of degree of Doctor of Philosophy of Tezpur University is an original piece of research work carried out by her under our supervision and guidance. The results embodied in this thesis have not been submitted to any other University or Institute for the award of any degree or diploma.



(D. Konwer)
Professor, Dept. of Energy
Tezpur University
Napaam, Tezpur –784028
Assam, India

Date: 29, July 2005



(S. K. Laskar)
Ex Consultant, DST-GPS Project
Dept. of Physics
Tezpur University
Napaam, Tezpur –784028
Assam, India

Date : 29, July 2005

ACKNOWLEDGEMENT

I am deeply indebted and grateful to Dr. S. K. Laskar for introducing me to potential theory and its application in geophysics. I extend my heartfelt gratitude to him for his painstaking guidance, constant encouragement, support and cooperation throughout the course of this work.

I also acknowledge my thankfulness to Prof. D. Konwer for his constant inspiration and supervision during the entire course of the work and preparation of this manuscript.

I would like to acknowledge my grandmother, father, brother, sister, aunt and my friend Nabamita without whose moral support and encouragement the work could not have been completed.

I would like to express my sincere thanks to Prof. P.C.Deka, Prof. P.Bhattacharyya, Dr. A. Kumar and Prof. P.K. Bordoloi for their kind help and cooperation throughout the work.

I am deeply thankful to Anjanda and Nava for their valuable help and useful discussions.

I will remain ever grateful to my friend Joya and Anindita for their constant encouragement and various help during the arduous time while working for this thesis.

I am thankful to all faculty members of Department of Mathematical Sciences and Department of Energy, Tezpur University for their timely help and support.

Thanks are also due to Prof. V.K.Gaur for his active interest in this work right from the beginning.

Financial support from the Department of Science and Technology, Govt, of India, is gratefully acknowledged.

Date : July 29, 2005
Place : Napaam, Tezpur

Pallabee Choudhury
(Pallabee Choudhury)

ABSTRACT

This work deals with up-continuation of a two-dimensional potential field from boundary data by reproducing it as a potential of simple as well as double layer boundary density. It is also achieved by Green's formula without finding Green's function for the boundary. For the field specified over a horizontal boundary, downward continuation of it to a flat-bottom curved boundary with its ends fixed and arms extending along the datum line is achieved as potential of double layer density belonging to the continuation boundary. Subsequently, down-continuation to a concave boundary with its ends fixed at the datum line and apex moving downward in steps along a vertical, giving the boundary a tapering shape as depth increases, is achieved. Finally, depth to the top of the subsurface causative mass is determined by the first maximum of the vertical gradient of the down-continued field computed along a vertical passing through it. The techniques developed are successfully tested on model data. The up-continued field obtained from model data agrees with the true response to a good degree of accuracy and the down-continued field appears with error proportional to that in the input data, the error increasing steadily with increase in depth without affecting the computed depth to the causative mass. When applied to aeromagnetic data of Umium valley of Shillong-Nongpoh area, the techniques identify the E-W trending basement faults and determine the sedimentary thickness in the valley.

CONTENTS

| | Page No. |
|--|-----------|
| Chapter I INTRODUCTION | 1 |
| Chapter II TWO-DIMENSIONAL POTENTIAL THEORY | 9 |
| 2.1 Potential due to Simple Sources | 9 |
| 2.1.1 Potential due to a Simple Source | 9 |
| 2.1.2 Potential due to simple sources placed over a closed contour | 10 |
| 2.2 Potential due to Double Sources | 13 |
| 2.2.1 Potential due to a Double Source | 13 |
| 2.2.2 Potential due to double sources placed over a closed contour | 14 |
| 2.3 Formulation of Dirichlet and Neumann Problem | 15 |
| 2.3.1 Interior Problems | 15 |
| 2.3.2 Exterior Problems | 18 |
| 2.4 Green's Formulae | 20 |
| 2.4.1 Green's Formulae for interior domain | 20 |
| 2.4.2 Green's Formulae for exterior domain | 20 |
| 2.4.3 Harmonic function as simple and double layer potential | 22 |
| Chapter III HALF-SPACE PROBLEMS | 26 |
| 3.1 Upward continuation from boundary data | 26 |
| 3.1.1 Simple layer formulation | 26 |
| 3.1.2 Double layer formulation | 27 |
| 3.1.3 Formulation by Green's formula | 28 |
| 3.2 Downward Continuation: A new formulation of the problem | 30 |
| Chapter IV APPLICATION IN GEOPHYSICS | 32 |
| 4.1 Upward continuation | 32 |
| 4.1.1 Gravity Magnetic Field by Simple Layer Boundary Density | 32 |
| 4.1.2 Gravity Magnetic Field by Double Layer Boundary Density | 34 |
| 4.1.3 Gravity Magnetic Field by Green's Formula | 35 |
| 4.2 Downward continuation | 36 |
| 4.2.1 Continuation to a curved boundary | 36 |
| 4.2.2 Continuation to a horizontal boundary | 39 |
| 4.2.3 Depth Determination | 40 |
| 4.2.4 Spacing of data | 42 |
| 4.2.5 Working data-length | 44 |
| Chapter V NUMERICAL PROCEDURE | 49 |
| 5.1 Discretisation of Equations in up-continuation | 49 |
| 5.1.1 Simple Layer Formulae | 49 |
| 5.1.2 Double Layer Formulae | 50 |
| 5.1.3 Green's Formulae | 51 |
| 5.2 Discretisation of Equations in down-continuation | 53 |
| 5.3 Evaluation of Integrals | 55 |
| 5.3.1 Analytical evaluation of simple layer Integrals | 57 |
| 5.3.2 Analytical evaluation of double layer Integrals | 58 |
| 5.4 Solution of the Equations | 60 |
| 5.4.1 Upward continuation | 60 |
| 5.4.2 Downward continuation | 62 |

| | | |
|---------------------|--|------------|
| Chapter VI | ANALYSIS OF MODEL DATA | 67 |
| 6.1 | Up-continuation of potential field | 67 |
| 6.1.1 | Boundary and the gravity-magnetic field | 67 |
| 6.1.2 | Up-continuation as simple layer potential | 70 |
| 6.1.3 | Up-continuation as double layer potential | 78 |
| 6.1.4 | Up-continuation by Green's formula | 82 |
| 6.1.5 | Summarization of results | 84 |
| 6.2 | Down-continuation of potential field | 85 |
| 6.2.1 | Continuation to a curved boundary | 85 |
| 6.2.2 | Uniqueness of solution | 89 |
| 6.2.3 | Continuation to horizontal and flat-bottom curved boundary | 94 |
| 6.3 | Depth Determination | 101 |
| 6.3.1 | Choice of boundary and spacing of data | 101 |
| 6.3.2 | Generation of input data | 102 |
| 6.3.3 | Down-continuation to a tapered parabolic boundary | 103 |
| 6.3.4 | Depth determination from down-continued field values | 107 |
| 6.3.5 | General remarks on down-continuation and depth determination | 110 |
| Chapter VII | APPLICATION TO FIELD DATA | 112 |
| 7.1 | Fault and sedimentary thickness in Shillong-Mawlong area | 112 |
| 7.1.1 | Introduction | 112 |
| 7.1.2 | Geology and topography | 115 |
| 7.1.3 | Analysis of aeromagnetic data | 116 |
| 7.1.4 | Comparative study of throw of faults | 127 |
| 7.1.5 | Sedimentary thickness in the area | 128 |
| 7.1.6 | Discussion | 130 |
| 7.1.7 | Conclusion | 132 |
| Chapter VIII | CONCLUSION | 133 |
| | APPENDIX I | 135 |
| | APPENDIX II | 140 |
| | APPENDIX III | 142 |
| | REFERENCE | 145 |

LIST OF TABLES

| <u>Table No.</u> | <u>Content</u> | <u>Page No.</u> |
|------------------|--|-----------------|
| Table 6.1.1 | Gravity and Magnetic responses over the boundary S | 69 |
| Table 6.1.2 | Simple and double layer boundary densities obtained from gravity data | 73 |
| Table 6.1.3 | Up-continuation of gravity field at level $z=1.5$ from boundary data | 74 |
| Table 6.1.4 | Simple and double layer boundary densities obtained from magnetic data | 76 |
| Table 6.1.5 | Up-continuation of magnetic field at level $z=1.5$ from boundary data | 77 |
| Table 6.2.1 | Uniqueness of solution in down-continuation of a magnetic field to a curved lower boundary | 91 |
| Table 6.2.2 | Uniqueness of solution in down-continuation of a gravity field to a curved lower boundary | 93 |
| Table 6.2.3 | Down-continuation of magnetic data to a horizontal and a flat-bottom curved lower boundary at a shallow depth | 96 |
| Table 6.2.4 | Down-continuation of gravity data to a horizontal and a flat-bottom curved lower boundary at a shallow depth | 98 |
| Table 6.2.5 | Down-continuation of magnetic data to a horizontal and a flat-bottom curved lower boundary at a deeper depth | 99 |
| Table 6.3.1 | Input gravity and magnetic data over a datum line \bar{S} | 103 |
| Table 6.3.2 | Down-continued gravity field along a vertical | 105 |
| Table 6.3.3 | Down-continued magnetic field along a vertical | 106 |
| Table 6.3.4 | Depth-determination by down-continuation of gravity data along a vertical from data specified over the interval $\bar{D}(-13.5,13.5)$ | 108 |
| Table 6.3.5 | Depth-determination by down-continuation of magnetic data along a vertical from data specified over the interval $\bar{D}(-13.5,13.5)$ | 109 |
| Table 6.3.6 | Computation of depth to the causative mass from gravity and magnetic data specified over $\bar{D}(-20.5,20.5)$ | 109 |

LIST OF FIGURES

| <u>Figure No.</u> | <u>Content</u> | <u>Page No.</u> |
|-------------------|---|-----------------|
| Fig. 2.1.1 | The source point q and the field point P in a xoz reference frame | 9 |
| Fig. 2.1.2 | Interior domain B_i is enclosed by the closed contour ∂B . Exterior domain B_e lies outside B_i . | 10 |
| Fig. 2.2.1 | The doublet of strength μ at the source point q and the field point P at a distance r from q | 13 |
| Fig. 2.4.1 | The closed domain B , bounded below by S and above by a semicircle S_u of Radius R | 22 |
| Fig. 3.2.1 | A closed domain B , bounded below by a curved boundary $S(= \bar{S}_o + S_L + \bar{S}_n)$ and above by a semicircle S_u of radius R | 30 |
| Fig. 4.1.1 | Boundary S , field point P and the outward normal \hat{i} to S at q | 32 |
| Fig. 4.2.1 | Continuation to a concave boundary extending downward in steps of Δz taking a tapering shape as depth increases | 44 |
| Fig. 5.3.1 | Evaluation of simple and double layer integrals over a subelement AB | 57 |
| Fig. 6.1.1 | The gravity-magnetic responses due to the polarised subsurface mass m are specified over S for their up-continuation to a higher level | 67 |
| Fig. 7.1.1 | Geological map of Shillong-Nongpoh area and NS lines over it | 116 |
| Fig. 7.1.2 | Aeromagnetic Map of Nongpoh-Shillong area showing 2-D NS lines | 117 |
| Fig. 7.1.3 | Vertical Component field and its horizontal and vertical gradients defining approx. location of basement faults along A2-B2 | 120 |
| Fig. 7.1.4 | Vertical Component field and its horizontal and vertical gradients defining approx. location of basement faults along A6-B6 | 120 |
| Fig. 7.1.5 | Contour map of vertical component magnetic field at level above | 123 |
| Fig. 7.1.6 | Regional Magnetic profile along Guwahati-Shillong highway and its harmonic components | 124 |
| Fig. 7.1.7 | Flight level, Continuation boundary, ground and basement topographic profiles along A2-B2 | 125 |
| Fig. 7.1.8 | Normalised Total field, Topography and basement profile along A6-B6 | 126 |
| Fig. 1 | Vertical component magnetic response and its gradients of step-faults approximating the basement in a geological basin | 142 |

LIST OF SYMBOLS USED AND THEIR MEANING

| <u>Symbol</u> | <u>Meaning</u> |
|-------------------------------------|--|
| ϕ | A logarithmic potential |
| P, q, p | Field point, source point and boundary point |
| σ | Logarithmic simple source density |
| μ | Logarithmic double source density or susceptibility in model study and field problem |
| G | Universal gravitational constant |
| H | A harmonic function, either an anomalous gravity or a component magnetic field |
| B_i, B_e | Interior and exterior domain respectively |
| $\log'_i \mathbf{q} - \mathbf{P} $ | Derivative of $\log \mathbf{q} - \mathbf{P} $ in the direction i at the point q keeping P fixed |
| ∂B | A closed contour |
| n_i, n_e | Interior and exterior normals respectively at any point p to the closed contour ∂B |
| \bar{S}_0 | Horizontal boundary |
| S_t | Concave boundary |
| S | General boundary |
| S_u | Semicircle of radius R |
| Δg | Gravimetric field |
| T_z | Vertical component magnetic field |

CHAPTER I

INTRODUCTION

Analysis and interpretation of gravity-magnetic (GM) data is the first geophysical method used in exploration of hydrocarbons in a basin. The GM anomaly maps prepared from the survey data provide a qualitative picture of the basin defining basement highs and lows and the basin boundary. Subsequently, depth to the basement can be computed from the observed GM data.

The primary goal of studying gravity and magnetic data is to provide a better understanding of the subsurface geology of the basin. Both gravity and magnetic measurements are non-destructive remote sensing methods that are relatively cheap, and are used to determine information about the subsurface that is useful especially for exploration of oil, gas and mineral deposits. The value and utility of gravity and magnetic methods today are greater than ever because of their low cost compared to seismic survey and drilling, availability of continent-scale data-sets for tectonic analysis and increasing resolution achieved through advanced acquisition and processing techniques.

Gravity data provide information about the densities of the subsurface rocks. Because there is a wide range in density among the rock types, geologists can make inferences about the distribution of strata that may be favourable for trapping oil and gas. The magnetic field of the earth is probably generated by electric currents in the liquid outer core (Gibson, 2005). Effectively, it is reasonable to think of the field as that due to a bar magnet at the earth's core. It affects the magnetic minerals that are distributed

in many rocks in the crust, so that the rocks have a component of magnetization. Because of variation in the magnetic properties of different rocks, the sedimentary rocks having the least magnetic effect, the geophysicists can determine the depth to the magnetite-rich rocks placed in general at the basement of a sedimentary basin.

A force field in general exhibits a three-dimensional behaviour. However, there are certain systems in which the field shows a two-dimensional behaviour, the field varying in a plane without yielding a component perpendicular to it. A field described in two-dimensions provides a quick computational facility to study its nature. Under certain approximations, many systems can be treated as two-dimensional and useful results can be obtained with less computational work.

Oil and mining industries acquire gravity and magnetic data to interpret them in terms of depth and geometry of the subsurface causative mass. For the field data H_i acquired over an irregular surface S these are required to be up-continued to a horizontal plane \bar{S} for subsequent use in qualitative and quantitative analysis of them. In two-dimensions, the field is to be up-continued to a horizontal line \bar{S} , S and \bar{S} both lying in a vertical plane. Subsequently, to determine depth to the basement from the observed data, the field is to be continued downward from \bar{S} to a boundary below it.

Both the problems stated above, up-continuation from an irregular boundary S to a horizontal boundary \bar{S} above it and down-continuation from \bar{S} to a lower boundary below it, involve solution of certain inverse problems. The former involves solution of a boundary value problem (Jaswon & Symm, 1977; Laskar & Bhattacharyya, 2002) that yields a stable solution for arbitrary data over the boundary, the later involves solution of an ill-posed problem (Tikhonov & Goncharsky, 1987) the solution of which is highly sensitive to error in input data. (Strakhov, 1963)

Gravity or a component magnetic field H due to subsurface causative mass is a harmonic function with asymptotic behaviour $H=O(r^{-n}), n \geq 2, r \rightarrow \infty$, in the upper half-space domain B_i bounded below by a half-space boundary S . In two-dimensions, $H=O(r^{-n}), n \geq 1, r \rightarrow \infty$, in B_i . Given H over S , computation of H in the upper half-space domain B_i requires finding of Green's function for the boundary S . Finding of Green's function for a horizontal boundary is straightforward, finding it for a general boundary is an extremely difficult task. Courtillot et. al. (1973) however, found it following a procedure that involves solution of a non-linear equation with a priori knowledge of the parameters.

Bhattacharyya and Chan (1977) attempted an alternative approach for up-continuation of gravity and magnetic fields from boundary data. They reproduced the gravity field, following Roy (1962), as derivative of potential due to a simple (monopole) layer boundary density σ on formulating the problem in an integral equation of the second kind in σ in terms of data specified over S . They reproduced a component of magnetic field as potential of double (dipole) layer boundary density μ on formulating the problem in an integral equation of the second kind in μ in terms of the component field data specified over S . The fact that the magnetostatic field H that vanishes at infinity in $O(r^{-3}), r \rightarrow \infty$, can also be reproduced as potential of double layer boundary density which vanishes at infinity in $O(r^{-2}), r \rightarrow \infty$ in general, remains unexplained in their work. Laskar (1984) showed that both gravity and magnetic fields could be reproduced from the respective boundary data as potentials of double layer boundary density. Subsequently, Laskar and Bhattacharyya (2002) have shown that gravity as well as a component magnetic field can be reproduced in upper half-space domain from respective boundary data as potential of simple as well as double layer boundary

density. Further, they have also reproduced the fields by Green's formula without finding Green's function for the boundary. The boundary densities in all the above cases are obtained as stable solution of inverse problems expressing the density in terms of the data specified over the boundary (Laskar & Bhattacharyya, 2002). Their discussion is confined in three-dimensions only.

Continuation of a potential field towards its source is supposed to exhibit an irregular behaviour on reaching the target as it is having a singularity at the source. This property of the continued field identifies a possible approach for determination of depth to the basement in a geological basin. Peters (1949) made the first attempt to find the depth to the basement by downward continuation of vertical component magnetic data from the ground level to a level below it as an inverse problem expressed in an integral equation of the first kind in the field value at the lower level in terms of the data observed at the ground level. Instead of solving the problem as formulated, Peters (1949) suggested analytical continuation of the field by Taylor's series extrapolation towards the source. Roy (1966) used Taylor's series extrapolation for continuation of a two-dimensional field and derived a 4-point formula to compute an approximate field at the lower level. On specific spacing of data, not explained in the work, he could show the electromagnetic field widely oscillates on reaching the target. The approach failed to produce valid results for gravity-magnetic fields (Roy, 1966).

Strakhov (1963) has discussed the inverse problem proposed by Peters (1949). He has shown that the problem has a closed form solution and it is highly sensitive to error in input data. He named it an incorrectly posed problem in potential theory. Strakhov (1967) however could construct a solution using successive approximation method.

This was quite stable relative to errors in the original data. The difficulty was that the rate of convergence of successive approximation was very low, particularly when the lower level, i.e., the level of continuation was near the source. The problem of finding stable approximate solution was finally solved by Glasko et. al. (1987) by using of regularisation technique (Tikhonov & Goncharsky, 1987). They named it an ill-posed problem in potential theory.

The above procedure of down-continuation of an observed potential field from a datum plane (line in two-dimensions) to a horizontal plane (line in two-dimensions) below it, cannot help us in finding point to point depth to an undulated basement of a geological basin. In this case, the continuation plane/ line passing through the bottom of a trough contains a portion of the neighbouring basement high above it. This violates Dirichlet condition that the domain of continuation, bounded below by the boundary of continuation, must be free from the causative mass.

Theoretically, the above formulation requires the boundaries to be extended from $-\infty$ to ∞ with space between them free from the causative mass and the field vanishing at infinity. In all practical problems we consider the data over a finite boundary and assume that the input data are zero outside it. This produces erroneous solution at the periphery of the boundary and the error propagates towards the central part as depth of continuation increases. As a result, down continuation of aeromagnetic data acquired over a narrow valley bounded by sharply rising high granitic hills, suffers from loss of reliable information over a strip of considerable width stretched all along the boundary of the valley. The question arises how to provide maximum possible coverage in the valley.

To find point to point depth to an undulated basement in a basin Laskar (1991) has proposed downward continuation of two-dimensional potential field to a concave lower boundary, with its arms coinciding with the datum line and apex moving downward in steps along a vertical line passing through the causative mass. At each downward step, the field value is computed at its apex and finally the gradient of the continued field is computed along the vertical to find the depth to the top of the causative mass without considering the error in the computed field and its effect on determination of depth to the causative mass.

The work of Laskar (1991) needs further development on (i) design of the convergence criterion in numerical solution of the ill-posed problem, (ii) choice of spacing of data over the datum line for obtaining a reliable continued field at a preassigned depth and (iii) a discussion on behaviour of error in the down-continued field whose gradient along the vertical defines the depth to the top of the causative mass.

In the present work **(I)** the basics of two-dimensional potential theory is presented in short for ready reference and existence and uniqueness of solution of close domain Dirichlet-Neumann problems are furnished in brief for their subsequent use in discussion on existence-uniqueness of solution of a half-space problem. Order of the boundary density at infinity is determined and the theory of half-space problem is discussed as a particular case of close domain problem when one part of the boundary goes to infinity. Next **(II)** reproduction of a two dimensional harmonic function ϕ with asymptotic behaviour $\phi=O(r^{-n})$, $n \geq 1$, $r \rightarrow \infty$, is achieved in the upper half-space domain B_1 bounded below by a half-space boundary S from boundary data as potential of single as well as double layer boundary density. The field is also reproduced in B_1

by Green's formula without finding Green's function for the boundary. Subsequently, **(III)** for ϕ specified over a horizontal boundary \bar{S} , downward continuation of ϕ to a curved lower boundary S with its arms extending along \bar{S} is discussed by formulating the problem in an integral equation of the first kind in double layer density over S in terms of data specified over \bar{S} . Assuming ϕ is defined on and above the continuation boundary S , it is shown that it has a unique solution over S . However, for the input data with error, this problem formulates an ill-posed problem in potential theory (Tikhonov & Goncharsky, 1987), a small perturbation in input data over \bar{S} creates an wide oscillation in solution over S .

The anomalous gravity field Δg and the component magnetic field T_z , we encounter in gravity-magnetic data analysis in geophysics, are harmonic functions vanishing at infinity in the upper half-space domain bounded below by the half-space boundary S . As such, **(IV)** the problems of continuation of a geo-potential field H , either Δg or T_z mentioned above, are expressed by replacing ϕ by H in the equations formulating the half-space problems. Since down continuation of data is highly sensitive to error in input data and the error goes on increasing with depth, a theoretical discussion is carried out for determination of spacing of data over the datum line for a reliable continued field at a given depth. It is also theoretically shown that for a finite length of the datum line \bar{S} , down continuation of the field at the apex z_k of a concave lower boundary S_L as S_L extends downward with its ends fixed at \bar{S} and z_k moving downward in steps along the axis of S_L , the error in the continued $H(z_k)$ increases steadily with depth of z_k below \bar{S} . As such, the error in the computed $H(z_k)$ does not affect the location of the first maximum of the gradient of $H(z_k)$ that defines the depth to the top of the causative mass below \bar{S} .

On discretization of equations (V) a discussion is carried out for finding a suitable method of solution of a equation formulating the up-continuation problem. Subsequently, a method of successive correction of a guess solution is described that yields a stable approximate solution of the ill-posed problem.

Subsequently model studies are carried out for numerical verification of theoretical results. (VI) It is shown numerically that each of the three formulations presented in the present work for up-continuation of a field from boundary data, yields the result to a good degree of accuracy. In down-continuation of data from a finite datum line, it is interesting to note that down-continuation of data to flat-bottom curved boundary presents a better result over the flat part than that produced by down-continuation to a horizontal boundary coinciding with it at the same depth below the datum line. Further, in a narrow valley bounded by sharply rising granitic hills, downward continuation of aeromagnetic data to a flat bottom curved boundary, provides a better coverage of the valley than that by down-continuation to a horizontal line.

Finally, (VII) the techniques are applied to aeromagnetic data of Shillong-Nongpoh area of the state of Meghalaya for identification of basement faults from the vertical component magnetic field and its gradients computed along NS lines above the flight level in the area. To identify a weak basement feature, if present in the area, the vertical component magnetic field is continued downward to a flat bottom curved boundary to enhance the response of the basement over the narrow valley, the flat part *proving the maximum possible coverage of the valley above the ground surface.* In the next step, point to point depth to the basement is computed from vertical component magnetic data to find the thickness of the sedimentary cover in the area. The depth-profile so obtained approximately agrees with the predicted basement faults across it and the exposed geology at Umsning, a small town in the area.

CHAPTER II

TWO-DIMENSIONAL POTENTIAL THEORY

2.1 Potential due to simple sources

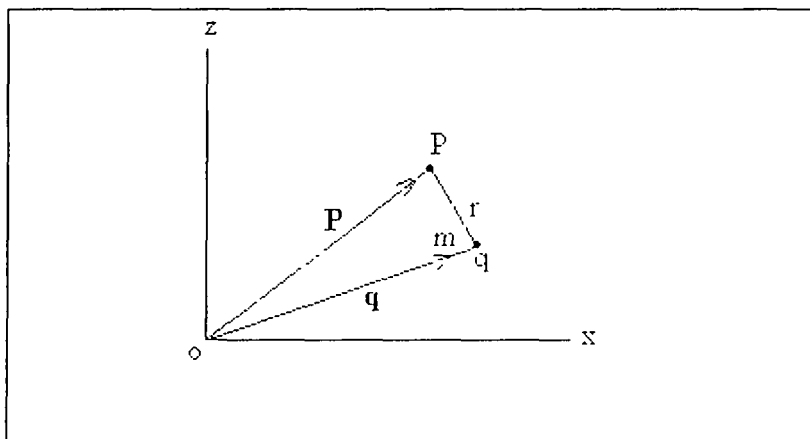
2.1.1 Potential due to a simple source

For a logarithmic simple source m placed at point q in a xoz plane (Fig. 2.1.1) the potential ϕ due to it at a point P in the same plane is given by

$$\phi(\mathbf{P}) = -m \log r = -m \log|\mathbf{P} - \mathbf{q}|, \quad (2.1.1)$$

where \mathbf{P} and \mathbf{q} are the position vectors specifying the points P and q respectively with respect to an arbitrary reference point O and r is the distance between P and q .

Fig. 2.1.1: The source point q and the field point P in a xoz reference frame with z -axis upward



Properties of Simple source potential

- ◆ The potential ϕ is defined everywhere except at the point q where it has a singularity.
- ◆ $\nabla^2\phi=0$ everywhere except at the source point q , i.e., the potential ϕ satisfies Laplace's equation everywhere except at q .
- ◆ The ϕ at infinity shows the behaviour

$$\phi(\mathbf{P}) = -\left[m \log|\mathbf{P}| - |\mathbf{P}|^{-1}(\mathbf{P} \cdot \mathbf{q})m + O(|\mathbf{P}|^{-2}) \right]$$

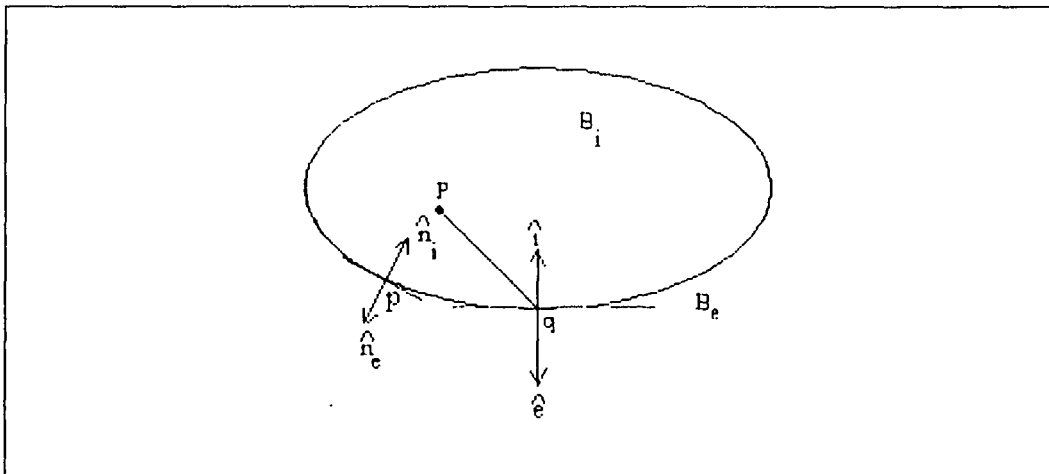
as $|\mathbf{P}| \rightarrow \infty$.

2.1.2 Potential due to simple sources over a closed contour

For a smooth closed contour ∂B defining the periphery of a vertical section of an infinitely long closed surface of density σ (Fig. 2.1.2), the potential ϕ at a point P in the plane of the contour is expressed as

$$\phi(\mathbf{P}) = - \int_{\partial B} \log|\mathbf{P} - \mathbf{q}| \sigma(\mathbf{q}) d\mathbf{q}, \tag{2.1.2}$$

Fig. 2.1.2: Interior domain B_i is enclosed by the closed contour ∂B . Exterior domain B_e lies outside B_i . Unit vectors \hat{i} and \hat{e} are internal and external normals respectively to ∂B at q .



where $|\mathbf{P} - \mathbf{q}|$ defines the distance between the points \mathbf{P} and \mathbf{q} , $\sigma(\mathbf{q})$ represents the line density at the boundary point \mathbf{q} and dq represents the elementary arc length at \mathbf{q} . For the sake of further mathematical analysis, let us omit the negative sign to the integral and write the logarithmic potentials as

$$\phi(\mathbf{P}) = \int_{\partial B} \log|\mathbf{P} - \mathbf{q}| \sigma(\mathbf{q}) dq, \quad \mathbf{P} \in B_i \quad (2.1.3)$$

and
$$\phi(\mathbf{P}) = \int_{\partial B} \log|\mathbf{P} - \mathbf{q}| \sigma(\mathbf{q}) dq, \quad \mathbf{P} \in B_e \quad (2.1.4)$$

These define harmonic functions in B_i , B_e respectively and they remains continuous at ∂B as

$$\phi(\mathbf{p}) = \int_{\partial B} \log|\mathbf{P} - \mathbf{q}| \sigma(\mathbf{q}) dq, \quad \mathbf{p} \in \partial B \quad (2.1.5)$$

It is evident from (2.1.3), (2.1.4) and (2.1.5) that

- ◆ The potential ϕ is continuous everywhere including the boundary
- ◆ $\nabla^2 \phi = 0$ everywhere except at the boundary.
- ◆ The ϕ at infinity shows the behaviour

$$\phi(\mathbf{P}) = \log|\mathbf{P}| \int_{\partial B} \sigma(\mathbf{q}) dq - |\mathbf{P}|^{-1} \int_{\partial B} (\mathbf{P} \cdot \mathbf{q}) \sigma(\mathbf{q}) dq + O(|\mathbf{P}|^{-2})$$

as $|\mathbf{P}| \rightarrow \infty$.

The tangential derivatives exist and continuous at $\mathbf{p} \in \partial B$ provided σ is Hölder continuous at \mathbf{p} , but the normal derivatives are discontinuous.

We write

$$\frac{\partial}{\partial n_i} \log|\mathbf{p} - \mathbf{q}| \equiv \log_i |\mathbf{p} - \mathbf{q}| \equiv \log|\mathbf{q} - \mathbf{p}|_i$$

$$\frac{\partial}{\partial n_e} \log|\mathbf{p} - \mathbf{q}| \equiv \log'_e |\mathbf{p} - \mathbf{q}| \equiv \log|\mathbf{q} - \mathbf{p}|_e,$$

for the interior and exterior derivatives of $\log|\mathbf{p} - \mathbf{q}|$ at \mathbf{p} keeping \mathbf{q} fixed. These have equal status and are connected by

$$\log'_i |\mathbf{p} - \mathbf{q}| + \log'_e |\mathbf{p} - \mathbf{q}| = 0, \quad \mathbf{p} \in \partial B \quad (2.1.6)$$

For an interior point \mathbf{P} , the derivative of ϕ at \mathbf{P} in the direction \hat{n} is given by

$$\begin{aligned} \frac{\partial}{\partial n} \phi(\mathbf{P}) &= \phi'_n(\mathbf{P}) = \int_{\partial B} \frac{\partial}{\partial n} \log|\mathbf{P} - \mathbf{q}| \sigma(\mathbf{q}) d\mathbf{q} \\ &= \int_{\partial B} \log'_n |\mathbf{P} - \mathbf{q}| \sigma(\mathbf{q}) d\mathbf{q}, \quad \mathbf{P} \in B_i, \end{aligned} \quad (2.1.7)$$

exists and continuous in B_i for the integrand being regular and uniformly convergent in \mathbf{P} . As $\mathbf{P} \rightarrow \mathbf{p} \in \partial B$, the integrand in (2.1.7) has a singularity at \mathbf{p} . Following Kellogg (1929), it can be established for σ satisfying Hölder continuity at \mathbf{p} and \mathbf{n} representing the interior normal \mathbf{i} at ∂B ,

$$\frac{\partial}{\partial n_i} \phi(\mathbf{p}) = \phi'_i(\mathbf{p}) = \pi\sigma(\mathbf{p}) + \int_{\partial B} \log'_i |\mathbf{p} - \mathbf{q}| \sigma(\mathbf{q}) d\mathbf{q}, \quad \mathbf{p} \in \partial B. \quad (2.1.8)$$

Following the sign convention of Jaswon (1963), treating both sides of ∂B as positive,

$$\frac{\partial}{\partial n_e} \phi(\mathbf{p}) = \phi'_e(\mathbf{p}) = \pi\sigma(\mathbf{p}) + \int_{\partial B} \log'_e |\mathbf{p} - \mathbf{q}| \sigma(\mathbf{q}) d\mathbf{q}, \quad \mathbf{p} \in \partial B, \quad (2.1.9)$$

for ϕ defined in the exterior domain B_e (Fig. 2.1.2) and σ satisfying Hölder continuity at $\mathbf{p} \in \partial B$.

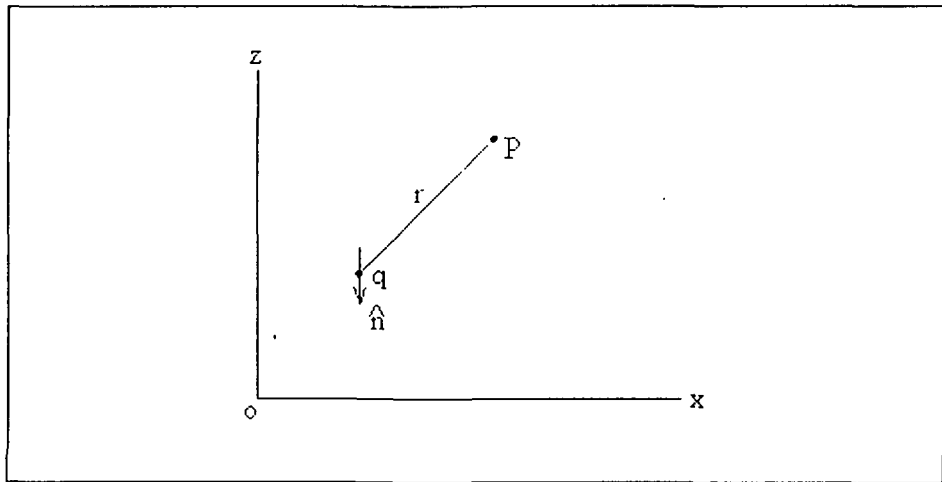
2.2 Potential due to double sources

2.2.1 Potential due to a double source

For a dipole of strength μ placed at a point q in the direction \hat{n} (Fig. 2.2.1), the potential W due to it at a point P is given by

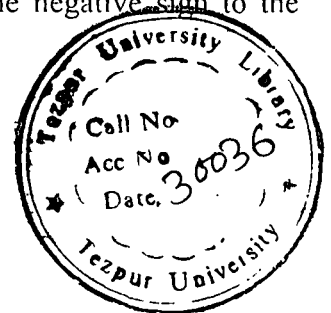
$$W(\mathbf{P}) = -\mu \log|\mathbf{P} - \mathbf{q}|_{\hat{n}} \quad (2.2.1)$$

Fig 2.2.1: The doublet of strength μ having direction \hat{n} is placed at the source point q and P defines the field point at a distance r from q



For the sake of further mathematical analysis, let us omit the negative sign to the integral and write the logarithmic potentials as

$$W(\mathbf{P}) = \mu \log|\mathbf{P} - \mathbf{q}|_{\hat{n}}$$



Properties of Double source potential

- ◆ The potential W is defined everywhere except at the point q where it has a singularity.
- ◆ $\nabla^2 W = 0$ everywhere except at the dipole at q .
- ◆ The W vanishes at infinity with asymptotic behaviour $W = O(|\mathbf{P}|^{-1})$, $|\mathbf{P}| \rightarrow \infty$

2.2.2 Potential due to double sources over a closed contour

A continuous distribution of double sources of strength μ over ∂B generates the double layer logarithmic potentials

$$W(\mathbf{P}) = \int_{\partial B} \log|\mathbf{P} - \mathbf{q}|_i \mu(\mathbf{q}) d\mathbf{q}, \mathbf{P} \in B_i \quad (2.2.2)$$

and
$$W(\mathbf{P}) = \int_{\partial B} \log|\mathbf{P} - \mathbf{q}|_e \mu(\mathbf{q}) d\mathbf{q}, \mathbf{P} \in B_e \quad (2.2.3)$$

These are harmonic functions in B_i, B_e respectively and

$$W(\mathbf{P}) = O(|\mathbf{P}|^{-1}), \text{ as } |\mathbf{P}| \rightarrow \infty. \quad (2.2.4)$$

The integral (2.2.2) suffers a discontinuity at ∂B as

$$\lim_{\mathbf{P}_i \rightarrow \mathbf{p}} W(\mathbf{P}_i) = W(\mathbf{p}) - \pi\mu(\mathbf{p}) \quad (2.2.5)$$

and
$$\lim_{\mathbf{P}_e \rightarrow \mathbf{p}} W(\mathbf{P}_e) = W(\mathbf{p}) + \pi\mu(\mathbf{p}), \quad (2.2.6)$$

where \mathbf{P}_i and \mathbf{P}_e are points on n_i and n_e respectively both emanating from $\mathbf{p} \in \partial B$.

It is evident from (2.2.2) and (2.2.5) that

- ◆ The potential W is continuous everywhere except at the boundary
- ◆ The potential W jumps by an amount $\pi\mu$ at the boundary
- ◆ The W vanishes at infinity with asymptotic behaviour $W = O(|\mathbf{P}|^{-1}), |\mathbf{P}| \rightarrow \infty$

2.3 Formulation of Dirichlet and Neumann Problems

2.3.1 Interior Problems

(a) Interior Dirichlet Problems

For a two-dimensional harmonic function ϕ given over a smooth closed contour ∂B , ϕ in the interior domain B , can be reproduced by simple layer logarithmic boundary density σ as

$$\phi(\mathbf{P}) = \int_{\partial B} \log|\mathbf{P} - \mathbf{q}| \sigma(\mathbf{q}) d\mathbf{q}, \quad \mathbf{P} \in B, \quad (2.3.1)$$

As $\mathbf{P} \rightarrow \mathbf{p} \in \partial B$, we obtain the boundary relation

$$\phi(\mathbf{p}) = \int_{\partial B} \log|\mathbf{p} - \mathbf{q}| \sigma(\mathbf{q}) d\mathbf{q}, \quad \mathbf{p} \in \overline{\partial B}. \quad (2.3.2)$$

Given ϕ over ∂B , (2.3.2) formulates a Dirichlet problem in an integral equation of the first kind in σ in terms of ϕ over ∂B .

This general equation was formulated by Hamel (1949) and Volterra (1959) without any further discussion on it. It has been shown by Jaswon and Symm (1977) that the equation (2.3.2) has a general solution

$$\sigma = \sigma_0 + k\lambda, \quad (2.3.3)$$

where σ_0 is a particular solution of (2.3.2), k is an arbitrary constant and λ satisfies

$$1 = \phi(\mathbf{p}) = \int_{\partial B} \log|\mathbf{p} - \mathbf{q}| \lambda(\mathbf{q}) d\mathbf{q}, \quad \mathbf{p} \in \partial B \quad (2.3.4)$$

for $\partial B \neq \Gamma$ -contour for which equation (2.3.4) does not have a solution (Jaswon, 1963). The solution can be made unique on a particular choice of k .

Given ϕ over ∂B the interior Dirichlet problem can also be formulated following (2.2.5) by a double layer logarithmic boundary density μ as

$$\phi(\mathbf{p}) = -\pi\mu(\mathbf{p}) + \int_{\partial B} \log|\mathbf{p} - \mathbf{q}| \mu(\mathbf{q})d\mathbf{q}, \mathbf{p} \in \partial B. \quad (2.3.5)$$

Following Kellogg (1929), equation (2.3.5) in μ has a solution if

$$\int_{\partial B} \phi(\mathbf{p})\lambda(\mathbf{p})d\mathbf{p} = 0, \quad (2.3.6)$$

where λ is the solution of the corresponding adjoint homogeneous equation

$$0 = -\pi\lambda(\mathbf{p}) + \int_{\partial B} \log|\mathbf{p} - \mathbf{q}| \lambda(\mathbf{q})d\mathbf{q}, \mathbf{p} \in \partial B \quad (2.3.7)$$

which is mathematically equivalent to

$$0 = \pi\lambda(\mathbf{p}) + \int_{\partial B} \log_c|\mathbf{p} - \mathbf{q}| \lambda(\mathbf{q})d\mathbf{q}, \mathbf{p} \in \partial B \quad (2.3.8)$$

by virtue of (2.1.6). It can be established that the equation (2.3.8) does not have a non-trivial λ . This λ satisfies (2.3.6) for an arbitrary ϕ on ∂B . Hence, following Kellogg (1929), equation (2.3.5) has a unique solution μ for an arbitrary ϕ over ∂B .

(b) Interior Neumann Problems

For ϕ_n prescribed over ∂B , the σ that reproduces the ϕ in $B, +\partial B$, can be obtained for $\partial B \neq \Gamma$ as a solution of the normal derivative equation

$$\phi_n(\mathbf{p}) = \pi\sigma(\mathbf{p}) + \int_{\partial B} \log_c|\mathbf{p} - \mathbf{q}| \sigma(\mathbf{q})d\mathbf{q}, \mathbf{p} \in \partial B, \quad (2.3.9)$$

formed by (2.1.8). Equation (2.3.9) expresses an interior Neumann problem by a Fredholm integral equation of the second kind in σ in terms of ϕ_n given on ∂B .

Following Kellogg (1929), this has a solution if

$$\int_{\partial B} \phi_n(\mathbf{p})\lambda(\mathbf{p})d\mathbf{p} = 0 \quad (2.3.10)$$

where λ is the solution of the corresponding adjoint homogeneous equation

$$0 = \pi\lambda(\mathbf{p}) + \int_{\partial B} \log|\mathbf{p} - \mathbf{q}|_i \lambda(\mathbf{q}) d\mathbf{q}, \mathbf{p} \in \partial B \quad (2.3.11)$$

which, by virtue of

$$\int_{\partial B} \log|\mathbf{p} - \mathbf{q}|_i d\mathbf{q} = -\pi, \mathbf{p} \in \partial B \quad (2.3.12)$$

has a non-trivial solution $\lambda = 1$ on ∂B . On substitution of this λ in (2.3.10), we arrive at the Gauss' condition

$$\int_{\partial B} \phi'_i(\mathbf{p}) d\mathbf{p} = 0 \quad (2.3.13)$$

for a ϕ harmonic in B_i . This ensures the existence of a solution of equation (2.3.9).

The solution can be written as

$$\sigma = \sigma_0 + k\lambda \quad (2.3.14)$$

where σ_0 is a particular solution of (2.3.9), k is an arbitrary constant and λ is the solution of (2.3.4). This solution when substituted in (2.3.1) produces a series of ϕ in B_i as

$$\phi = \phi_0 + k \quad (2.3.15)$$

having the interior normal derivative as prescribed on ∂B . The solution can be made unique on proper choice of k .

2.3.2 Exterior Problems

(a) Exterior Dirichlet Problems

The boundary density σ obtained as solution of equation (2.3.2) i.e .

$$\phi(\mathbf{p}) = \int_{\partial B} \log|\mathbf{p} - \mathbf{q}| \sigma(\mathbf{q}) d\mathbf{q}, \mathbf{p} \in \overline{\partial B}, \quad (2.3.16)$$

for $\partial B \neq \Gamma$, generates a potential V in B , that solves the interior Dirichlet problem for \overline{B} . The σ generates an exterior potential V_o characterized by logarithmic behaviour at infinity, whereas the classical existence-uniqueness theorem (Kellogg 1929) specifies $O(1)$ behaviour, implying boundedness on V_o at infinity.

It has been shown by Jaswon and Symm (1977) that the equation (2.3.16) for the exterior domain B_c has a solution

$$\sigma = \sigma_o + k\lambda \quad (2.3.17)$$

$$1 = \int_{\partial B} \log|\mathbf{p} - \mathbf{q}| \lambda(\mathbf{q}) d\mathbf{q}, \mathbf{p} \in \partial B, \quad (2.3.18)$$

where σ_o satisfies

$$\phi_o(\mathbf{p}) = \int_{\partial B} \log|\mathbf{p} - \mathbf{q}| \sigma_o(\mathbf{q}) d\mathbf{q}, \mathbf{p} \in \partial B \quad (2.3.19)$$

with existence condition

$$\int_{\partial B} \phi_o(\mathbf{p}) \lambda(\mathbf{p}) d\mathbf{p} = \int_{\partial B} \sigma_o(\mathbf{q}) d\mathbf{q} = 0 \quad (2.3.20)$$

implying $\phi_o = O(r^{-1})$, $r \rightarrow \infty$, and σ_o is the unique solution of (2.3.19).

The solution (2.3.17) can be made unique on proper choice of k .

(a) Exterior Neumann Problems

For ϕ'_c defining the exterior normal derivative of an exterior harmonic function ϕ , with asymptotic behaviour $\phi = O(r^{-1})$, $r \rightarrow \infty$, given ϕ'_c over ∂B (Fig.2.1.2), ϕ in B_c can be obtained as a potential due to a simple layer boundary density σ on ∂B ($\neq \Gamma$ contour) as

$$\phi(\mathbf{P}) = \int_{\partial B} \log|\mathbf{P} - \mathbf{q}| \sigma(\mathbf{q}) d\mathbf{q}, \mathbf{P} \in B_c \quad (2.3.21)$$

Following (2.1.9), the σ of (2.3.21) is related to ϕ'_c on ∂B as

$$\phi'_c(\mathbf{p}) = \pi\sigma(\mathbf{p}) + \int_{\partial B} \log'_c|\mathbf{p} - \mathbf{q}| \sigma(\mathbf{q}) d\mathbf{q}, \mathbf{p} \in \partial B \quad (2.3.22)$$

Given ϕ'_c over ∂B , equation (2.3.22) expresses an exterior Neumann problem in a Fredholm boundary integral equation of the second kind for σ in terms of ϕ'_c over ∂B . This equation has a solution if

$$\int_{\partial B} \phi'_c(\mathbf{p}) \lambda(\mathbf{p}) d\mathbf{p} = 0 \quad (2.3.23)$$

where λ satisfies the adjoint homogeneous equation

$$0 = \pi\lambda(\mathbf{p}) + \int_{\partial B} \log|\mathbf{p} - \mathbf{q}'_c| \lambda(\mathbf{q}) d\mathbf{q}, \mathbf{p} \in \partial B. \quad (2.3.24)$$

That the homogeneous component of (2.3.22)

$$0 = \pi\sigma(\mathbf{p}) - \int_{\partial B} \log'_c|\mathbf{p} - \mathbf{q}| \sigma(\mathbf{q}) d\mathbf{q}, \mathbf{p} \in \partial B,$$

does not have a non-trivial solution. Hence, following Kellogg (1929), we conclude that the adjoint homogeneous equation (2.3.24) does not have a non-trivial solution. This implies, the condition (2.3.23) is satisfied for an arbitrary ϕ'_c on ∂B . Consequently, the equation (2.3.22) has a solution for an arbitrary ϕ'_c on ∂B and this solution is unique.

2.4 Green's Formulae

2.4.1 Green's Formulae for interior domain

For a harmonic function ϕ defined in an interior domain B , bounded by a smooth closed contour ∂B , Green's formula in two dimensions takes the form

$$\int_{\partial B} \log|\mathbf{P}-\mathbf{q}|_i \phi(\mathbf{q})d\mathbf{q} - \int_{\partial B} \log|\mathbf{P}-\mathbf{q}| \phi'_i(\mathbf{q})d\mathbf{q} = -2\pi\phi(\mathbf{P}), \mathbf{P} \in B, \quad (2.4.1)$$

For the field point P located on ∂B , the boundary formula in two-dimensions is written as,

$$\int_{\partial B} \log|\mathbf{p}-\mathbf{q}|_i \phi(\mathbf{q})d\mathbf{q} - \int_{\partial B} \log|\mathbf{p}-\mathbf{q}| \phi'_i(\mathbf{q})d\mathbf{q} = -\pi\phi(\mathbf{p}), \mathbf{p} \in \partial B \quad (2.4.2)$$

Given ϕ on ∂B , equation (2.4.2) expresses an interior Dirichlet problem for ϕ'_i in terms of ϕ , by a Fredholm boundary integral equation of the first kind in ϕ'_i as

$$\int_{\partial B} \log|\mathbf{p}-\mathbf{q}| \phi'_i(\mathbf{q})d\mathbf{q} = \pi\phi(\mathbf{p}) + \int_{\partial B} \log|\mathbf{p}-\mathbf{q}|_i \phi(\mathbf{q})d\mathbf{q}, \mathbf{p} \in \partial B. \quad (2.4.3)$$

This equation is of the type (2.3.2) which has been proved to have a unique solution.

2.4.2 Green's Formulae for exterior domain

To discuss Green's formulae for the exterior domain B_e , let us assume $\phi = O(r^{-1}), r \rightarrow \infty$. We know changing of i into e yields the analogous exterior formulae under the new sign convention of Jaswon (1963). For example, under this rule, the formula (2.4.1) yields the exterior formula

$$\int_{\partial B} \log|\mathbf{P}-\mathbf{q}|_e \phi(\mathbf{q})d\mathbf{q} - \int_{\partial B} \log|\mathbf{P}-\mathbf{q}| \phi'_e(\mathbf{q})d\mathbf{q} = -2\pi\phi(\mathbf{P}), \mathbf{P} \in B_e \quad (2.4.4)$$

and (2.4.2) yields the boundary formula for the exterior ϕ as

$$\int_{\partial B} \log|\mathbf{p}-\mathbf{q}|_c \phi(\mathbf{q})d\mathbf{q} - \int_{\partial B} \log|\mathbf{p}-\mathbf{q}| \phi'_c(\mathbf{q})d\mathbf{q} = -\pi\phi(\mathbf{p}), \mathbf{p} \in \partial B \quad (2.4.5)$$

where π signifies the external angle at \mathbf{p} .

Given ϕ on ∂B , the relation (2.4.5) yields the Boundary equation

$$\int_{\partial B} \log|\mathbf{p}-\mathbf{q}| \phi'_c(\mathbf{q})d\mathbf{q} = \pi\phi(\mathbf{p}) + \int_{\partial B} \log|\mathbf{p}-\mathbf{q}|_c \phi(\mathbf{q})d\mathbf{q}, \mathbf{p} \in \partial B \quad (2.4.6)$$

which expresses the exterior Dirichlet Problem for ϕ'_c in a Fredholm integral equation of the first kind in ϕ'_c in terms of ϕ on ∂B .

This equation is of type (2.3.16) for the exterior domain B_c which has a solution for $O(1)$ behaviour of ϕ and that can be made unique. Since the ϕ under discussion vanishes at infinity, the equation (2.4.6) has a unique solution.

Given ϕ'_c on ∂B , equation (2.4.6) expresses an exterior Neumann Problem in a Fredholm integral equation of the second kind in ϕ as

$$\int_{\partial B} \log|\mathbf{p}-\mathbf{q}|_c \phi(\mathbf{q})d\mathbf{q} + \pi\phi(\mathbf{p}) = \int_{\partial B} \log|\mathbf{p}-\mathbf{q}| \phi'_c(\mathbf{q})d\mathbf{q} \quad (2.4.7)$$

Following Kellogg (1929), this has a solution if and only if

$$\int_{\partial B} \left\{ \int_{\partial B} \log|\mathbf{p}-\mathbf{q}| \phi'_c(\mathbf{q})d\mathbf{q} \right\} \lambda(\mathbf{p})d\mathbf{q} = 0,$$

where λ satisfies the adjoint homogenous equation

$$0 = \pi\lambda(\mathbf{p}) + \int_{\partial B} \log|_c|\mathbf{p}-\mathbf{q}| \lambda(\mathbf{q})d\mathbf{q}, \mathbf{p} \in \partial B$$

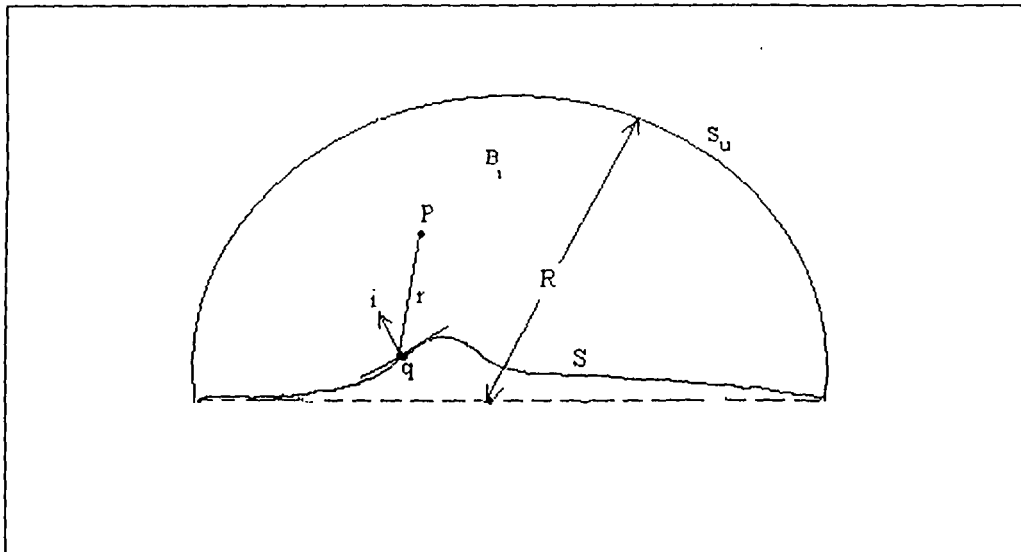
This equation does not have a non-trivial solution λ as discussed in the equation (2.3.22). Hence, the exterior Neumann problem, expressed by equation (2.4.7) has a unique solution for $\phi = O(r^{-1}), r \rightarrow \infty$ and $\partial B \neq \Gamma$ contour.

2.4.3 Reproduction of a Harmonic function as Simple and double layer potential

Let a two-dimensional harmonic function ϕ with asymptotic behaviour $\phi=O(r^{-n})$, $n \geq 1$, $r \rightarrow \infty$, be defined in the upper half-space domain bounded below by a general half-space boundary S . Let us consider the ϕ above S in a closed domain B_i as shown in Fig.2.4.1, bounded above by a semicircle S_u of radius R . Given ϕ and its interior normal derivative ϕ'_i over $\partial B(=S+S_u)$, ϕ in the interior is given by Green's formula as

$$-2\pi\phi(P) = \int_{\partial B} \log_i |\mathbf{q} - \mathbf{P}| \phi(q) dq - \int_{\partial B} \log |\mathbf{q} - \mathbf{P}| \phi'_i(q) dq, P \in B_i \quad (2.4.8)$$

Fig. 2.4.1: The closed domain B_i bounded below by S and above by a semicircle S_u of Radius R , $R \rightarrow \infty$



Let us now consider an exterior harmonic function f with asymptotic behaviour $f=O(r^{-n})$, $n \geq 1$, $r \rightarrow \infty$ defined in the exterior domain B_e bounded at interior by ∂B .

Following Green's identity II, its boundary data satisfy

$$\int_{\partial B} \log_i |\mathbf{q} - \mathbf{P}| f(\mathbf{q}) d\mathbf{q} - \int_{\partial B} \log |\mathbf{q} - \mathbf{P}| f'_c(\mathbf{q}) d\mathbf{q} = 0, \mathbf{P} \in B, \quad (2.4.9)$$

Superposition of (2.4.9) on formula (2.4.8) yields, by virtue of $\log_i |\mathbf{q} - \mathbf{P}| = \log_c |\mathbf{q} - \mathbf{P}|, \mathbf{q} \in \partial B,$

$$\int_{\partial B} \log_i |\mathbf{q} - \mathbf{P}| \{\phi(\mathbf{q}) - f(\mathbf{q})\} d\mathbf{q} - \int_{\partial B} \log |\mathbf{q} - \mathbf{P}| \{\phi'_i(\mathbf{q}) + f'_c(\mathbf{q})\} d\mathbf{q} = -2\pi\phi(\mathbf{P}), \mathbf{P} \in B, , \quad (2.4.10)$$

already shown by Jaswon and Symm (1977).

Now we consider two distinct possibilities for f

(a) For $f=\phi$ over ∂B , we find

$$\int_{\partial B} \log |\mathbf{q} - \mathbf{P}| \{\phi'_i(\mathbf{q}) + f'_c(\mathbf{q})\} d\mathbf{q} = 2\pi\phi(\mathbf{P}), \mathbf{P} \in B, , \quad (2.4.11)$$

This provides a simple layer representation of ϕ in B , with source density

$$\sigma(\mathbf{q}) = +\frac{1}{2\pi} \{\phi'_i(\mathbf{q}) + f'_c(\mathbf{q})\} \quad (2.4.12)$$

Existence of a unique exterior f with asymptotic behaviour as assumed above, satisfying $f=\phi$ over ∂B , is ensured by the exterior Dirichlet existence theorem.

(b) The second possibility $f'_c = -\phi'_i$ over ∂B , provides the representation

$$\int_{\partial B} \log_i |\mathbf{q} - \mathbf{P}| \{\phi(\mathbf{q}) - f(\mathbf{q})\} d\mathbf{q} = -2\pi\phi(\mathbf{P}), \mathbf{P} \in B, ,$$

This is a double layer potential generated by source density

$$\mu(\mathbf{q}) = -\frac{1}{2\pi} \{\phi(\mathbf{q}) - f(\mathbf{q})\}. \quad (2.4.13)$$

Existence of a unique f in B_c satisfying $f'_c = -\phi'_c$ over ∂B is ensured by exterior Neumann existence theorem.

For f and ϕ vanishing at infinity in same order over S_u (Fig. 2.4.1) as $r \rightarrow \infty$, we find for $\mathbf{q} \in S_u$

$$\sigma(\mathbf{q}) = O(\phi'_c), |\mathbf{q}| \rightarrow \infty, \quad (2.4.14)$$

and $\mu(\mathbf{q}) = O(\phi), |\mathbf{q}| \rightarrow \infty, \quad (2.4.15)$

from (2.4.12) and (2.4.13) respectively.

A quick verification of (2.4.14) and (2.4.15) comes from the boundary relations of ϕ'_c and σ and that of ϕ and μ over a half-space horizontal boundary \bar{S} . For ϕ in B_1 (Fig. 2.4.1) given by

$$\phi(\mathbf{P}) = \int_{\bar{S}} |\log|\mathbf{P} - \mathbf{q}|| \sigma(\mathbf{q}) d\mathbf{q}, \mathbf{P} \in B_1,$$

the normal derivative relation ϕ and σ over \bar{S} is

$$\phi'_c(\mathbf{p}) = \pi\sigma(\mathbf{p}) + \int_{\bar{S}} |\log|\mathbf{p} - \mathbf{q}|| \sigma(\mathbf{q}) d\mathbf{q} = \pi\sigma(\mathbf{p}), \mathbf{p} \in \bar{S} \quad (2.4.16)$$

the integral over \bar{S} being zero for both $\mathbf{p}, \mathbf{q} \in \bar{S}$. For ϕ in B_1 given by

$$\phi(\mathbf{P}) = \int_{\bar{S}} \log|\mathbf{P} - \mathbf{q}| \mu(\mathbf{q}) d\mathbf{q}, \mathbf{P} \in B, ,$$

and the boundary relation of ϕ and μ over \bar{S} is

$$\phi(\mathbf{p}) = -\pi\mu(\mathbf{p}) + \int_{\bar{S}} \log|\mathbf{p} - \mathbf{q}| \mu(\mathbf{q}) d\mathbf{q} = -\pi\mu(\mathbf{p}), \mathbf{p} \in \bar{S}, \quad (2.4.17)$$

the integral on the right hand side of (2.4.17) vanishing for $\mathbf{p}, \mathbf{q} \in \bar{S}$.

CHAPTER III

HALF-SPACE PROBLEMS

3.1 Upward Continuation from Boundary Data

3.1.1 Simple layer Formulation

Let a two-dimensional harmonic function ϕ with asymptotic behaviour $\phi = O(r^{-n}), n \geq 1, r \rightarrow \infty$, be defined in a closed domain B_i bounded below by a general boundary S and above by a semicircle S_u of radius $R, R \rightarrow \infty$, as shown in Fig. 2.4.1. Following (2.3.1), ϕ in B_i can be reproduced by a simple layer boundary density σ as

$$\begin{aligned}\phi(\mathbf{P}) &= \int_{\partial B} \log|\mathbf{P} - \mathbf{q}| \sigma(\mathbf{q}) d\mathbf{q}, \mathbf{P} \in B_i \\ &= \int_S \log|\mathbf{P} - \mathbf{q}| \sigma(\mathbf{q}) d\mathbf{q} + \int_{S_u} \log|\mathbf{P} - \mathbf{q}| \sigma(\mathbf{q}) d\mathbf{q}, \mathbf{P} \in B_i\end{aligned}\quad (3.1.1)$$

As $R \rightarrow \infty$, i.e., as S_u moves to infinity, the formula (3.1.1) yields

$$\phi(\mathbf{P}) = \int_S \log|\mathbf{P} - \mathbf{q}| \sigma(\mathbf{q}) d\mathbf{q}, \mathbf{P} \in B_i, \quad (3.1.2)$$

the second integral of (3.1.1) having no contribution to ϕ at \mathbf{P} , for $\sigma(\mathbf{q}) = O(\phi') = O(R^{-(n+1)})$, $n \geq 1$, by (2.4.14), $d\mathbf{q} = O(R)O(1)$, $\mathbf{q} \in S_u$ and $\lim_{R \rightarrow \infty} (\log R / R) = 0$.

As $\mathbf{P} \rightarrow \mathbf{p} \in S$, by virtue of continuity of ϕ in $B_i + S$, we obtain

$$\phi(\mathbf{p}) = \int_S \log|\mathbf{p} - \mathbf{q}| \sigma(\mathbf{q}) d\mathbf{q}, \mathbf{p} \in S \quad (3.1.3)$$

To discuss the existence-uniqueness of the solution of (3.1.3), let us consider the boundary formula

$$\phi(\mathbf{p}) = \int_{\partial B} \log|\mathbf{p} - \mathbf{q}| \sigma(\mathbf{q}) d\mathbf{q}, \mathbf{p} \in \partial B \quad (3.1.4)$$

Given ϕ over ∂B , equation (3.1.4) expresses an interior Dirichlet problem in σ in terms of ϕ specified over ∂B . This equation, by (2.3.3), has a solution $\sigma = \sigma_0 + k\lambda$, which can be made unique on proper choice of k , σ_0 being the particular solution of (3.1.4)

Since (3.1.4) has a solution that can be made unique, the solution of

$$\begin{aligned} \phi(\mathbf{p}) &= \int_S \log|\mathbf{p} - \mathbf{q}| \sigma(\mathbf{q}) d\mathbf{q} + \int_{S_u} \log|\mathbf{p} - \mathbf{q}| \sigma(\mathbf{q}) d\mathbf{q}, \mathbf{p} \in \partial B \\ &= \int_S \log|\mathbf{p} - \mathbf{q}| \sigma(\mathbf{q}) d\mathbf{q}, \mathbf{p} \in S, \end{aligned} \quad (3.1.5)$$

has a unique solution σ_0 for the choice $k=0$, ϕ and σ being $O(R^{-1})$ and $O(R^{-2})$ over S_u as $R \rightarrow \infty$. The $\sigma (= \sigma_0)$ reproduces the ϕ on and above the half-space boundary S .

3.1.2 Double layer Formulation

Let a two dimensional harmonic function ϕ with asymptotic behaviour $\phi = O(r^{-n}), n \geq 1, r \rightarrow \infty$, be defined in a closed domain B , bounded below by a general boundary S and above by a semicircle S_u of radius $R, R \rightarrow \infty$, as shown in Fig. 2.4.1. Following (2.2.2), ϕ in B , can be reproduced as potential of a double layer boundary density μ as

$$\phi(\mathbf{P}) = \int_{\partial B} \log|\mathbf{P} - \mathbf{q}| \mu(\mathbf{q}) d\mathbf{q}, \mathbf{P} \in B, \quad (3.1.6)$$

yielding the boundary relation, by (2.2.5)

$$\phi(\mathbf{p}) = -\pi\mu(\mathbf{p}) + \int_{\partial B} \log|\mathbf{p} - \mathbf{q}| \mu(\mathbf{q}) d\mathbf{q}, \mathbf{p} \in \partial B. \quad (3.1.7)$$

Given ϕ over ∂B , the equation (3.1.7), following (2.3.5), has a unique solution μ for an arbitrary ϕ over ∂B .

As $R \rightarrow \infty$, i.e., S_u goes to infinity, (3.1.6) becomes

$$\phi(\mathbf{P}) = \int_S \log|\mathbf{P} - \mathbf{q}| \mu(\mathbf{q}) d\mathbf{q}, \mathbf{P} \in B, \quad (3.1.8)$$

and (3.1.7) becomes

$$\phi(\mathbf{p}) = -\pi\mu(\mathbf{p}) + \int_S \log|\mathbf{p} - \mathbf{q}| \mu(\mathbf{q}) d\mathbf{q}, \mathbf{p} \in S \quad (3.1.9)$$

the integral over S_u having no contribution to ϕ at \mathbf{P} for $\mu = O(\phi) = O(r^{-n})$, $n \geq 1$, $r \rightarrow \infty$ and $|\log|q - P||$ being bounded for all locations of \mathbf{P} in $B_r + S$.

Since the equation (3.1.7) has a unique solution for an arbitrary ϕ specified over ∂B , the equation (3.1.9), a particular case of (3.1.7) for ϕ and μ vanishing over S_u , has a unique μ over S for an arbitrary ϕ over S . This μ reproduces the ϕ in B , by (3.1.8).

3.1.3 Formulation by Green's Formula

For a two-dimensional harmonic function ϕ with asymptotic behaviour $\phi = O(r^{-n})$, $n \geq 1$, $r \rightarrow \infty$, defined in a closed domain B , bounded below by a general boundary S and above by a semicircle of radius R , $R \rightarrow \infty$, as shown in Fig. 2.4.1, given ϕ and ϕ'_e over $\partial B (= S + S_u)$, Fig. 2.4.1), ϕ in B , can be obtained by (2.4.1) as

$$-2\pi\phi(\mathbf{P}) = \int_{\partial B} \log|\mathbf{P} - \mathbf{q}| \phi(\mathbf{q}) d\mathbf{q} - \int_{\partial B} \log|\mathbf{P} - \mathbf{q}| \phi'_e(\mathbf{q}) d\mathbf{q}, \mathbf{P} \in B, \quad (3.1.10)$$

For $\partial B = S + S_u$, the above formula can be written as

$$\begin{aligned}
 -2\pi\phi(\mathbf{P}) &= \int_S \log|\mathbf{P} - \mathbf{q}| \phi(\mathbf{q}) d\mathbf{q} - \int_S \log|\mathbf{P} - \mathbf{q}| \phi'(\mathbf{q}) d\mathbf{q} \\
 &+ \int_{S_u} \log|\mathbf{P} - \mathbf{q}| \phi(\mathbf{q}) d\mathbf{q} - \int_{S_u} \log|\mathbf{P} - \mathbf{q}| \phi'(\mathbf{q}) d\mathbf{q}, \mathbf{P} \in B,
 \end{aligned}$$

As $R \rightarrow \infty$, S_u goes to infinity and the above formula becomes

$$-2\pi\phi(\mathbf{P}) = \int_S \log|\mathbf{P} - \mathbf{q}| \phi(\mathbf{q}) d\mathbf{q} - \int_S \log|\mathbf{P} - \mathbf{q}| \phi'(\mathbf{q}) d\mathbf{q}, \mathbf{P} \in B, \quad (3.1.11)$$

the integrals over S_u vanishing at least in $O(R^{-1})$, $R \rightarrow \infty$. The formula (3.1.11) expresses ϕ in the upper half-space domain B , in terms of ϕ and ϕ' given on S . As

$\mathbf{P} \rightarrow \mathbf{p} \in S$ and $R \rightarrow \infty$, the formula (2.4.2) becomes

$$-\pi\phi(\mathbf{p}) = \int_S \log|\mathbf{p} - \mathbf{q}| \phi(\mathbf{q}) d\mathbf{q} - \int_S \log|\mathbf{p} - \mathbf{q}| \phi'(\mathbf{q}) d\mathbf{q}, \mathbf{p} \in S, \quad (3.1.12)$$

the integrals over S_u vanishing at least in $O(R^{-1})$, $R \rightarrow \infty$.

Given ϕ on S , the formula (3.1.12) defines a Dirichlet problem for ϕ' in terms of ϕ as

$$\int_S \log|\mathbf{p} - \mathbf{q}| \phi'(\mathbf{q}) d\mathbf{q} = \pi\phi(\mathbf{p}) + \int_S \log|\mathbf{p} - \mathbf{q}| \phi(\mathbf{q}) d\mathbf{q}, \mathbf{p} \in S. \quad (3.1.13)$$

for the upper half-space domain bounded below by S .

Introducing the upper part S_u of the boundary, the equation can be expressed as

$$\int_{\partial B} \log|\mathbf{p} - \mathbf{q}| \phi'(\mathbf{q}) d\mathbf{q} = \pi\phi(\mathbf{p}) + \int_{\partial B} \log|\mathbf{p} - \mathbf{q}| \phi(\mathbf{q}) d\mathbf{q}, \mathbf{p} \in \partial B. \quad (3.1.14)$$

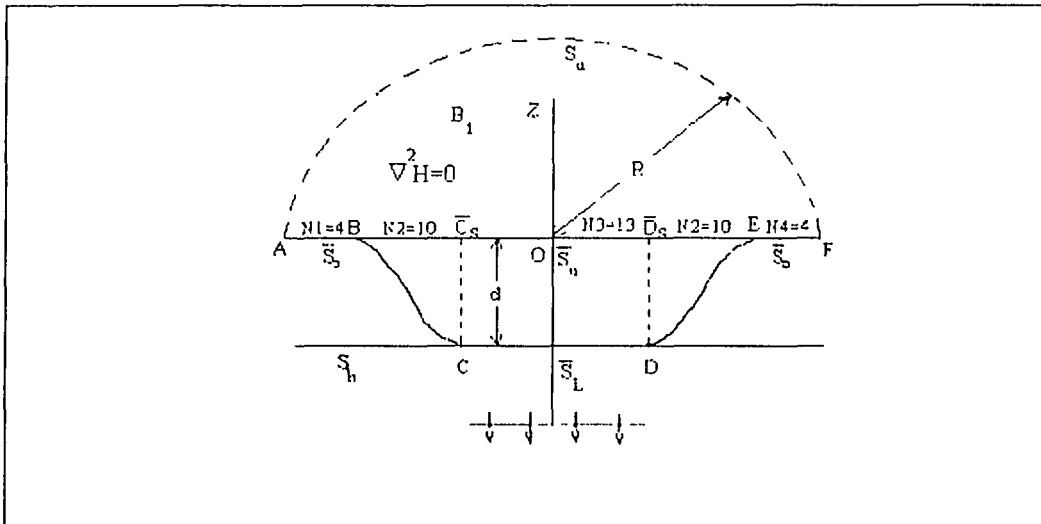
This equation, by (2.4.3), has a unique solution. Hence, the half-space problem formulated by (3.1.13), a particular case of (3.1.14), has unique ϕ' over S for ϕ given over S .

3.2 Downward Continuation from Boundary Data

For a two-dimensional harmonic function ϕ with asymptotic behaviour $\phi = O(r^{-n})$, $n \geq 1$, $r \rightarrow \infty$, defined in the upper half-space domain B_1 bounded below by a half-space boundary $S (= \bar{S}_0 + S_L + \bar{S}_0)$, Fig.3.2.1), given ϕ over S , by (3.1.8), there exists a double layer boundary density μ over S that reproduces the $\sqrt{\phi}$ in B_1 as

$$\phi(\mathbf{P}) = \int_S \log_1 |\mathbf{q} - \mathbf{P}| \mu(\mathbf{q}) d\mathbf{q}, \mathbf{P} \in B_1. \quad (3.2.1)$$

Fig. 3.2.1: A closed domain B_1 bounded below by a curved boundary $S (= \bar{S}_0 + S_L + \bar{S}_0)$ and above by a semicircle S_u of radius R , $R \rightarrow \infty$



As $\mathbf{P} \rightarrow \mathbf{p} \in S$, by (3.1.9), the formula (3.2.1) yields the boundary relation between ϕ and μ as

$$\phi(\mathbf{p}) = -\pi\mu(\mathbf{p}) + \int_S \log_1 |\mathbf{q} - \mathbf{p}| \mu(\mathbf{q}) d\mathbf{q}, \mathbf{p} \in S. \quad (3.2.2)$$

Given ϕ over S , the equation (3.2.2) formulates a Dirichlet problem in μ for the upper half-space domain B_1 in terms of ϕ specified over S . It has already been shown in

subsection 3.1.2 that the above equation has a unique μ over S and this μ reproduces the ϕ on and above S .

Let us now assume that the ϕ be specified over a horizontal half-space boundary $\bar{S}(= \bar{S}_0 + \bar{S}_u + \bar{S}_v, \text{Fig. 3.2.1})$ and the curved continuation boundary S , having a central concave part S_L with its ends common to those of \bar{S}_u , extend to infinity along \bar{S}_v on both sides of \bar{S}_u . Now for $P \in \bar{S}_u$, excluding its end points, the half-space formula (3.2.1) yields

$$\begin{aligned} \phi(P) &= \int_{S_L} \log_i |\mathbf{q} - \mathbf{P}| \mu(\mathbf{q}) d\mathbf{q} + \int_{\bar{S}_v} \log_i |\mathbf{q} - \mathbf{P}| \mu(\mathbf{q}) d\mathbf{q} \\ &= \int_{S_L} \log_i |\mathbf{q} - \mathbf{P}| \mu(\mathbf{q}) d\mathbf{q}, \quad \mathbf{P} \in \bar{S}_u, \end{aligned} \quad (3.2.3)$$

the integral over \bar{S}_0 having no contribution to ϕ at $\mathbf{P} \in \bar{S}_u$. This is evident from the fact that $\log_i |\mathbf{q} - \mathbf{P}| = 0$ for $\mathbf{P}, \mathbf{q} \in \bar{S}$ and $\mathbf{P} \neq \mathbf{q}$. Once the μ over S_L is obtained as solution of the equation (3.2.3), μ over \bar{S}_0 is given by (3.2.2) rewritten as

$$\begin{aligned} \pi\mu(P) &= \phi(P) + \int_{S_L + \bar{S}_0} \log_i |\mathbf{q} - \mathbf{P}| \mu(\mathbf{q}) d\mathbf{q}, \quad \mathbf{P} \in \bar{S}_0, \\ &= \phi(P) + \int_{S_L} \log_i |\mathbf{q} - \mathbf{P}| \mu(\mathbf{q}) d\mathbf{q}, \quad \mathbf{P} \in \bar{S}_0, \end{aligned} \quad (3.2.4)$$

the integral over \bar{S}_0 being zero for $\mathbf{P} \neq \mathbf{q}$, $\log_i |\mathbf{q} - \mathbf{P}| = 0$, $\mathbf{P}, \mathbf{q} \in \bar{S}_0$ and for $\mathbf{P} = \mathbf{q}$, the integral being singular at an isolated point P , a set of measure zero.

CHAPTER IV

APPLICATION IN GEOPHYSICS

4.1 Upward Continuation

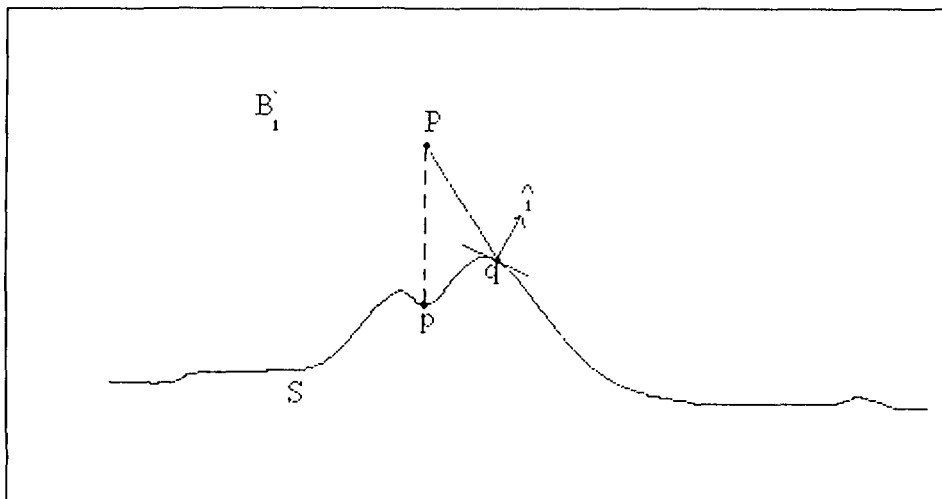
4.1.1 Reproduction of Gravity-Magnetic Fields from boundary data as potential due to Simple Layer Boundary Density

Let H be a harmonic function, an anomalous gravity field Δg or component magnetic field T_z , in two-dimensions with asymptotic behaviour $H=O(r^{-n})$, $n \geq 1$, $r \rightarrow \infty$ in the upper half-space domain B_i , bounded below by a half-space boundary S , given H over S , H in B_i can be reproduced by (3.1.2) as potential due to simple layer logarithmic boundary density σ as

$$H(P) = - \int_S \log|q - P| \sigma(q) dq, \quad P \in B_i, \quad (4.1.1)$$

introducing the original negative sign to the integral and $\sigma(q)$ is the simple layer boundary density over S at the point q .

Fig. 4.1.1: Boundary S , field point P and the outward (towards B_i) normal \hat{i} to S at boundary point q



The H in (4.1.1) is continuous in B_i+S . For the field point P coinciding with the boundary point p , we obtain the boundary formula

$$H(p) = - \int_S \log|q - p| \sigma(q) dq, \quad p \in S. \quad (4.1.2)$$

Given H over S , equation (4.1.2) expresses a Fredholm integral equation of first kind in σ in terms of H specified over S . It has been shown in (3.1.5) that the equation has a unique σ over S . Once the σ is known as solution of equation (4.1.2), H in B_i can be computed by (4.1.1).

Now, as P moves to infinity, the formula (4.1.1) yields

$$H(P) = O(\log|P|) \int_S \sigma(q) dq, \quad |P| \rightarrow \infty.$$

For H representing a two-dimensional gravity field, $H = O(r^{-1})$, $r \rightarrow \infty$. As such, in this case

$$\int_S \sigma(q) dq = 0,$$

for $\log|P| \neq 0$, $|P| \rightarrow \infty$.

For H representing a two-dimensional component magnetostatic field, $H = O(r^{-2})$, $r \rightarrow \infty$. As such, for this case also

$$\int_S \sigma(q) dq = 0$$

Hence for both the cases, H representing either a gravimetric or a component magnetostatic field in two-dimensions,

$$\int_S \sigma(q) dq = 0. \quad (4.1.3)$$

4.1.2 Reproduction of Gravity-Magnetic Fields from boundary data as potential due to Double Layer Boundary Density

For H denoting either a gravimetric or a component magnetostatic field in B_i+S , H in B_i is a harmonic function with asymptotic behaviour $H=O(r^{-n})$, $n \geq 1$, as $r \rightarrow \infty$. As such, upward continuation of H in B_i can be obtained following (3.1.8) as a potential due to a double layer boundary density as

$$H(\mathbf{P}) = - \int_S \log \frac{1}{|\mathbf{q} - \mathbf{P}|} \mu(\mathbf{q}) \, dq, \quad \mathbf{P} \in B_i, \quad (4.1.4)$$

introducing the original negative sign to the integral, $\mu(\mathbf{q})$ defining the double layer boundary density at the point \mathbf{q} over S . For the field point \mathbf{P} coinciding with a boundary point \mathbf{p} , as \mathbf{P} approaches S , we obtain by boundary formula (3.1.9),

$$H(\mathbf{p}) = \pi \mu(\mathbf{p}) - \int_S \frac{1}{|\mathbf{q} - \mathbf{p}|} \mu(\mathbf{q}) \, dq, \quad \mathbf{p} \in S. \quad (4.1.5)$$

Given H over S , equation (4.1.5) presents a boundary integral equation of the second kind in μ . This expresses a Dirichlet problem in μ in terms of H over S . Since the equation (3.1.9) has a unique solution for an arbitrary ϕ over S , this equation has a unique solution for an arbitrary H over S . Once μ is known over S , H at $\mathbf{P} \in B_i$ can be computed by (4.1.4).

As $|\mathbf{P}| \rightarrow \infty$, formula (4.1.4) yields

$$H(\mathbf{P}) = O(|\mathbf{P}|^{-1}) \int_S \mu(\mathbf{q}) \, dq, \quad |\mathbf{P}| \rightarrow \infty. \quad (4.1.6)$$

For H representing a two-dimensional gravimetric field, $H = O(|\mathbf{P}|^{-1})$, $|\mathbf{P}| \rightarrow \infty$. It is evident from (4.1.6) that for H representing a gravity field,

$$\int_S \mu(\mathbf{q}) \, dq \neq 0 \quad (4.1.7)$$

necessarily.

For H representing a two-dimensional magnetostatic component field, $H = O(|\mathbf{P}|^{-2})$, $|\mathbf{P}| \rightarrow \infty$. Hence, it is evident from (4.1.5) that for the magnetostatic case,

$$\int_S \mu(q) dq = 0. \quad (4.1.8)$$

4.1.3 Reproduction of Gravity-Magnetic Fields from boundary data by Green's Formula

For H representing a gravity or a component magnetostatic field in the upper half-space domain B_1 bounded below by S , H is a harmonic function in B_1 with asymptotic behaviour $H = O(r^{-n})$, $n \geq 1$, $r \rightarrow \infty$. As such given H over S , following (3.1.11), H in B_1 can be obtained by Green's formula

$$-2\pi H(\mathbf{P}) = \int_S \log|\mathbf{q} - \mathbf{P}| H(\mathbf{q}) dq - \int_S \log|\mathbf{q} - \mathbf{P}| H'_1(\mathbf{q}) dq, \quad \mathbf{P} \in B_1, \quad (4.1.9)$$

on obtaining H'_1 over S as a solution of the boundary integral equation

$$-\pi H(\mathbf{p}) = \int_S \log|\mathbf{q} - \mathbf{p}| H(\mathbf{q}) dq - \int_S \log|\mathbf{q} - \mathbf{p}| H'_1(\mathbf{q}) dq, \quad \mathbf{p} \in S. \quad (4.1.10)$$

Given H over S , equation (4.1.10) represents a boundary integral equation of the first kind in H'_1 in terms of H specified over S . Following (3.1.13), we conclude that this equation has a unique H'_1 over S . With this H'_1 over S , H at a point $\mathbf{P} \in B_1$ can be obtained by (4.1.9).

4.2 Downward continuation

4.2.1 Continuation to a curved lower boundary

Let a two-dimensional harmonic function H , a gravity field Δg or a magnetostatic component field T_z , with asymptotic behaviour $H = O(r^{-n})$, $n \geq 1$, $r \rightarrow \infty$, be defined in the upper half space domain B_1 bounded below by a curved half-space boundary $S (= \bar{S}_0 + S_1 + \bar{S}_0$, Fig.3.2.1) such that its central part S_L is concave upward with its ends fixed at the datum line and arms extending along it.

Let us now assume that the upper half-space domain B_1 , bounded below by S , be also bounded above by a semicircular arc S_u of radius R , $R \rightarrow \infty$. The domain so bounded by $S+S_u$ ($=\partial B$, say) be considered as an interior domain B_i . For the causative mass lying below S , the field H is a harmonic function in B_1 . As such, given H over ∂B , H in B_i can be reproduced as potential due to a double layer boundary density μ (Jaswon and Symm, 1977) as

$$H(\mathbf{P}) = - \int_{\partial B} \log_{,i} |\mathbf{q} - \mathbf{P}| \mu(\mathbf{q}) dq = - \int_{S+S_u} \log_{,i} |\mathbf{q} - \mathbf{P}| \mu(\mathbf{q}) dq, \quad \mathbf{P} \in B_i, \quad (4.2.1)$$

where \mathbf{P} and \mathbf{q} represent the position vectors of the field point P and the boundary point q respectively, $\log_{,i} |\mathbf{q} - \mathbf{P}|$ represents the interior (towards B_i) normal derivative of $\log |\mathbf{q} - \mathbf{P}|$ at the point q keeping P fixed, $\mu(\mathbf{q})$ represents the double layer logarithmic boundary density μ at the point q and dq represents the arc element at q .

Since the boundary density $\mu(\mathbf{q})=O(H)$, $|\mathbf{q}| \rightarrow \infty$, by (2.4.15), contribution of the μ of S_u to H at P in formula (4.2.1) vanishes as $R \rightarrow \infty$. Consequently, formula (4.2.1) reduces to the half-space formula

$$H(\mathbf{P}) = - \int_S \log_i |\mathbf{q} - \mathbf{P}| \mu(\mathbf{q}) d\mathbf{q}, \quad \mathbf{P} \in B_i, \quad (4.2.2)$$

for the upper half-space domain B_i bounded below by S .

Since the μ of (4.2.2) reproduces the H on and above S , it must reproduce the field on a horizontal line \bar{S} in B_i+S . Let us now assume that the field H be specified over the horizontal half-space boundary $\bar{S} (= \bar{S}_o + \bar{S}_u + \bar{S}_l)$, Fig.3.2.1) and let the curved lower boundary S_L lie vertically below \bar{S}_u with end-points common to them. Now for $\mathbf{P} \in \bar{S}_u$ excluding its end points, the half-space formula (4.2.2) yields

$$\begin{aligned} H(\mathbf{P}) &= - \left[\int_{S_i} \log_i |\mathbf{q} - \mathbf{P}| \mu(\mathbf{q}) d\mathbf{q} + \int_{\bar{S}_o} \log_i |\mathbf{q} - \mathbf{P}| \mu(\mathbf{q}) d\mathbf{q} \right], \\ &= - \int_{S_L} \log_i |\mathbf{q} - \mathbf{P}| \mu(\mathbf{q}) d\mathbf{q}, \quad \mathbf{P} \in \bar{S}_u, \end{aligned} \quad (4.2.3)$$

the integral over \bar{S}_o having no contribution to H at $\mathbf{P} \in \bar{S}_u$ for $\log_i |\mathbf{q} - \mathbf{P}| = 0$, $\mathbf{P} \neq \mathbf{q}$, $\mathbf{P}, \mathbf{q} \in \bar{S} (= \bar{S}_o + \bar{S}_u + \bar{S}_l)$, Fig.3.2.1).

It is to be mentioned here that for an erroneous input data, equation (4.2.3) formulates an ill-posed problem (Tikhonov and Goncharsky, 1987) in μ in terms of H specified over \bar{S}_u . A small perturbation in H creates a wide oscillation in $\mu \in S_L$.

Assuming that the input data are free from error, given H over \bar{S}_u , equation (4.2.3) has a unique solution (Appendix I). To find the μ over \bar{S}_o , let us consider, following Jawson and Symm (1977), the boundary equation as

$$H(\mathbf{P}) = \pi \mu(\mathbf{P}) - \int_S \log_i |\mathbf{q} - \mathbf{P}| \mu(\mathbf{q}) d\mathbf{q}, \quad \mathbf{P} \in \bar{S}_o$$

$$\begin{aligned}
 &= \pi\mu(\mathbf{P}) - \left[\int_{S_L} \log_i |\mathbf{q} - \mathbf{P}| \mu(\mathbf{q}) d\mathbf{q} + \int_{\bar{S}_0} \log_i |\mathbf{q} - \mathbf{P}| \tilde{\mu}(\mathbf{q}) d\mathbf{q} \right], \quad \mathbf{P} \in \bar{S}_0. \\
 &= \pi\mu(\mathbf{P}) - \int_{S_L} \log_i |\mathbf{q} - \mathbf{P}| \mu(\mathbf{q}) d\mathbf{q}, \quad \mathbf{P} \in \bar{S}_0, \tag{4.2.4}
 \end{aligned}$$

the integral over \bar{S}_0 vanishing for $\log_i |\mathbf{q} - \mathbf{P}| = 0$, $\mathbf{P}, \mathbf{q} \in \bar{S}_0$, $\mathbf{P} \neq \mathbf{q}$, and for $\mathbf{P} = \mathbf{q}$, the integral having a singularity at the isolated point \mathbf{P} , a set of measure zero. Once the μ over S_L is obtained as solution of the equation (4.2.3), the μ over \bar{S}_0 can be directly obtained from (4.2.4).

For the μ known over $S (= \bar{S}_0 + S_L + \bar{S}_0)$, Fig.3.2.1), H at a point $\mathbf{p} \in S_L$ can be computed as potential due to $\mu(\mathbf{q})$, $\mathbf{q} \in S$, by the boundary formula

$$H(\mathbf{p}) = \pi\mu(\mathbf{p}) - \int_S \log_i |\mathbf{q} - \mathbf{p}| \mu(\mathbf{q}) d\mathbf{q}, \quad \mathbf{p} \in S. \tag{4.2.5}$$

To examine the validity of μ obtained over S_L and \bar{S}_0 as solution of equations (4.2.3) and (4.2.4) respectively, let us obtain the μ over $S (= \bar{S}_0 + S_L + \bar{S}_0)$, Fig.3.2.1) as solution of Dirichlet problem expressed by (4.2.5), assuming that the H is known over S . This provides an opportunity to examine the uniqueness of the solution of (4.2.3), assuming that the input data are free from error.

4.2.2 Continuation to a horizontal lower boundary

For S_L coinciding with a horizontal half-space boundary \bar{S}_L (say) placed at a depth d below \bar{S} , the boundary relation between H and μ over \bar{S}_L , by (4.2.5), is

$$\begin{aligned} H(\mathbf{p}) &= \pi\mu(\mathbf{p}) - \int_{\bar{S}_L} \log_i |\mathbf{q} - \mathbf{p}| \mu(\mathbf{q}) d\mathbf{q}, \quad \mathbf{p} \in \bar{S}_L \\ &= \pi\mu(\mathbf{p}), \quad \mathbf{p} \in \bar{S}_L, \end{aligned} \quad (4.2.6)$$

for $\int_{\bar{S}_L} \log_i |\mathbf{q} - \mathbf{p}| \mu(\mathbf{q}) d\mathbf{q} = 0$, $\mathbf{p}, \mathbf{q} \in \bar{S}_L$, as shown earlier in (4.2.3) and (4.2.4). This

expresses μ in terms of H belonging to \bar{S}_L as

$$\mu(\mathbf{q}) = H(\mathbf{q}) / \pi, \quad \mathbf{q} \in \bar{S}_L. \quad (4.2.7)$$

For \bar{S}_u and S_L both representing half-space horizontal boundaries, $S_L (= \bar{S}_L)$ placed at depth d below \bar{S}_u , the μ over S_L in equation (4.2.3) can be replaced by $H(\mathbf{q})/\pi$. Putting this μ in equation (4.2.3) with \bar{S}_u and $S_L (= \bar{S}_L)$ both extending to infinity, we obtain downward continuation of H to a horizontal boundary \bar{S}_L at a depth d below \bar{S} as

$$\begin{aligned} H(\mathbf{P}) &= - \int_{\bar{S}_L} \log_i |\mathbf{q} - \mathbf{P}| H(\mathbf{q}) d\mathbf{q}, \quad \mathbf{P} \in \bar{S}_u \\ &= - \frac{1}{\pi} \int_{\bar{S}_L} \log_i |\mathbf{q} - \mathbf{P}| H(\mathbf{q}) d\mathbf{q}, \end{aligned} \quad (4.2.8)$$

for $\mu(\mathbf{q})$ replaced by $H(\mathbf{q})/\pi$.

For \mathbf{P} and \mathbf{q} defined by the co-ordinates $(X,0)$ and $(x,-d)$ respectively in a cartesian frame with z -axis upward, the formula (4.2.8) leads to the well known downward continuation formula of Peters(1949).

$$H(X,0) = \frac{d}{\pi} \int_{-\infty}^{\infty} \frac{H(x,-d)}{[(x-X)^2 + d^2]} dx, \quad (4.2.9)$$

for \bar{S}_u defined by $z=0$ and \bar{S}_l defined by $z=-d$.

4.2.3 Depth-Determination from Gradient of Down-Continued Field: A New Approach

For a potential field continued towards its source, the field is supposed to exhibit a wild behavior on reaching the target. This property of the field suggests a possible approach for finding the depth to the magnetic basement from the observed magnetic data in a geological basin.

To determine point to point depth to the basement, we are to continue the field to a concave boundary, tapering in shape as depth increases, its apex moving along a vertical defining the axis of the boundary. This can be achieved by down-continuation of data to a concave lower boundary that extends downward with its ends fixed at the datum line and apex moving downward in steps along the vertical.

Since the solution technique discussed in subsection 5.4.2 ensures convergence and produces a stable approximate numerical solution for all positions of S_L above or below the causative mass, it is likely that contrary to expectation the computed $H(z_k)$, z_k defining the apex of S_L , will show a smooth behaviour at the boundary of the causative mass. However, as the field rapidly increases as we approach the target and the formulation becomes invalid for the field point passing through the causative mass (Laskar 2000), the vertical gradient of the computed field, under such a situation, is expected to show its first maximum at the boundary of the target. As such, the depth

of the first maximum of the vertical gradient of the continued field is supposed to define the depth to the top of the causative mass.

On finding $H(z_k)$ as z_k moves downward in a regular step Δz along the vertical, the vertical gradient of $H(z)$ at $z=z_k$ is computed, following Scarborough (1966), by the finite difference formula

$$\left. \nabla_z H_k = \frac{\partial H}{\partial z} \right|_{z=z_k} \approx \frac{1}{\Delta z} \left[(\Delta_1 H_{k,1} + \Delta_1 H_{k,2})/2 - (\Delta_3 H_{k,11} + \Delta_3 H_{k,12})/12 + \dots \right], \quad (4.2.10)$$

where $\nabla_z H_k$ denotes the vertical gradient of H_k at the point $z=z_k$, $H_k=H(z_0+k\Delta z)$, $\Delta_j H_k$ is the j^{th} order difference of H_k placed against the depth value z_k in a horizontal difference table of H .

To provide a graphical representation of the behaviour of the gradient values as depth increases, the normalised deviation of $\nabla_z H_k$ from $\nabla_z H_3$ is computed by the formula

$$\eta_k = \frac{\nabla_z H_k - \nabla_z H_3}{|\nabla_z H_k - \nabla_z H_3|_{\max}}, \quad k = 3, 4, \dots, (n_s - 2), \quad (4.2.11)$$

where $|\nabla_z H_k - \nabla_z H_3|_{\max}$ represents the largest absolute value of the deviation of $\nabla_z H_k$ from $\nabla_z H_3$, as k varies from 3 to (n_s-2) , n_s defining the last step taken along the vertical at which the continued field $H(z_k)$ is computed.

4.2.4 Spacing of data over the datum line

It is always preferable to have equispaced data over the datum line \bar{S} . The question arises what should be the spacing of data for obtaining a reliable down-continued field value to a pre-assigned depth below \bar{S} . This means we are to find the spacing of data over \bar{S} for which equation (4.2.3) yields a good approximate μ over S_L . This can be achieved when the matrix $|a_{ij}|$, appearing in the discretised version of (4.2.3), presents a system with $\det|a_{ij}|$ having a significant value. To arrive at a working rule, let us divide the lower boundary S_L into n sub-intervals and the corresponding \bar{S}_u that lies vertically above S_L also be divided into n equal sub-intervals such that $\Delta\bar{S}_j$ of \bar{S}_u becomes the projection of ΔS_j of S_L on \bar{S}_u , $j=1,2,\dots,n$. Under this subdivision, the discretised version of (4.2.3) appears in n simultaneous linear algebraic equations in n unknown μ_j as

$$\sum_{j=1}^n a_{kj} \mu_j = H_k, \quad k=1,2,\dots,n, \quad (4.2.12)$$

where

$$a_{ki} = - \int_{\Delta S_i} \log|P_k - q|_i dq, \quad P_k \in \Delta\bar{S}_k. \quad (4.2.13)$$

In the above equation $\det|a_{kj}|$ gradually decreases with increase in depth of S_L . This in turn deteriorates the solution μ at depths, particularly when the input data are with error. To improve the condition of $\det|a_{kj}|$, let us choose a h such that the diagonal element a_{kk} , for a given depth of continuation, satisfies the condition

$$a_{kk} \geq 0.25, \quad k=1,2,\dots,n. \quad (4.2.14)$$

That yields a well-conditioned matrix $|A|$ for its use in finding a reliable μ as solution of (4.2.12).

A relation between h and depth of investigation D_s can however be established on finding an approximate a_{kk} by the centroid rule (Hess and Smith 1967) as

$$a_{kk} = - \int_{\Delta S_k} \log |p_k - q|_i dq, P_k \in \Delta \bar{S}_k$$

$$\cong -\Delta S_k (\hat{r} \cdot \hat{n}_i) / r = \frac{h}{r}, k = 1, 2, \dots, n, \quad (4.2.15)$$

where $-\Delta S_k (\hat{r} \cdot \hat{n}_i) = h$, \hat{r} is vertically downward over $\Delta S_k \in S_L$, \hat{n}_i is the inward (towards B,) normal to ΔS_k , h is the uniform spacing of data over \bar{S}_n and r is the vertical distance from the nodal point $p_k \in \Delta \bar{S}_k$ to the nodal point $q_k \in \Delta S_k$, q_k lying vertically below p_k . (Fig. 4.2.1)

It is evident from (4.2.15) that a_{kk} attains its lowest value at the deepest location of ΔS_k that defines the depth of apex z_k in the k^{th} configuration of S_L . If D_s be the depth of investigation, by (4.2.14) and (4.2.15), we obtain

$$\frac{h}{D_s} \geq 0.25 \quad \text{or} \quad h \geq \frac{D_s}{4}. \quad (4.2.16)$$

Hence, for a depth of investigation D_s , spacing of data $h=D_s/4$ is expected to provide a reasonable approximate solution of (4.2.12), the discretised version of (4.2.3) over S_L .

a) Error in Reproduced Down-continued Field

Down-continuation of an observed two-dimensional potential field H , a gravity field Δg or a component magnetic field ΔT , from the datum line $\bar{S} = (\bar{S}_o + \bar{S}_u + \bar{S}_o, \text{Fig.4.2.1})$ to a lower boundary $S (= \bar{S}_o + S_L + \bar{S}_o, \text{Fig.4.2.1})$ having a central concave part S_L with its ends fixed at the end-points of \bar{S}_u and arms extending along the datum line, has been discussed in subsection 4.2.1. It has been shown that for H specified over \bar{S} , H can be reproduced at z_k at depth D_k below \bar{S} , by (4.2.5), as a double layer potential .

$$H(\mathbf{z}_k) = \pi\mu(\mathbf{z}_k) - \int_S \log_i |\mathbf{q} - \mathbf{z}_k| \mu(\mathbf{q}) d\mathbf{q}, \quad \mathbf{z}_k \in S_L, \quad (4.2.17)$$

provided the upper half-space domain B_i bounded below by S is free from the causative mass. The boundary density μ over S_L can be obtained as a stable approximate solution of the equation (4.2.3) written as

$$H(\mathbf{P}) = - \int_{S_L} \log_i |\mathbf{q} - \mathbf{P}| \mu(\mathbf{q}) d\mathbf{q}, \quad \mathbf{P} \in \bar{S}_u \quad (4.2.18)$$

and that over \bar{S}_o can be directly obtained from the boundary relation (4.2.4) written as

$$\pi\mu(\mathbf{q}_m) = H(\mathbf{q}_m) + \int_{S_L} \log_i |\mathbf{q} - \mathbf{q}_m| \mu(\mathbf{q}) d\mathbf{q}, \quad \mathbf{q}_m \in \bar{S}_o, \quad (4.2.19)$$

for H specified at $\mathbf{q}_m \in \bar{S}_o$ and μ over S_L is obtained as solution of (4.2.18). Once the μ is known over $S (= \bar{S}_o + S_L + \bar{S}_o)$, the field at the apex z_k of S_L can be computed by (4.2.17).

Let us assume that the input data are specified over an interval \bar{D} of the datum line \bar{S} that coincides with the x -axis of a cartesian reference frame and \bar{D} extends from –

$(x_n+h/2)$ to $(x_n+h/2)$ containing $(2n+1)$ equal subintervals of length h each. Let the central part \bar{S}_n of \bar{S} extend from $-(x_{m-1}+h/2)$ to $(x_{m-1}+h/2)$ containing $2(m-1)+1$ subintervals and the concave lower boundary S_L , with its apex at z_k on the vertical $x=0$, lies vertically below \bar{S}_n . As such, the m^{th} subinterval $\Delta\bar{S}_m$ lie just outside \bar{S}_n with its node point at a distance mh from the axis of S_L . Now the contribution of $\Delta\bar{S}_m$ to $H(z_k)$, z_k lying at depth $D_k(=kh)$ below \bar{S} , is

$$E_m^k = - \int_{\Delta\bar{S}_m} \log_e |\mathbf{q} - \mathbf{q}_k| \mu(\mathbf{q}) d\mathbf{q}$$

$$\cong - \frac{h(\mathbf{q}_m - \mathbf{q}_k) \cdot \hat{n}_i}{|\mathbf{q}_m - \mathbf{q}_k|^2} \mu_m^k, \quad (4.2.20)$$

by centroid rule (Hess and Smith, 1967), μ_m^k defining the constant value of μ over $\Delta\bar{S}_m$ for the k^{th} configuration of S_L , (Fig. 4.2.1) $z_k=q_k$ and \hat{n}_i defining the upward (inward to B.) normal to $\Delta\bar{S}_m$ at q_m . On further simplification, we find

$$E_m^k \cong - \frac{D_k h}{(mh)^2 + D_k^2} \mu_m^k = - \frac{kh^2}{(m^2 + k^2)h^2} \mu_m^k = - \frac{k}{m^2 + k^2} \mu_m^k \quad (4.2.21)$$

Following the same procedure, we find the contribution of $\Delta\bar{S}_m$ to $H(z_{k+1})$ at depth $D_{k+1}[=(k+1)h]$ below \bar{S} for the $(k+1)^{\text{th}}$ configuration of S_L is

$$E_m^{k+1} = - \frac{k+1}{m^2 + (k+1)^2} \mu_m^{k+1}. \quad (4.2.22)$$

For \bar{D} extending from $-(x_n+h/2)$ to $(x_n+h/2)$, as mentioned earlier, the contribution to $H(z_k)$ from the sub-elements over the half-space datum line \bar{S} lying outside $(-x_n-h/2, x_n+h/2)$ on both sides of \bar{S}_n , is

$$C_r = - \left[\sum_{m=m_1}^{\infty} \frac{k}{m^2 + k^2} \mu_m^k + \sum_{m=-m_1}^{-\infty} \frac{k}{m^2 + k^2} \mu_m^k \right],$$

by (4.2.21), where $m_1 = n+1$. This contribution C is left out to be added to $H(z_k)$ and as such, the error E in the continued $H(z_k)$ is

$$E = -C = \left[\sum_{m=m_1}^{\infty} \frac{k}{m^2 + k^2} \mu_m^k + \sum_{m=-m_1}^{-\infty} \frac{k}{m^2 + k^2} \mu_m^k \right]. \quad (4.2.23)$$

It is evident from (4.2.21) that for a fixed z_k , the error in the reproduced $H(z_k)$ decreases with increase in m , i.e., increase in data-length, as expected.

b) Behaviour of Error in Vertical Gradient of the Down-continued Field at apex of S_L

To understand the behaviour of error in $H(z_k)$ as z_k moves downward in steps along $x=0$, we are to examine the change in μ_m from μ_m^k to μ_m^{k+1} over $\Delta \bar{S}_m$ as S_L changes its configuration from $S_{L(k)}$ to $S_{L(k+1)}$ shown in Fig. 4.2.1 with depth of z_k increasing from kh to $(k+1)h$ below \bar{S} .

For a gravimetric or a magnetostatic component field H defined in the upper half-space domain B , bounded below by a half-space boundary $S (= \bar{S}_0 + S_L + \bar{S}_0)$, Fig.4.2.1) with its arms \bar{S}_0 coinciding with the half-space datum line \bar{S} , it is shown in Appendix II that the line integral of the double layer boundary density μ reproducing H in $B_1 + S$ exhibits the property

$$\int_S \mu(q) dq = \int_{\bar{S}_0(L)} \mu(q) dq + \int_{S_L} \mu(q) dq + \int_{\bar{S}_0(R)} \mu(q) dq = \int_{\bar{S}} \bar{\mu}(q) dq,$$

where $\bar{\mu}$ is the density over \bar{S} and $\bar{S}_0(L)$ and $\bar{S}_0(R)$ are the arms of S at left and right of \bar{S}_0 respectively. Further, as $|\mathbf{q}| \rightarrow \infty$,

$$\bar{\mu}(\mathbf{q}) = \mu(\mathbf{q}) = 0,$$

q lying over \bar{S}_0 as it extends to infinity where the field vanishes. As such, a change in the line integral of μ over S_L , as S_L changes from $S_{L(k)}$ to $S_{L(k+1)}$, is compensated in the

μ -integral over \bar{S}_0, \bar{S}_0 extending to infinity on both sides S_L . This brings a very minor change in μ over $\Delta\bar{S}_m$ compared to a significant increment in $k/(m^2+k^2)$ as S_L changes from $S_{L(k)}$ to $S_{L(k+1)}$. As such, the product terms show the property

$$\left| \frac{k+1}{m^2+(k+1)^2} \mu_m^{k+1} \right| > \left| \frac{k}{m^2+k^2} \mu_m^k \right|, \quad (4.2.24)$$

for a positive or negative μ_m over $\Delta\bar{S}_m$. Subsequently, the error in the computed $H(z_k)$ will be steadily increasing or decreasing according to μ_m is positive or negative over $\Delta\bar{S}_m$ as depth of z_k increases.

It is to be noted here that the field is measured positive downward and the magnetic causative is polarised by downward doublets. As such, the field becomes positive and it rapidly increases near the causative mass.

It is now evident from the above discussion that for a potential field H specified over a finite interval \bar{D} of the datum line \bar{S} , the error in the down-continued field along a vertical, steadily increases or decreases with depth along the vertical when the field increasing rapidly near the causative mass. As such, this error does not affect the true position of the first maximum of the gradient of the field that defines the depth to the top of the causative mass along the vertical. Hence, the data over a short data-length $\bar{D} > \bar{S}_u$ is sufficient enough to determine the depth to the causative mass below it, though the computed field might have large error in it. It is our working experience that for a causative mass lying within a search depth D_s , $\bar{S}_u \geq 5D_s$ provides the reproduced field $H(z_k)$ along the axis of S_L that leads to determination of a reliable depth to the top of the causative mass.

CHAPTER V

NUMERICAL PROCEDURE

5.1 Discretisation of Equations formulating Up-continuation Problems

5.1.1 Simple Layer Formulae

For a two-dimensional potential field H , an anomalous gravity field Δg or a component magnetic field T , with asymptotic behaviour $H = O(r^{-n})$, $n \geq 1$, $r \rightarrow \infty$, defined in the upper half-space domain B , bounded below by a general half-space boundary S , given H over S , H in B , can be reproduced by (4.1.1.) as potential of simple layer logarithmic boundary density σ as

$$H(\mathbf{P}) = - \int_S \log|\mathbf{q} - \mathbf{P}| \sigma(\mathbf{q}) \, d\mathbf{q}, \quad \mathbf{P} \in B, \quad (5.1.1)$$

on obtaining the σ over S as solution of the boundary equation (4.1.2)

$$H(\mathbf{p}) = - \int_S \log|\mathbf{p} - \mathbf{q}| \sigma(\mathbf{q}) \, d\mathbf{q}, \quad \mathbf{p} \in S. \quad (5.1.2)$$

To solve the equation (5.1.2) numerically, we divide a large finite boundary S into n piecewise straight subintervals ΔS_j , $j=1, 2, \dots, n$ and make the fundamental assumption that σ is constant over a subinterval. For \mathbf{q}_k defining the nodal point (centroid) of k^{th} subinterval ΔS_k and σ_j defining the constant value of σ over the j^{th} subinterval ΔS_j , the H at \mathbf{q}_k given by (5.1.2) can be expressed as

$$H_k = \sum_{j=1}^n -\sigma_j \int_{\Delta S_j} \log|\mathbf{q} - \mathbf{q}_k| \, d\mathbf{q}$$

$$= \sum_{j=1}^n -a_{kj} \sigma_j,$$

where H_k is the value of H at the nodal point q_k , σ_j is the constant value of σ over j^{th} subinterval ΔS_j and

$$a_{kj} = \int_{\Delta S_j} \log|q - q_k| dq. \quad (5.1.3)$$

For k successively assuming the values $1, 2, 3, \dots, n$, the equation (5.1.2) yields

$$\sum_{j=1}^n -a_{kj} \sigma_j = H_k, \quad k = 1, 2, 3, \dots, n, \quad (5.1.4)$$

a system of n simultaneous linear algebraic equations in n unknown σ_j .

On finding the σ_j as solution of (5.1.4) for H_k specified over S , the field H at a point

$P \in B_1$ can be computed by the discretised version of (5.1.1) expressed as

$$\tilde{H}(P) = - \sum_{j=1}^n \sigma_j \int_{\Delta S_j} \log|P - q| dq, \quad (5.1.5)$$

where $\tilde{H}(P)$ denotes the approximate value of H at P .

5.1.2 Double Layer Formulae

For the same harmonic function H , a potential field described in subsection 5.1.1, given H over S , H in B_1 can be reproduced by (4.1.4) as a double layer potential

$$H(P) = - \int_S \log_i|q - P| \mu(q) dq, \quad P \in B_1, \quad (5.1.6)$$

on obtaining the μ over S as solution of the boundary equation (4.1.5)

$$H(p) = \pi \mu(p) - \int_S \log_i|q - p| \mu(q) dq, \quad p \in S \quad (5.1.7)$$

To solve the equation (5.1.7) numerically, we divide a large finite boundary S into n piecewise straight subintervals and make the fundamental assumption that μ is constant over a subinterval. For the field point \mathbf{P} coinciding with \mathbf{q}_k , the nodal point of the k^{th} subinterval ΔS_k of S , the equation (5.1.7) is discretised as

$$\begin{aligned} H_k &= \pi\mu_k + \sum_{j=1}^n -\mu_j \int_{\Delta S_j} \log_i |\mathbf{q} - \mathbf{q}_k| d\mathbf{q}, \\ &= (\pi\delta_{kj} - b_{kj})\mu_j, \quad k = 1, 2, \dots, n, \end{aligned} \quad (5.1.8)$$

where H_k is the value of H at the nodal point \mathbf{q}_k of ΔS_k , μ_j is the constant value of μ over the j^{th} subinterval ΔS_j , δ_{kj} is the Kronecker delta and

$$b_{kj} = \int_{\Delta S_j} \log_i |\mathbf{q} - \mathbf{q}_k| d\mathbf{q} \quad (5.1.9)$$

The equation (5.1.8) represent a system of n simultaneous linear algebraic equations in n unknown μ_j . On finding the μ_j as solution of (5.1.7), the field H at a point $\mathbf{P} \in B_i$ can be computed by

$$H(\mathbf{P}) = -\sum_{j=1}^n \mu_j \int_{\Delta S_j} \log_i |\mathbf{q} - \mathbf{P}| d\mathbf{q}, \quad (5.1.10)$$

the discretised version of (5.1.6).

5.1.3 Green's Formulae

For a harmonic function H with asymptotic behaviour $H = O(r^{-n})$, $n \geq 1, r \rightarrow \infty$, defined in the upper half-space domain B_i bounded below by a half-space boundary S , given H over S , H in B_i can be obtained by Green's formula (4.1.9) on obtaining H_i over S as a unique solution of (4.1.10). For a numerical approach to solve the equations (4.1.10) and subsequently to reproduce H in B_i , let us divide as before a

large finite boundary S into n piecewise straight subintervals ΔS_j , $j=1, 2, 3, \dots, n$ and assume that H is constant over a subinterval, its value being associated with the nodal point of the subinterval. Under this condition the discretised version of the formula (4.1.9) becomes

$$-2\pi\tilde{H}(\mathbf{P}) = \sum_{i=1}^n \left[H_j \int_{\Delta S_j} \log|\mathbf{q} - \mathbf{P}| \, d\mathbf{q} - H_i \int_{\Delta S_i} \log|\mathbf{q} - \mathbf{P}| \, d\mathbf{q} \right], \quad (5.1.11)$$

where $\tilde{H}(\mathbf{P})$ is the approximate value of H at \mathbf{P} , H_j is the constant value of H over j^{th} subinterval ΔS_j and H_i is constant value of H , assumed constant over ΔS_i . Under the same assumptions that H_i and H_j are constant over ΔS_i , discretised version of the boundary equation (4.1.10) becomes

$$-\pi H_k = \sum_{i=1}^n \left[H_j \int_{\Delta S_j} \log|\mathbf{q} - \mathbf{q}_k| \, d\mathbf{q} - H_i \int_{\Delta S_i} \log|\mathbf{q} - \mathbf{q}_k| \, d\mathbf{q} \right], \quad k=1,2,\dots,n,$$

where H_k is the value of H at the nodal point \mathbf{q}_k of ΔS_k . On reorganization, the above equations become

$$\sum_{j=1}^n H_j \int_{\Delta S_j} \log|\mathbf{q} - \mathbf{q}_k| \, d\mathbf{q} = \sum_{i=1}^n H_i \int_{\Delta S_i} \log|\mathbf{q} - \mathbf{q}_k| \, d\mathbf{q} + \pi H_k, \quad k = 1,2,\dots,n. \quad (5.1.12)$$

Denoting $\int_{\Delta S_i} \log|\mathbf{q} - \mathbf{q}_k| \, d\mathbf{q}$ and $\int_{\Delta S_j} \log|\mathbf{q} - \mathbf{q}_k| \, d\mathbf{q}$ by a_{ki} and b_{kj} respectively, the n

equations (5.1.12) in n unknown H_i take the form

$$\begin{aligned} \sum_{j=1}^n H_j a_{kj} &= \sum_{i=1}^n H_i b_{ki} + \pi H_k, \quad k=1, 2, 3, \dots, n \\ &= D_k, \quad k=1, 2, 3, \dots, n, \end{aligned} \quad (5.1.13)$$

where $D_k = \sum_{j=1}^n H_j b_{kj} + \pi H_k$.

The equations (5.1.13) represent a system of n simultaneous linear algebraic equations in n unknown H_j . On solving the equations (5.1.13) for H_j , H at a point $P \in B_i$ can be computed by (5.1.11), the discretised version of (4.1.9).

5.2 Discretisation of Equations formulating Down-continuation Problem

For a two-dimensional harmonic function H , an anomalous gravity field Δg or a component magnetic field T_z with asymptotic behaviour $H = O(r^{-n})$, $n \geq 1$, $r \rightarrow \infty$, defined in the upper half-space domain B_i bounded below by a half-space boundary $S (= \bar{S}_o + S_L + \bar{S}_o$, Fig.3.2.1) with the curved part S_L below the datum line $\bar{S} (= \bar{S}_o + \bar{S}_u + \bar{S}_o$, Fig.3.2.1), given H over \bar{S} , H over S can be computed by (4.2.5) as

$$H(\mathbf{p}) = \pi\mu(\mathbf{p}) - \int_S \log_i |\mathbf{q} - \mathbf{p}| \mu(\mathbf{q}) d\mathbf{q}, \quad \mathbf{p} \in S. \quad (5.2.1)$$

on obtaining the μ over S_L as solution of (4.2.3)

$$H(\mathbf{P}_k) = - \int_{S_L} \log_i |\mathbf{q} - \mathbf{P}_k| \mu(\mathbf{q}) d\mathbf{q}, \quad \mathbf{P}_k \in \bar{S}_u, \quad (5.2.2)$$

and that over \bar{S}_o obtained directly from (4.2.4)

$$\pi\mu(\mathbf{p}) = H(\mathbf{p}) + \int_{S_L} \log_i |\mathbf{q} - \mathbf{p}| \mu(\mathbf{q}) d\mathbf{q}, \quad \mathbf{p} \in \bar{S}_o, \quad (5.2.3)$$

when the μ over S_L is known as solution of (5.2.2).

To solve the equations (5.2.2) and (5.2.3) and to compute H over S by (5.2.1) numerically, let us divide a large finite datum line \bar{S} into N equal subintervals ΔS_k , $k=1,2,\dots,N$ and assign the input data H_k at the nodal point P_k of ΔS_k , $k=1,2,\dots,N$ with

n of them over \bar{S}_0 that lies directly over S_L with end-points common to them. Let us now divide S_L into n piecewise straight subintervals $\Delta S_j, j=1,2,\dots,n$, such that the projection of ΔS_j over \bar{S} coincides with $\Delta \bar{S}_j, j=1,2,\dots,n$ of \bar{S}_0 .

Now assuming, as before, μ is constant over a subinterval, the equation (5.2.2) can be written as

$$H_k = -\sum_{j=1}^n \mu_j \int_{\Delta S_j} \log_i |\mathbf{q} - \mathbf{P}_k| dq, \quad k=1,2,\dots,n, \quad (5.2.4)$$

where H_k is the input data over \bar{S}_0 at the nodal point \mathbf{P}_k of $\Delta \bar{S}_k$, μ_j is the constant value of μ over the j^{th} subinterval ΔS_j of S_L . The equations (5.2.4) represent a system of n simultaneous linear algebraic equations in n unknown μ_j over S_L . It has already been mentioned earlier that the equation (5.2.2) formulates an ill-posed problem in potential theory, a small perturbation in H_k creates a wide oscillation in solution. However, a stable approximate μ_j over S_L can be obtained by successive correction of an initial guess described in subsection 5.4.

On obtaining the μ_j over S_L , the $\mu(\mathbf{q}_k)$ over \bar{S}_0 can be obtained directly from the discretised version of (5.2.3) written as

$$\pi\mu(\mathbf{q}_k) = H(\mathbf{q}_k) + \sum_{j=1}^n \mu_j \int_{\Delta S_j} \log_i |\mathbf{q} - \mathbf{q}_k| dq, \quad \mathbf{q}_k \in \bar{S}_0. \quad (5.2.5)$$

On finding the μ_j over $S(= \bar{S}_0 + S_L + \bar{S}_0)$, the down-continued field $H(\mathbf{z}_k), \mathbf{z}_k \in S$ can be computed by the discretised version of (5.2.1) written as

$$H(\mathbf{z}_k) = \pi\mu(\mathbf{z}_k) - \sum_{j=1}^n \mu_j \int_{\Delta S_j} \log_i |\mathbf{q} - \mathbf{z}_k| dq, \quad \mathbf{z}_k \in S. \quad (5.2.6)$$

5.3 Evaluation of the Integrals over a Line Element

It is evident from the previous subsections that numerical solutions of the boundary integral equations in up-continuation of a potential field from boundary data, solution of an ill-posed problem in down continuation of a field from the datum line and reproduction of a field in the upper half-space domain involve evaluation of certain integrals over the subelement of the boundary.

The integrals involved are

$$I_p = \int_{\Delta S_j} \log|\mathbf{q} - \mathbf{P}| d\mathbf{q} \quad (5.3.1)$$

and $J_p = \int_{\Delta S_j} \log'_i |\mathbf{q} - \mathbf{P}| d\mathbf{q} \quad (5.3.2)$

for the field point P lying outside or in the line element ΔS_j .

For P coinciding with the nodal point \mathbf{q}_k of a subelement ΔS_k , the simple layer integral (5.3.1) is denoted by a_{kj} and the double layer integral (5.3.2) is denoted by b_{kj} in the subsection 5.1. Hence, under this setup, we express (5.3.1) and (5.3.2) as

$$a_{kj} = \int_{\Delta S_j} \log|\mathbf{q} - \mathbf{q}_k| d\mathbf{q} \quad (5.3.3)$$

and $b_{kj} = \int_{\Delta S_j} \log'_i |\mathbf{q} - \mathbf{q}_k| d\mathbf{q} \quad (5.3.4)$

respectively.

For P lying outside ΔS_j , the integrals are regular and these can be evaluated analytically or approximations to them by Centroid rule (Hess and Smith 1967) may suffice the purpose. For P lying on ΔS_j , the integrals are singular and these are to be evaluated analytically.

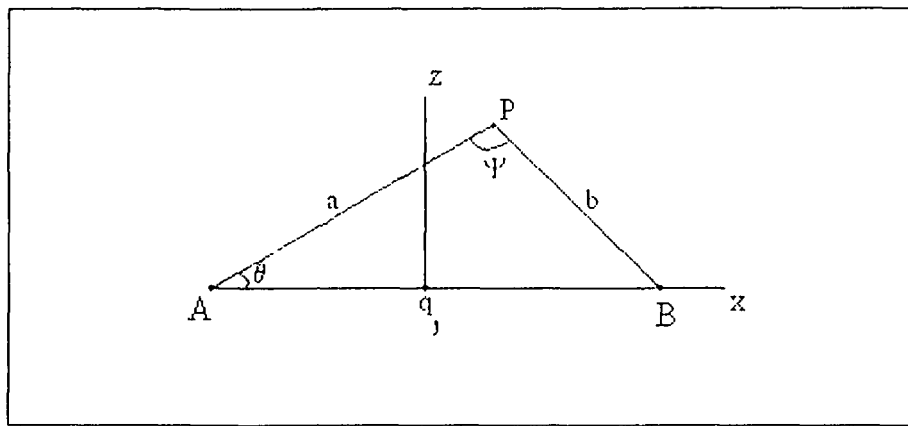
It is to be noted here that in downward continuation of a potential field from the datum line \bar{S} , the equation (5.2.2) formulating the problem involves evaluation of the double layer integral (5.3.4) over the subelement ΔS_j of the continuation boundary S_L , the field point P lying on the central part \bar{S}_u of \bar{S} . Since the equation (5.2.2) formulates an ill-posed problem, the integral (5.3.4) is to be evaluated analytically for a better stable approximate solution of the equation.

An extensive discussion on the above integrals has been carried out by Jaswon and Symm (1977) for an arbitrary alignment of ΔS_j . Keeping in view the geophysical problems in which the field point P lies on and above a half-space boundary S , the coordinates of P are expressed in a new reference frame xoz with its origin at the centroid q_j of ΔS_j , x -axis coinciding with ΔS_j and z -axis pointing towards the upper half-space domain B_j above S as shown in Fig. 5.3.1. This brings a good simplification in the approach for implementation of the simple layer integral (5.3.1) presented by Jaswon and Symm (1977). Under this transformation, the double layer integral (5.3.2) also comes up in a simple form for its easy implementation on a computer.

5.3.1 Analytical Evaluation of Simple Layer Integral

Let a straight line segment ΔB of length h represent the subelement ΔS_1 in a local xoz reference frame with its origin at the nodal (centroid) point q_1 of ΔS_1 , x -axis coinciding with ΔS_1 and z -axis pointing towards the upper half-space domain above ΔS_1 as shown in Fig. 5.3.1.

Fig. 5.3.1: Evaluation of simple and double layer integrals over a subelement AB



Let the field point P in this frame be defined by (X, Z) , the end-points A, B defined by $(-h/2, 0)$ and $(h/2, 0)$ respectively, ΔB subtends an angle Ψ at P and PB subtends an angle θ at A . For PA and PB denoted by a and b respectively, following Jaswon and Symm (1977), we express the integral (5.3.1) as

$$I_p = \int_{\Delta S_1} \log |\mathbf{q} - \mathbf{P}| dq$$

$$= a \cos \theta (\log a - \log b) + h (\log b - 1) + a \psi \sin \theta \quad (5.3.5)$$

For P representing the nodal point q_k of a subelement ΔS_k of S , the expression for a_{kj} of (5.3.3) also stands as

$$a_{kj} = a \cos \theta (\log a - \log b) + h (\log b - 1) + a \psi \sin \theta \quad (5.3.6)$$

Special Case I: Regular Integral

When P, A and B are collinear, $\theta=0$ or π and therefore $\sin\theta=0$ and $\cos\theta=1$ or -1 respectively.

(i) when $\theta = 0$, i.e., when P is at the right side of the subinterval $\Delta S_j (=AB)$.

$$a_{kj} = a(\log a - 1) - b(\log b - 1) \quad (5.3.7)$$

(ii) when $\theta = \pi$, i.e., when P is at the left side of the subinterval $\Delta S_j (=AB)$

$$a_{kj} = a(1 - \log a) - b(1 - \log b) \quad (5.3.8)$$

Special Case II: Singular Integral

When the field point P coincides with the nodal (centroid) point of ΔS_j , the integral is singular. In this case, considering $\theta=0$ and $b=0$, the contribution from the left half of

ΔS_j at q_j , by (5.3.8), is $\frac{h}{2} \left(\log \frac{h}{2} - 1 \right)$. The same contribution appears at q_j from the

other half of the subinterval placed at right side of q_j . Hence, the singular integral

$$\begin{aligned} a_{jj} = a_{kk} &= 2 \left[\frac{h}{2} \left(\log \frac{h}{2} - 1 \right) \right] \\ &= h \left(\log \frac{h}{2} - 1 \right) \end{aligned} \quad (5.3.9)$$

5.3.2 Analytical Evaluation of Double Layer Integral

To evaluate the double layer integral (5.3.2) over the j^{th} subinterval ΔS_j , we fix up a local reference frame xoz , its origin coinciding with the nodal point q_j of ΔS_j , x -axis coinciding with ΔS_j and z -axis pointing upward in the upper half-space domain B_j above ΔS_j as shown in Fig. 5.3.1. For ΔS_j of length h , the coordinates of the end points

of ΔS_j are defined by $A(-h/2, 0)$ and $B(h/2, 0)$. Let (\bar{X}, \bar{Z}) define the coordinates of the field point \mathbf{P} and (x, z) define the coordinates q in this frame.

$$\begin{aligned} J_p &= \int_{\Delta S_k} \log_i |\mathbf{q} - \mathbf{P}| dq \\ &= \int_{x=-h/2}^{x=h/2} \bar{Z} [(x - \bar{X})^2 + (z - \bar{Z})^2]^{-1/2} dx \\ &= \tan^{-1} \frac{x - \bar{X}}{\bar{Z}} \Bigg|_{x=-h/2}^{x=h/2} \end{aligned} \quad (5.3.10)$$

For \mathbf{P} coinciding with the nodal point q_k of the subinterval ΔS_k , the J_p in (5.3.10) stands for b_{kj} of (5.3.4) and hence,

$$b_{kj} = \tan^{-1} \frac{x - \bar{X}}{\bar{Z}} \Bigg|_{x=-h/2}^{x=h/2}, \quad j \neq k. \quad (5.3.11)$$

For q_k and q_j defined by (X_k, Z_k) and (x_j, z_j) respectively in the original reference frame XOZ , we find

$$\begin{cases} \bar{x} = l_1 (X_k - x_j) + m_1 (Z_k - z_j) \\ \bar{z} = l_2 (X_k - x_j) + m_2 (Z_k - z_j) \end{cases} \quad (5.3.12)$$

for (l_1, m_1) and (l_2, m_2) defining the direction cosines of x -axis and z -axis respectively of local frame in the original reference frame. For x -axis of the local frame making an angle θ with the x -axis of the original frame, we find, $l_1 = \cos \theta$, $m_1 = \sin \theta$, $l_2 = -\sin \theta$, and $m_2 = \cos \theta$.

Special Case : Evaluation of Singular Integral

For the field point \mathbf{P} or the nodal point q_k coinciding with q_j , the integral becomes singular. In this case, on expansion of the integrand, we find

$$b_{kk} = \int_{\Delta S_k} \log_i |\mathbf{q} - \mathbf{q}_k| dq$$

$$\begin{aligned}
 &= \iint_{\Delta S_k} |\mathbf{q} - \mathbf{q}_k|^{-2} (\mathbf{q} - \mathbf{q}_k) \cdot \hat{\mathbf{n}}_i \, d\mathbf{q} \\
 &= 0,
 \end{aligned} \tag{5.3.13}$$

for $\mathbf{q} \neq \mathbf{q}_k$, the outward normal $\hat{\mathbf{n}}_i$ to ΔS_k at \mathbf{q}_k being normal to $(\mathbf{q} - \mathbf{q}_k)$ and for $\mathbf{q} = \mathbf{q}_k$, the integral having a singularity at the isolated point \mathbf{q}_k , a set of measure zero.

5.4 Solution of equations

For computation of the solution of equations, three solution techniques are used:

- (i) Gauss-Seidal iterative method used for diagonal dominant system for solving boundary integral equations formulating up-continuation problem
- (ii) Gauss Elimination method used for diagonal having non-zero element for solving boundary integral equations formulating up-continuation problem
- (iii) Successive correction of initial guess solution used for solving integral equations formulating ill-posed problem

5.4.1 Upward Continuation: Solution of Boundary Integral Equation

(i) Choice of numerical methods of solution

In simple layer formulation of up-continuation problem we come across (5.1.4), the digitized version of the boundary equation (5.1.2)

$$H_k = - \sum_{l=1}^n \iint_{\Delta S_l} \log |\mathbf{q} - \mathbf{q}_k| \sigma(\mathbf{q}) \, d\mathbf{q} = - \sum_{l=1}^n a_{kl} \sigma_l, \quad k = 1, 2, \dots, n \tag{5.4.1}$$

for its solution in n unknown σ_j where the analytical expressions for a_{kj} and a_{kk} are given by (5.3.6) and (5.3.9) respectively. It is evident from the expressions of a_{kj} and

a_{kk} that $a_{kk} \neq 0$ and (5.4.1) does not form a diagonal dominant system. In such a case, Gauss elimination method provides the suitable numerical technique for its solution.

The same is true for numerical solution of Green's boundary equation (5.1.12) in H_1 , given by (5.1.13) as

$$\sum_{j=1}^n a_{kj} H_j = D_k, \quad k=1, 2, 3, \dots, n. \quad (5.4.2)$$

In double layer formulation of the up-continuation problem, we come across the boundary equation (5.1.8) in μ_j

$$\begin{aligned} H_k &= \pi\mu_k - \sum_{j=1}^n \mu_j \int_{\Lambda S_j} \log_i |\mathbf{q} - \mathbf{q}_k| d\mathbf{q}, \\ &= \pi\mu_k - \sum_{j=1}^n b_{kj} \mu_j, \quad k = 1, 2, \dots, n, \end{aligned} \quad (5.4.3)$$

where $b_{kk}=0$, by (5.3.13).

We know,

$$\sum_{j=1}^n b_{kj} = \sum_{j=1}^n \int_{\Lambda S_j} \log_i |\mathbf{q} - \mathbf{q}_k| d\mathbf{q} = \int_S \log_i |\mathbf{q} - \mathbf{q}_k| d\mathbf{q}. \quad (5.4.4)$$

For B , enclosed by $\partial B = S + S_u$ (Fig. 2.4.1), where S_u is a semicircle of radius R , Gauss integral in 2-D over ∂B is

$$\int_{\partial B} \log_i |\mathbf{q} - \mathbf{q}_k| d\mathbf{q} = \int_S \log_i |\mathbf{q} - \mathbf{q}_k| d\mathbf{q} + \int_{S_u} \log_i |\mathbf{q} - \mathbf{q}_k| d\mathbf{q} = -\pi.$$

As $R \rightarrow \infty$, the integral over S_u is $-\pi$. Hence, the integral over the half-space boundary S is

$$\int_S \log_i |\mathbf{q} - \mathbf{q}_k| d\mathbf{q} = \sum_{j=1}^n b_{kj} = 0 \quad (5.4.5)$$

It is now evident that the system of equations in μ_i in (5.4.3) forms a highly diagonal dominant system for the presence of $\pi\delta_{kk}$, $k=1,2,\dots,n$, in it. As such, the equations (5.4.3) can be best solved by Gauss-Seidal iterative method yielding quick convergence of solution.

(ii) Gauss-Seidal iterative method of solution of equations:

In this method, the zeroth order approximation to solution x_i is assumed to be zero and the m^{th} order approximate solution is given by

$$x_j^{(m)} = [H_k - \{ \sum_{j=1}^{k-1} a_{kj}x_j^{(m-1)} + \sum_{j=k+1}^n a_{kj}x_j^{(m-1)} \}] / (\pi + a_{kk}), k=1,2,\dots,n, \tag{5.4.6}$$

where $x_j^{(m-1)}$ stands for $(m-1)^{\text{th}}$ order approximate value of x_j . The iterative process of obtaining of the solution terminates at the p th iterative step, if for a pre-assigned small value ϵ

$$|x_j^{(m)} - x_j^{(m-1)}| < \epsilon, j=1,2,\dots,n, \tag{5.4.7}$$

The ϵ in general is taken as 0.000001 that yields the solution correct upto 5 decimal places.

5.4.2 Downward Continuation: Solution of Ill-posed Problems

It has been shown that for H without error specified over \bar{S} , the equation

$$H(\mathbf{P}) = - \int_{S_i} \log_i |\mathbf{q} - \mathbf{P}| \mu(\mathbf{q}) d\mathbf{q}, \quad \mathbf{P} \in \bar{S}_u, \tag{5.4.8}$$

has a unique solution (Appendix I). However, as already mentioned earlier, the solution is highly sensitive to error in input data. A solution, built by successive

correction of the initial choice is expected to provide a stable approximate solution of the equation. A numerical procedure to construct a stable approximate solution is described below.

The equation (5.4.8) can be rewritten in a general form

$$H(\mathbf{P}) = \int_{S_L} K(\mathbf{P}, \mathbf{q}) \mu(\mathbf{q}) d\mathbf{q}, \quad \mathbf{P} \in \bar{S}_u, \quad (5.4.9)$$

where the kernel $K(\mathbf{P}, \mathbf{q})$ is $-\log |\mathbf{q} - \mathbf{P}|$. To make a numerical approach to solve the equation (5.4.9), let us divide S_L into n piecewise straight sub-intervals and project them on \bar{S}_u such that \bar{S}_u is divided into n equal sub-intervals. The input data $H_k (= H(\mathbf{P}_k), \mathbf{P}_k \in \bar{S}_u)$ are then specified at the n nodal points (centroid) of the subintervals over \bar{S}_u .

As the approximate solution μ reproduces a field that deviates from the original data H_i , let us find a μ such that the sum E of the squared deviations with an additional term λ times the integral of $\mu^2(\mathbf{q})$ over S_L , expressed as

$$E = \sum_{i=1}^n \left[H_i - \int_{S_L} K(\mathbf{P}_i, \mathbf{q}) \mu(\mathbf{q}) d\mathbf{q} \right]^2 + \lambda \int_{S_L} \mu^2(\mathbf{q}) d\mathbf{q}, \quad (5.4.10)$$

is a minimum. The μ under question can be obtained from the equation $\partial E / \partial \mu = 0$.

On discretisation, this equation appears in a matrix form with λds_k as an additional term at the diagonal. This enhances the diagonal of the resultant matrix and thereby makes the inverse always computable. On discretisation of the integrals in (5.4.10) and carrying out differentiation with respect to μ_k , we arrive at the equation

$$\frac{\partial E}{\partial \mu_k} = \sum_{i=1}^n -2 \left[H_i - \sum_{j=1}^n \int_{S_L} K(\mathbf{P}_i, \mathbf{q}) \mu_j d\mathbf{q} \right] \int_{S_L} K(\mathbf{P}_i, \mathbf{q}) d\mathbf{q} + 2\lambda \int_{S_L} \mu_k d\mathbf{q} = 0, \quad k=1, 2, \dots, n \quad (5.4.11)$$

in μ_j , that produces the minimum of E , μ_j being the value of μ treated constant over the j^{th} subinterval of S_L , and \int_k denotes the integral over the subinterval ΔS_k .

Using the notation

$$a_{ij} = \int_i K(\mathbf{p}_i, \mathbf{q}) dq, \quad \mathbf{p}_i \in \bar{S}_v,$$

the equations (5.4.11) can be written as

$$\sum_{j=1}^n \left(\sum_{i=1}^n a_{ij} a_{ik} \right) \mu_j + \lambda \mu_k dS_k = \sum_{i=1}^n H_i a_{ik}, k = 1, 2, \dots, n, \quad (5.4.12)$$

where $dS_k = \int_k dq$.

For synthetic input data the equations (5.4.12) with $\lambda=0$ lead to a reasonable solution for a shallow depth of S_L . For the input data with error, say within 1% of the absolute value of true H_i , it is our experience that the traditional Marquardt-Levenberg formulation (Marquardt 1963, Bard 1970, Himmelblau 1972) that uses scalar times ad-hoc diagonal matrix $[\lambda]_n$ produces results within 5% error to a shallow depth (less than 2h units), h defining the uniform spacing of data over \bar{S} . The convergence however becomes slow as depth increases. The choice of λ_j is quite critical to the convergence rate for the algorithm. An iterative update for λ_j of the form

$$[D_{i+1}]_{jj} = [D_i]_{jj} / a_j = [(\lambda dS_j)_i]_{jj} / a_j, \quad (5.4.13)$$

$$a_j = 1 - [\bar{g}_i]_j / [\bar{g}_{i+1} - \bar{g}_i]_j, \quad (5.4.14)$$

obtained following Mendal (1983), solves the equations (5.4.12) satisfactorily. Here, $(i+1)$ denotes the current operation of estimation of the vector D_j for

$$[D_i]_{jj} = [(\lambda dS_j)_i]_{jj}, \quad (5.4.15)$$

$$[\bar{g}_i]_j = \left[\sum_{k=1}^n H_k a_{kj} \right]_j, \quad (5.4.16)$$

$$[\bar{g}_{i+1}]_j = \left[\sum_{k=1}^n \Delta H_k a_{kj} \right]_j, \quad (5.4.17)$$

$$\text{where } \Delta H_k = H_k - \int_{S_i} K(\mathbf{P}_k, \mathbf{q}) \bar{\mu}_i^{(i)} d\mathbf{q}; \quad (5.4.18)$$

$\bar{\mu}_i^{(i)}$ being the estimation of μ_j in the i^{th} correction. The estimation of $[D_i]_j$ is due to Mendal (1983) and it has been suggested that the a_j of (5.4.14) to be kept in the bounds $0.1 \leq a_j \leq 10$.

To find the initial choice of μ_j , we observe that for the lower boundary S_L coinciding with the datum line \bar{S} , the μ_j of (5.4.12) assumes the value H_j/π , by (4.2.7). This provides a good choice for the initial approximation to μ_j of equation (5.4.12). Further, $\lambda = \pi$ in (5.4.15) also provides a good initial estimation of D_i . An approximate stable solution μ_j can be obtained in the form

$$\mu_j = \sum_{i=0}^m \mu_j^{(i)}, \quad j=1,2,\dots,n, \quad (5.4.19)$$

where $\mu_j^{(0)} = H_j/\pi$ and $\mu_j^{(i)}$ is the correction to μ_j at the i^{th} iterative step, the details of which is given below:

Considering the initial choice of μ_j as $\mu_j^{(0)} = H_j/\pi$, the deviations $\Delta H_k, k=1,2,\dots,n$ are computed by (5.4.18). In the next step, $[D_i]_j$ of (5.4.15) is initialized by putting $\lambda = \pi$ and $[D_{i+1}]_j$ of (5.4.13) is computed on finding $[\bar{g}_i]_j$ and $[\bar{g}_{i+1}]_j$ by (5.4.16) and (5.4.17) respectively. Subsequently, H_k of (5.4.12) are replaced by ΔH_k and the equations are

solved for μ_j to be treated as $\mu_j^{(1)}$ of (5.4.19). On finding the first order approximation of μ_j as $\bar{\mu}_j^{(1)} = \mu_j^{(0)} + \mu_j^{(1)}$, the ΔH_k are computed by (5.4.18) for finding the next correction term $\mu_j^{(2)}$ using the iterative process as described in the case of $\mu_j^{(1)}$.

On finding the m^{th} order estimation of μ_j as a sum of the correction terms $\mu_j^{(i)}$, $i=1,2,\dots,m$, the solution μ_j is used to see that the mean squared deviation, i.e., the mean squared error (MSE) satisfies the termination condition

$$\sum_{k=1}^n (\Delta H_k)^2 / n \leq \xi, \quad (5.4.20)$$

ξ defining the square of assumed level of error in input data specified over \bar{S}_n . In a field problem, this information is usually made available in the field book.

It is evident from the above discussion that $\Delta H_k^{(i)}$, the deviation at $\Delta \bar{S}_k$ at the i^{th} operation, gradually decreases in magnitude in general as i increases. Consequently, the $\mu_j^{(i)}$ of (5.4.19) approaches zero as i increases yielding a stable convergent summation series for μ_j .

CHAPTER VI

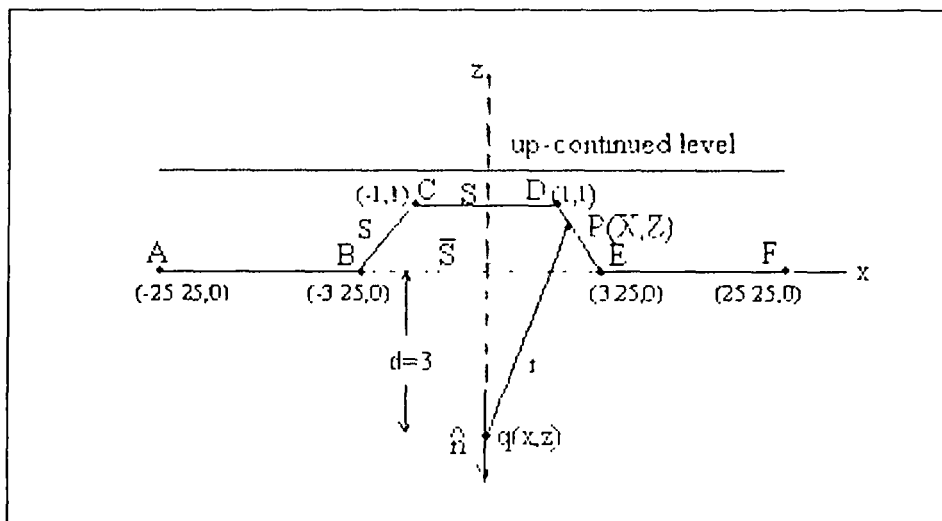
ANALYSIS OF MODEL DATA

6.1 Up-continuation of a Potential Field from Boundary data

6.1.1 The boundary and the Gravity-Magnetic Data over it

Let a vertically polarised unit logarithmic mass m be placed at point $q(x,z)$ at a depth d below the datum line \bar{S} defined by $z=0$ in a xoz reference frame with z -axis upward. Let us now construct an irregular boundary S by the line segments joining the points $(-25.25,0)$, $(-3.25,0)$, $(-1,1)$, $(1,1)$, $(3.25,0)$ and $(25.25,0)$. The boundary S so obtained is divided into $N=100$ unequal subintervals ΔS_j , each of length $h \cong 0.5$ and their nodal points are noted. The boundary so constructed is shown in Fig.6.1.1

Fig. 6.1.1: The gravity-magnetic responses due to the polarised subsurface mass m are specified over S for their up-continuation to a higher level



The gravity response Δg at a nodal point $P(X,Z)$ of S due to the mass m placed at $q(x,z)$ is given by the formula

$$H(P)=\Delta g(X,Z)=Gm \frac{Z-z}{(X-x)^2+(Z-z)^2} \quad (6.1.1)$$

Assuming the universal gravitational constant $G=1$ the Δg values are computed by (6.1.1) for $m=1$ at the nodal points of the subelements. The boundary data so obtained over S , are shown at some representative points in column 3 of Table 6.1.1. Subsequently, the downward vertical component magnetic field T_z at a nodal point $P(X,Z)$ is computed by the formula

$$H(P) = T_z(X,Z) = \mu \left[\frac{2(z-Z)^{-2}}{[(x-X)^2+(z-Z)^2]^2} - \frac{1}{(x-X)^2+(z-Z)^2} \right] \quad (6.1.2)$$

with $\mu=1$ and these are shown at some representative points in column 4 of Table 6.1.1, μ defining the vertically downward doublet placed at q .

Table 6.1.1: Gravity and magnetic responses over the boundary S

| Nodal point | | Gravity field | Magnetic field |
|-------------|-------|---------------|----------------|
| x | z | Δg | T_z |
| -25.0 | 0.0 | 0.0047 | -0.0015 |
| -23.0 | 0.0 | 0.0056 | -0.0018 |
| -21.0 | 0.0 | 0.0067 | -0.0021 |
| -19.0 | 0.0 | 0.0081 | -0.0026 |
| -17.0 | 0.0 | 0.0101 | -0.0032 |
| -15.0 | 0.0 | 0.0128 | -0.0039 |
| -13.0 | 0.0 | 0.0169 | -0.0051 |
| -11.0 | 0.0 | 0.0231 | -0.0066 |
| -9.0 | 0.0 | 0.0333 | -0.0089 |
| -7.0 | 0.0 | 0.0517 | -0.0119 |
| -5.0 | 0.0 | 0.0882 | -0.0138 |
| -3.0 | 0.125 | 0.1682 | 0.0028 |
| -0.75 | 1.0 | 0.2415 | 0.0563 |
| 0.75 | 1.0 | 0.2415 | 0.0563 |
| 3.0 | 0.125 | 0.1682 | 0.0028 |
| 5.0 | 0.0 | 0.0882 | -0.0138 |
| 7.0 | 0.0 | 0.0517 | -0.0119 |
| 9.0 | 0.0 | 0.0333 | -0.0089 |
| 11.0 | 0.0 | 0.0231 | -0.0066 |
| 13.0 | 0.0 | 0.0169 | -0.0051 |
| 15.0 | 0.0 | 0.0128 | -0.0039 |
| 17.0 | 0.0 | 0.0101 | -0.0032 |
| 19.0 | 0.0 | 0.0081 | -0.0026 |
| 21.0 | 0.0 | 0.0067 | -0.0021 |
| 23.0 | 0.0 | 0.0056 | -0.0018 |
| 25.0 | 0.0 | 0.0047 | -0.0015 |

[Vertically polarised unit logarithmic point mass m is placed at a depth $d=3$ units below the datum line \bar{S} defined by $z=0$ in a xoz frame with z -axis upward]

6.1.2 Up-continuation as Simple Layer Potential

Gravity or a component magnetostatic field H is a harmonic function in the upper half-space domain B_i . Both of them vanish at infinity with asymptotic behavior $H = O(r^{-n})$, $n \geq 1$, $r \rightarrow \infty$. As such, following (4.1.1), these fields can be reproduced in B_i from respective boundary data as potentials due to simple layer boundary density σ as

$$H(\mathbf{P}) = - \int_S \log|\mathbf{q} - \mathbf{P}| \sigma(\mathbf{q}) \, d\mathbf{q}, \quad \mathbf{P} \in B \quad (6.1.3)$$

It has been shown in subsection 4.1.1 that the σ in (6.1.3) can be obtained as a unique solution of the boundary equation (4.1.2), i.e.,

$$H(\mathbf{p}) = - \int_S \log|\mathbf{q} - \mathbf{p}| \sigma(\mathbf{q}) \, d\mathbf{q}, \quad \mathbf{p} \in S. \quad (6.1.4)$$

Dividing the boundary S into piecewise straight subelements ΔS_j and assuming σ is constant over a subelement, the formula (6.1.3) can be expressed in the form of (5.1.5) as

$$\tilde{H}(\mathbf{P}) = \sum_{j=1}^n -\sigma_j \int_{\Delta S_j} \log|\mathbf{q} - \mathbf{P}| \, d\mathbf{q}, \quad (6.1.5)$$

where, $\tilde{H}(\mathbf{P})$ is the approximate value of H at \mathbf{P} and the equation (6.1.4) can be written as

$$H(\mathbf{q}_k) = \sum_{j=1}^n -\sigma_j \int_{\Delta S_j} \log|\mathbf{q} - \mathbf{q}_k| \, d\mathbf{q}, \quad k=1,2,3,\dots,n,$$

$$\text{or,} \quad b_k = \sum_{j=1}^n -a_{kj} \sigma_j, \quad k = 1,2,3,\dots,n, \quad (6.1.6)$$

where,

$$a_{kj} = \int_{\Delta S_j} \log |\mathbf{q} - \mathbf{q}_k| d\mathbf{q} \quad (6.1.7)$$

and $b_k = H(\mathbf{q}_k)$. (6.1.8)

The analytical expression of (6.1.7), following (5.3.6), is given by

$$\begin{aligned} a_{kj} &= \int_{\Delta S_j} \log |\mathbf{q} - \mathbf{q}_k| d\mathbf{q}, \quad \mathbf{q}_k \in \Delta S_k, \\ &= \{a \cos \theta (\log a - \log b) + h (\log b - 1) + a \psi \sin \theta\}, \end{aligned} \quad (6.1.9)$$

where a , b , h , θ and ψ are explained in Fig. 5.3.1. For the end points of the subelement are collinear with \mathbf{q}_k , we find by (5.3.7) and (5.3.8)

$$a_{kj} = a(\log a - 1) - b(\log b - 1) \quad (6.1.10)$$

for \mathbf{q}_k lying at the right side of ΔS_j

$$a_{kj} = a(1 - \log a) - b(1 - \log b) \quad (6.1.11)$$

for \mathbf{q}_k lying at the left of ΔS_j

For \mathbf{q}_j coinciding with the nodal point of \mathbf{q}_k of ΔS_k , i.e., for $j=k$,

$$a_{kk} = h \left(\log \frac{h}{2} - 1 \right) \quad (6.1.12)$$

by (5.3.9).

On evaluation of the co-efficients a_{kj} , the b_k are to be computed by (6.1.1) for the gravimetric case and by (6.1.2) for the magnetostatic case. Then the $n(=100)$ equations (6.1.6) can be solved for σ_j . Since the equations do not form a diagonal dominant system, these are to be solved by Gauss Elimination method mentioned in subsection 5.4.1. On finding the σ_j values over S , the field at a point $P(X,Z)$ above S can be computed by (6.1.5), the discretised version of (6.1.3).

(i) Gravimetric case

For the boundary S divided into $n=100$ subelements ΔS_j , the Δg values at the n nodal points $P_k(X_k, Z_k)$ of ΔS_k , $k=1, 2, \dots, n$, are computed by formula (6.1.1) with $G=1$, $m=1$, $Z=Z_k$, $x=0$ and $z=-3$ and the coefficients a_{kj} are evaluated analytically for all positions of k and j over S as described in (6.1.9), (6.1.10), (6.1.11) and (6.1.12). Subsequently, the equations (6.1.6) are solved by Gauss Elimination method. The σ_j so obtained are shown at some representative points in column 3 of Table 6.1.2.

The line integral of σ is found to be -0.01547 which by (4.1.3) is expected to be zero. Since the σ_j are negative at the outer sides of S , as evident in Table 6.1.2, it is expected that the line integral of numerical σ will attain the zero value on further extension of the boundary. On finding the σ_j over S , the up-continued Δg values at level $z=1.5$ are computed by formula (6.1.5) on evaluating the integrals by the analytical means. The values so obtained are shown in column 3 of Table 6.1.3 along with the true values in column 2 for comparison.

It is evident from Table 6.1.3 that the up-continued values of Δg obtained by the discretised version of (6.1.3) agree with the true values to a good degree of accuracy but the end values of the reproduced field contain large errors in them and the error goes on decreasing at the central part of the continued level. This is due to the fact that the datum was considered finite in length but theoretically the datum line extends from $-\infty$ to $+\infty$.

Table 6.1.2: Simple and double layer boundary densities obtained from boundary gravity data

| Boundary point | | Simple layer | Double layer | Green's Sigma |
|----------------|-------|--------------|--------------|---------------|
| x | z | σ_1 | μ_j | H' |
| -25.0 | 0.0 | -0.0062 | 0.0015 | 0.0209 |
| -23.0 | 0.0 | -0.0018 | 0.0018 | 0.0060 |
| -21.0 | 0.0 | -0.0015 | 0.0022 | 0.0051 |
| -19.0 | 0.0 | -0.0015 | 0.0026 | 0.0050 |
| -17.0 | 0.0 | -0.0015 | 0.0033 | 0.0052 |
| -15.0 | 0.0 | -0.0017 | 0.0042 | 0.0058 |
| -13.0 | 0.0 | -0.0020 | 0.0055 | 0.0067 |
| -11.0 | 0.0 | -0.0024 | 0.0075 | 0.0082 |
| -9.0 | 0.0 | -0.0030 | 0.0108 | 0.0104 |
| -7.0 | 0.0 | -0.0038 | 0.0169 | 0.0134 |
| -5.0 | 0.0 | -0.0038 | 0.0289 | 0.0153 |
| -3.0 | 0.125 | 0.0060 | 0.0596 | -0.0241 |
| -0.75 | 1.0 | 0.0141 | 0.0889 | -0.0541 |
| 0.75 | 1.0 | 0.0141 | 0.0889 | -0.0541 |
| 3.0 | 0.125 | 0.0060 | 0.0596 | -0.0241 |
| 5.0 | 0.0 | -0.0038 | 0.0289 | 0.0153 |
| 7.0 | 0.0 | -0.0038 | 0.0169 | 0.0134 |
| 9.0 | 0.0 | -0.0030 | 0.0108 | 0.0104 |
| 11.0 | 0.0 | -0.0024 | 0.0075 | 0.0082 |
| 13.0 | 0.0 | -0.0020 | 0.0055 | 0.0067 |
| 15.0 | 0.0 | -0.0017 | 0.0042 | 0.0058 |
| 17.0 | 0.0 | -0.0015 | 0.0033 | 0.0052 |
| 19.0 | 0.0 | -0.0015 | 0.0026 | 0.0050 |
| 21.0 | 0.0 | -0.0015 | 0.0022 | 0.0051 |
| 23.0 | 0.0 | -0.0018 | 0.0018 | 0.0060 |
| 25.0 | 0.0 | -0.0062 | 0.0015 | 0.0209 |

[The boundary S with a central high extends at both ends along the datum line \bar{S} defined by $z=0$]

Table 6.1.3: Up-continuation of gravity field at level $z=1.5$ from boundary data

| x | True field $\Delta g[t]$ | Field as potential of | | By use of |
|--------|-----------------------------|----------------------------|---------------------------|--------------------------------|
| | | Smpl lyr. $\Delta g[S]$ | Dbl lyr. $\Delta g[D]$ | Green's frml. $\Delta g[G]$ |
| -10.25 | 0.0359 | 0.0381 | 0.0346 | 0.0511 |
| -9.25 | 0.0425 | 0.0446 | 0.0410 | 0.0569 |
| -8.25 | 0.0510 | 0.0530 | 0.0490 | 0.0643 |
| -7.25 | 0.0618 | 0.0638 | 0.0591 | 0.0740 |
| -6.25 | 0.0759 | 0.0778 | 0.0721 | 0.0866 |
| -5.25 | 0.0941 | 0.0960 | 0.0884 | 0.1027 |
| -4.25 | 0.1175 | 0.1193 | 0.1079 | 0.1229 |
| -3.25 | 0.1460 | 0.1477 | 0.1296 | 0.1465 |
| -2.25 | 0.1778 | 0.1792 | 0.1541 | 0.1732 |
| -1.25 | 0.2063 | 0.2076 | 0.1862 | 0.2023 |
| -0.25 | 0.2215 | 0.2224 | 0.2196 | 0.2256 |
| 0.25 | 0.2215 | 0.2224 | 0.2196 | 0.2257 |
| 1.25 | 0.2063 | 0.2076 | 0.1862 | 0.2025 |
| 2.25 | 0.1778 | 0.1792 | 0.1541 | 0.1735 |
| 3.25 | 0.1460 | 0.1477 | 0.1296 | 0.1470 |
| 4.25 | 0.1175 | 0.1193 | 0.1079 | 0.1234 |
| 5.25 | 0.0941 | 0.0960 | 0.0884 | 0.1033 |
| 6.25 | 0.0759 | 0.0778 | 0.0721 | 0.0872 |
| 7.25 | 0.0618 | 0.0638 | 0.0591 | 0.0747 |
| 8.25 | 0.0510 | 0.0530 | 0.0490 | 0.0650 |
| 9.25 | 0.0425 | 0.0446 | 0.0410 | 0.0576 |
| 10.25 | 0.0359 | 0.0381 | 0.0346 | 0.0517 |

$[\Delta g[t] \text{ \& } \Delta g[S], \Delta g[D], \Delta g[G]$ are the true & reproduced gravity values by simple layer boundary density, double layer boundary density and Green's formula respectively]

(ii) Magnetostatic case:

In this case, the vertical component magnetic data T_z at the nodal points of S are computed by formula (6.1.2) with $\mu=1$ and the values so obtained are shown at some representative points in column 4 of Table 6.1.1. It has been theoretically shown that this field also can be reproduced in the upper half-space domain as potential of simple

layer boundary density σ on obtaining it as solution of equations (6.1.6). Considering the a_{kj} values already computed for the gravimetric case, the equations (6.1.6) are solved by Gauss-elimination method treating $T_z(q_k)$ value as b_k , $k=1,2,\dots,n$. The σ_j values so obtained are shown in column 3 of Table 6.1.4 at some representative points over S.

The line integral of σ in this case is found to be 0.00035, as theoretically expected in (4.1.3). Subsequently, the T_z values at level lines $z=1.5$ are computed by formula (6.1.5) on evaluation of the integrals by analytical means. The values so obtained are shown in column 3 of Table 6.1.5 along with the true values in column 2 for comparison. It is evident from Table 6.1.5 that the up-continued T_z values agree with the true values to a good degree of accuracy.

Table 6.1.4: Simple and double layer boundary densities obtained from boundary magnetic data

| Boundary point | | Simple layer | Double layer | Green's Sigma |
|----------------|-------|--------------|--------------|---------------|
| x | z | σ_j | μ_j | H' |
| -25.0 | 0.0 | 0.0001 | -0.0005 | 0.0002 |
| -23.0 | 0.0 | 0.0000 | -0.0006 | 0.0001 |
| -21.0 | 0.0 | 0.0000 | -0.0007 | 0.0001 |
| -19.0 | 0.0 | 0.0000 | -0.0008 | 0.0001 |
| -17.0 | 0.0 | 0.0000 | -0.0010 | 0.0002 |
| -15.0 | 0.0 | 0.0000 | -0.0012 | 0.0003 |
| -13.0 | 0.0 | -0.0001 | -0.0015 | 0.0005 |
| -11.0 | 0.0 | -0.0002 | -0.0020 | 0.0010 |
| -9.0 | 0.0 | -0.0005 | -0.0027 | 0.0019 |
| -7.0 | 0.0 | -0.0012 | -0.0035 | 0.0042 |
| -5.0 | 0.0 | -0.0028 | -0.0039 | 0.0101 |
| -3.0 | 0.125 | -0.0034 | 0.0035 | 0.0070 |
| -0.75 | 1.0 | 0.0074 | 0.0216 | -0.0246 |
| 0.75 | 1.0 | 0.0074 | 0.0216 | -0.0246 |
| 3.0 | 0.125 | -0.0034 | 0.0035 | 0.0070 |
| 5.0 | 0.0 | -0.0028 | -0.0039 | 0.0101 |
| 7.0 | 0.0 | -0.0012 | -0.0035 | 0.0042 |
| 9.0 | 0.0 | -0.0005 | -0.0027 | 0.0019 |
| 11.0 | 0.0 | -0.0002 | -0.0020 | 0.0010 |
| 13.0 | 0.0 | -0.0001 | -0.0015 | 0.0005 |
| 15.0 | 0.0 | 0.0000 | -0.0012 | 0.0003 |
| 17.0 | 0.0 | 0.0000 | -0.0010 | 0.0002 |
| 19.0 | 0.0 | 0.0000 | -0.0008 | 0.0001 |
| 21.0 | 0.0 | 0.0000 | -0.0007 | 0.0001 |
| 23.0 | 0.0 | 0.0000 | -0.0006 | 0.0001 |
| 25.0 | 0.0 | 0.0001 | -0.0005 | 0.0002 |

[The boundary S with a central high extends at both ends along the datum line \bar{S} defined by $z=0$]

Table 6.1.5: Up-continuation of Magnetic field at level $z=1.5$ from boundary data

| x | True field $\Delta T[t]$ | Field as potential of | | By use of |
|--------|-----------------------------|----------------------------|---------------------------|--------------------------------|
| | | Smpl lyr. $\Delta T[S]$ | Dbl lyr. $\Delta T[D]$ | Green's frml. $\Delta T[G]$ |
| -10.25 | -0.0054 | -0.0054 | -0.0055 | -0.0021 |
| -9.25 | -0.0058 | -0.0059 | -0.0060 | -0.0027 |
| -8.25 | -0.0061 | -0.0062 | -0.0064 | -0.0032 |
| -7.25 | -0.0061 | -0.0061 | -0.0064 | -0.0034 |
| -6.25 | -0.0053 | -0.0054 | -0.0058 | -0.0029 |
| -5.25 | -0.0032 | -0.0032 | -0.0039 | -0.0011 |
| -4.25 | 0.0015 | 0.0015 | 0.0003 | 0.0031 |
| -3.25 | 0.0102 | 0.0102 | 0.0079 | 0.0110 |
| -2.25 | 0.0237 | 0.0237 | 0.0197 | 0.0232 |
| -1.25 | 0.0393 | 0.0394 | 0.0351 | 0.0381 |
| -0.25 | 0.0489 | 0.0489 | 0.0484 | 0.0493 |
| 0.25 | 0.0489 | 0.0489 | 0.0484 | 0.0493 |
| 1.25 | 0.0393 | 0.0394 | 0.0351 | 0.0382 |
| 2.25 | 0.0237 | 0.0237 | 0.0197 | 0.0233 |
| 3.25 | 0.0102 | 0.0102 | 0.0079 | 0.0111 |
| 4.25 | 0.0015 | 0.0015 | 0.0003 | 0.0032 |
| 5.25 | -0.0032 | -0.0032 | -0.0039 | -0.0010 |
| 6.25 | -0.0053 | -0.0054 | -0.0058 | -0.0028 |
| 7.25 | -0.0061 | -0.0061 | -0.0064 | -0.0033 |
| 8.25 | -0.0061 | -0.0062 | -0.0064 | -0.0031 |
| 9.25 | -0.0058 | -0.0059 | -0.0060 | -0.0026 |
| 10.25 | -0.0054 | -0.0054 | -0.0055 | -0.0020 |

[$\Delta T[t]$ & $\Delta T[S]$, $\Delta T[D]$, $\Delta T[G]$ are the true & reproduced magnetic values by simple layer boundary density, double layer boundary density and Green's formula respectively]

6.1.3 Up-continuation as Double Layer Potential

We know that gravity or a component magnetic field H in two-dimensions due to a subsurface causative mass is a harmonic function in the upper half-space domain B_1 bounded below by the ground surface S . Both the fields vanish at infinity with asymptotic behaviour $H = O(r^{-n})$, $n \geq 1, r \rightarrow \infty$. As such, following (4.1.4), H can be reproduced in B_1 from the respective boundary data as potential of double layer boundary density μ as

$$H(\mathbf{P}) = - \int_S \log_i |\mathbf{q} - \mathbf{P}| \mu(\mathbf{q}) d\mathbf{q}, \mathbf{P} \in B_1. \quad (6.1.13)$$

For H specified over S , the μ over S can be obtained as a unique solution of the boundary integral equation (4.1.5), i.e.,

$$H(\mathbf{p}) = \pi\mu(\mathbf{p}) - \int_S \log_i |\mathbf{q} - \mathbf{p}| \mu(\mathbf{q}) d\mathbf{q}, \mathbf{p} \in S. \quad (6.1.14)$$

On discretisation, the formula (6.1.13) becomes

$$\tilde{H}(\mathbf{P}) = - \sum_{j=1}^n \mu_j \int_{\Delta S_j} \log_i |\mathbf{q} - \mathbf{P}| d\mathbf{q} \quad (6.1.15)$$

where $\tilde{H}(\mathbf{P})$ is the approximation to H at P and the boundary equation (6.1.14) becomes

$$H(\mathbf{q}_k) = \pi\mu(\mathbf{q}_k) - \sum_{j=1}^n \mu_j \int_{\Delta S_j} \log_i |\mathbf{q} - \mathbf{q}_k| d\mathbf{q}$$

$$\text{or, } H_k = \sum_{j=1}^n (\pi\delta_{kj} - b_{kj})\mu_j, k = 1,2,3,\dots,n, \quad (6.1.16)$$

$$\text{where } b_{kj} = \int_{\Delta S_j} \log_i |\mathbf{q} - \mathbf{q}_k| d\mathbf{q} = \int_{\Delta S_j} |\mathbf{q} - \mathbf{q}_k|^{-2} (\mathbf{q} - \mathbf{q}_k) \cdot \hat{i} d\mathbf{q}, \quad (6.1.17)$$

$H_k = H(q_k)$, \hat{i} is the normal towards B_1 at piecewise straight ΔS_j and δ_{kj} is the Kronecker delta defined as $\delta_{kj} = 0$ for $j \neq k$ and $\delta_{kk} = 1$ for $j = k$.

Two distinct cases arise in evaluation of the coefficient b_{kj}

Case 1:

For $j \neq k$, the integral is regular. Analytical evaluation of it is discussed in subsection 5.3.2. For the nodal point P_k of ΔS_k defined by (\bar{X}, \bar{Z}) in a local reference frame xoz with its origin at the nodal point q_j of ΔS_j and z -axis extending towards B_1 coinciding with the normal to ΔS_j , the b_{kj} over ΔS_j by (5.3.11) is

$$b_{kj} = \int_{\Delta S_j} \log_i |\mathbf{q} - \mathbf{P}_k| d\mathbf{q} = \left[\tan^{-1} \frac{x - \bar{X}}{\bar{Z}} \right]_{x=-h/2}^{x=h/2} \quad (6.1.18)$$

in defining the length of ΔS_j . For q_k and q_j defined by (X_k, Z_k) and (x_j, z_j) respectively in the original reference frame xoz and (\bar{X}, \bar{Z}) defining co-ordinates of P_k in the local frame xoz at the nodal point of ΔS_j , we find

$$\left. \begin{aligned} \bar{X} &= l_1 (X_k - x_j) + m_1 (Z_k - z_j) \\ \bar{Z} &= l_2 (X_k - x_j) + m_2 (Z_k - z_j) \end{aligned} \right\}$$

for (l_1, m_1) and (l_2, m_2) defining the direction cosines of x -axis and z -axis respectively of local frame in the original reference frame. For x -axis of the local frame making an angle θ with the x -axis of the original frame, we find, $l_1 = \cos \theta$, $m_1 = \sin \theta$, $l_2 = -\sin \theta$, and $m_2 = \cos \theta$.

Case 2:

For $j = k$,

$$b_{kk} = \int_{\Delta S_j} \log |\mathbf{q} - \mathbf{q}_k| d\mathbf{q} = 0, \quad (6.1.19)$$

since $(\mathbf{q} - \mathbf{q}_k) \cdot \hat{i} = 0$, $\mathbf{q} \neq \mathbf{q}_k$, $\mathbf{q}, \mathbf{q}_k \in \Delta S_k$ and the integral having a singularity at an isolated point \mathbf{q}_k , a set of measure zero.

Since the equations (6.1.16) form a diagonal dominant system, as shown in subsection 5.4.1, the equations (6.1.16) can be solved easily by Gauss-Seidal iterative method with convergence condition $\epsilon = 0.000001$. On finding the μ over S , the field at a point P above S can be computed by (6.1.15)

(i) Gravimetric case

On computing the gravity values at the $n (= 100)$ nodal points of the sub-elements over S , as described in the previous subsection and shown in column 3 of Table 6.1.1, the coefficient b_{kj} are computed by (6.1.18) for $j \neq k$ and by (6.1.19) for $j = k$. The equations (6.1.16) are then solved for μ_j by Gauss-Seidal iterative method with convergence condition $\epsilon = 0.000001$. The equations took only 6 iterations to converge as expected and the surface integral of μ is found to be 0.95454 ($\neq 0$) as theoretically expected in (4.1.7). The μ values so obtained are shown at some representative points in column 4 of Table 6.1.2.

The gravity values along the level $z = 1.5$ are then computed as potential of double layer density μ by the formula (6.1.13) and these are exhibited in column 4 of Table 6.1.3 along with the true values in column 2 for comparison. It is evident from Table

6.1.3 that the gravity values, reproduced from the boundary data as potential of double layer boundary density, agree with the true values to a good degree of accuracy in general. The error at few points over the middle part is due to the steep nature of the input field and the boundary having edge and corners over the central part.

(ii) Magnetostatic case

Subsequently, vertical component magnetic data due to a unit vertically downward doublet are computed as H_k at the nodal points of S by the formula (6.1.2). The coefficients b_{kj} are computed as above and the equations (6.1.16) are solved for μ_j by Gauss–Seidal iterative method with convergence condition $\varepsilon = 0.000001$. The equations took 6 iterations to converge as expected. The solution at some of the representative points over S are shown in column 4 of Table 6.1.4. The solutions are positive over the central part of S and negative over the outer part. The surface integral of μ over S is found to be 0.028669 where its theoretically expected value, by (4.1.8), is 0. Since the μ values are negative at the outer part of S , the surface integral of the numerical μ over S is expected to be zero as S extends to infinity.

The vertical component magnetic values at the level $z = 1.5$ are then computed as potential of the boundary μ by (6.1.15) and these are shown in column 4 of Table 6.1.5 along with the true values in column 2 for comparison. It is evident from Table 6.1.5 that the magnetic values obtained as double layer potential of boundary density agree with the true values to a good degree of accuracy over the central part of S .

6.1.4 Up-continuation by Green's Formula

For a harmonic function H , a gravity field Δg or a magnetostatic component field T_z , with asymptotic behavior $H = O(r^{-n})$, $n \geq 1$, $r \rightarrow \infty$, defined in the upper half-space domain B_1 bounded below by a half-space boundary S , given H and H_1' over S , H in B_1 can be reproduced by Green's formula (4.1.9) as

$$-2\pi H(\mathbf{P}) = \int_S \log_i |\mathbf{q} - \mathbf{P}| H(\mathbf{q}) d\mathbf{q} - \int_S \log |\mathbf{q} - \mathbf{P}| H_1'(\mathbf{q}) d\mathbf{q}, \quad \mathbf{P} \in B_1. \quad (6.1.20)$$

As $\mathbf{P} \rightarrow \mathbf{p} \in S$, the boundary relation between H and H_1' over S is given by (4.1.10) as

$$-\pi H(\mathbf{p}) = \int_S \log_i |\mathbf{q} - \mathbf{p}| H(\mathbf{q}) d\mathbf{q} - \int_S \log |\mathbf{q} - \mathbf{p}| H_1'(\mathbf{q}) d\mathbf{q}, \quad \mathbf{p} \in S. \quad (6.1.21)$$

As discussed in subsection 4.1.3, given H over S , H_1' over S can be obtained as a unique solution of the boundary integral equation

$$\int_S \log |\mathbf{q} - \mathbf{p}| H_1'(\mathbf{q}) d\mathbf{q} = \int_S \log_i |\mathbf{q} - \mathbf{p}| H(\mathbf{q}) d\mathbf{q} + \pi H(\mathbf{p}), \quad \mathbf{p} \in S. \quad (6.1.22)$$

The discretised versions of (6.1.20) and (6.1.22) are given below

$$-2\pi H(\mathbf{P}) = \sum_{j=1}^n H(\mathbf{q}_j) \int_{\Delta S_j} \log_i |\mathbf{q} - \mathbf{P}| d\mathbf{q} - \sum_{j=1}^n H_1'(\mathbf{q}_j) \int_{\Delta S_j} \log |\mathbf{q} - \mathbf{P}| d\mathbf{q}, \quad \mathbf{P} \in B_1, \quad (6.1.23)$$

and

$$\sum_{i=1}^n H_1'(\mathbf{q}_i) \int_{\Delta S_i} \log |\mathbf{q} - \mathbf{q}_k| d\mathbf{q} = \sum_{j=1}^n H(\mathbf{q}_j) \int_{\Delta S_j} \log_i |\mathbf{q} - \mathbf{q}_k| d\mathbf{q} + \pi H(\mathbf{q}_k), \quad (6.1.24)$$

respectively where $k=1,2,\dots,n$ and $H_1'(\mathbf{q}_i)$ and $H(\mathbf{q}_j)$ stand for the constant values of $H_1'(\mathbf{q})$ and $H(\mathbf{q})$ respectively over the j^{th} subinterval ΔS_j . Following the notations used for the coefficients in (6.1.7) and (6.1.17), the equation (6.1.24) can be expressed as

$$\sum_{j=1}^n a_{kj} H'_j(\mathbf{q}_j) = \sum_{j=1}^n b_{kj} H(\mathbf{q}_j) + \pi H(\mathbf{q}_k), k = 1, 2, \dots, n$$

or,
$$\sum_{j=1}^n a_{kj} H'_j(\mathbf{q}_j) = \sum_{j=1}^n [b_{kj} + \delta_{kj} \pi] H(\mathbf{q}_j) = D_k \text{ (say)}, k = 1, 2, \dots, n, \quad (6.1.25)$$

where δ_{kj} is the Kronecker delta such that $\delta_{kj} = 0, k \neq j$ and $\delta_{kj} = 1, j = k$.

For H specified over the nodal points of the piecewise straight subelements ΔS_j , the equation (6.1.25) can be solved for H'_j by Gauss Elimination method on evaluation of the coefficients a_{kj} and b_{kj} . On finding H'_j over S , the field H in the upper half space domain B_1 can be computed by (6.1.23), the discretised version of (6.1.20).

(i) Gravimetric case

On computing the gravity values $\Delta g_j [= H(\mathbf{q}_j)]$ at the $n (= 100)$ nodal points of the subelements of S by (6.1.1) as described earlier and shown in column 3 of Table 6.1.1, the a_{kj} and D_k values of (6.1.25) are computed following the procedures mentioned in subsections 6.1.2 and 6.1.3 above. The n equations in H'_j are then solved by Gauss Elimination method. The H'_j values so obtained are shown column 5 of Table 6.1.2. On finding the $H'_j(\mathbf{q}_j)$ values over S , the gravity values H are then computed at the level $z = 1.5$ by the formula (6.1.23) and these are shown in column 5 of Table 6.1.3 along with the true values for comparison. It is evident from Table 6.1.3 that the computed values agree with the true values to a good degree of accuracy over the central part of the boundary S .

(ii) Magnetostatic case

Subsequently, the vertical component magnetic data T_z are computed at the $n(=100)$ nodal points of the subelements over S by use of formula (6.1.2) as described earlier and shown in column 4 of Table 6.1.1. On evaluation of coefficients a_{kj} and b_{kj} following the same procedure described earlier, the equations (6.1.25) are solved for H_j^* by Gauss Elimination method. The H_j^* values so obtained are shown in column 5 of Table 6.1.4. Finally, with these H_j^* values known over S , the vertical component magnetic field H is computed at the level $z = 1.5$ by the formula (6.1.20) and these are exhibited in column 5 of Table 6.1.5 along with true T_z values for comparison. It is evident from Table 6.1.5 that the computed T_z values agree with the true T_z values to a good degree of accuracy over the central part of the boundary S .

6.1.5 Summarization of Results on Up-continuation

- (i) Up-continuation of a two-dimensional potential field, an anomalous gravity field or a component magnetic field from its boundary data can be achieved as potential of simple as well as double layer boundary density. It can also be achieved by Green's formula without finding Green's function for the boundary.
- (ii) All the three formulations are theoretically sound, none superior to other. The double layer formulation is however numerically superior to others as in this case computation of the coefficients is straightforward and the equations, arriving from discretisation of the equation, form a highly diagonal dominant system making it amenable to quick solution by Gauss-Seidal iterative method.

6.2 Downward continuation of Gravity-Magnetic Data

6.2.1 Continuation to a curved lower boundary

(i) Theory in brief

Let a two-dimensional harmonic function H , a gravity field Δg or a magnetostatic component field T_z , with asymptotic behaviour $H = O(r^{-n})$, $n \geq 1$, $r \rightarrow \infty$, be defined in the upper half space domain B_i bounded below by a curved half-space boundary $S(= \bar{S}_o + S_L + \bar{S}_o$, Fig.3.2.1) such that its central part S_L is concave upward with its ends fixed at the datum line $\bar{S}(= \bar{S}_o + \bar{S}_u + \bar{S}_o$, Fig.3.2.1) and arms extending along it.

For H given over \bar{S} , H at a point q_k over S can be computed by (4.2.5) as

$$H(q_k) = \pi \mu(q_k) - \int_S \log_i |q - q_k| \mu(q) dq, \quad q_k \in S \quad (6.2.1)$$

The μ of (6.2.1) can be obtained over S_L as an approximate stable solution of the ill-posed problem (4.2.3)

$$H(P) = - \int_S \log_i |q - P| \mu(q) dq, \quad P \in \bar{S}_u \quad (6.2.2)$$

and that over \bar{S}_o as a direct solution of (4.2.4)

$$\pi \mu(P) = H(P) + \int_{S_L} \log_i |q - P| \mu(q) dq, \quad P \in \bar{S}_o \quad (6.2.3)$$

For synthetic input data, it has already been shown in Appendix I that the equation (6.2.2) has a unique solution. This can be verified in a model study, where H can be computed over S from the model response, by comparing the μ obtained as solution of the Dirichlet problem (4.2.5)

$$H(p) = \pi \mu(p) - \int_S \log_i |q - p| \mu(q) dq, \quad p \in S, \quad (6.2.4)$$

for H given over S .

For a horizontal S_l , say \bar{S}_l extending to infinity at both ends lying at a depth d below the datum line \bar{S} , the equation (6.2.2) takes the form (4.2.8) written as

$$H(\mathbf{P}) = -\frac{1}{\pi} \int_{\bar{S}_l} \log |\mathbf{q} - \mathbf{P}| H(\mathbf{q}) dq, \quad \mathbf{P} \in \bar{S}. \quad (6.2.5)$$

For \mathbf{P}, \mathbf{q} defined by $(X,0)$ and $(x,-d)$ respectively in a cartesian reference frame xoz with z -axis upward, the equation (6.2.5) becomes

$$H(X,0) = \frac{d}{\pi} \int_{-\infty}^{\infty} \frac{H(x,-d)}{[(x-X)^2 + d^2]} dx, \quad (6.2.6)$$

the well-known Peters (1949) down-continuation formula, for \bar{S}_u defined by $z=0$ and \bar{S}_l defined by $z=-d$.

(ii) Model Response

To carry out a model study, let us assume that a vertically polarised logarithmic line-mass of line-density λ be placed at a depth d units below the datum line \bar{S} coinciding with x -axis of a reference frame xoz with z -axis upward. For the line-mass extending from $x=x_1$ to $x=x_2$, its gravity and downward vertical component magnetic fields at a point $P_k(x_k, z_k)$ are given by

$$H(P_k) = \Delta g(x_k, z_k) = G\lambda \tan^{-1} \frac{x - x_k}{z_k - z} \Big|_{x=x_1}^{x=x_2} \quad (6.2.7)$$

$$\text{and } H(P_k) = T_z(x_k, z_k) = \mu \left[\frac{(z - z_k)l - (x - x_k)m}{(x - x_k)^2 + (z - z_k)^2} \right]_{x=x_1}^{x=x_2}, \quad (6.2.8)$$

respectively, where G is the universal gravitational constant, μ is the uniform strength of the logarithmic doublets per unit length of the line mass, (l, m) are the direction cosines of the doublets, (x, z) are the coordinates of the point q on the line-mass, T_z is

the downward vertical component magnetic field and Δg is the gravity field due to the line-mass.

Assuming $G=1$, $\lambda=1$, $z=-d=-3$, $x_1=-12$, $x_2=12$, $\mu=1$ and assigning $l=0$, $m=-1$ for vertically downward doublets, the gravity and the vertical component magnetic responses of the line mass can be computed by (6.2.7) and (6.2.8) respectively at the nodal points over \bar{S} taking $z_k=0$.

(iii) The Datum line and the Down-continuation Boundary

To solve the equations (6.2.2) and (6.2.3) and to compute the H over S ($=\bar{S}_o+S_l+\bar{S}_o$, Fig.3.2.1) numerically, let us assume that N equidistant H_k values are specified over a large data-length \bar{S} ($=AB \bar{C}_s \bar{D}_s EF=AB + \bar{S}_u + EF$, Fig. 3.2.1) for downward continuation of H to the lower boundary S_L ($=BC+CD+DE$, Fig.3.2.1). The boundaries are such that C and D of S_L lie vertically below \bar{C}_s and \bar{D}_s respectively of \bar{S} to a depth d below \bar{S} . Let us now divide the line $\bar{S}(=AF)$ into N equal subintervals $\Delta\bar{S}_1, \Delta\bar{S}_2, \dots, \Delta\bar{S}_N$ such that $AB, B\bar{C}_s, \bar{C}_s \bar{D}_s, \bar{D}_s E$ and EF contain N_1, N_2, N_3, N_2, N_4 subintervals respectively. When the end-points of $\Delta\bar{S}_k$ are projected downward, these divide the lower boundary $S(= AB + BC + CD + DE +EF$, Fig.3.2.1) into N unequal subintervals. Let us make the subintervals piecewise straight and denote them as $\Delta S_j, j=1,2,\dots,N$.

It is to be noted here that the segments AB and EF are common to both the boundaries \bar{S} and S , CD is parallel to \bar{S} and each of the curved parts BC and DE at flanks is formed of two parabolic arcs, one above the other.

(iv) **Discretised version of the Equations**

Now locating the N input data H_k at the centroids of the subintervals $\Delta\bar{S}_k$, $k = 1, 2, \dots, N$ over \bar{S} and assuming that the boundary density μ is constant over a subinterval ΔS_j of S , we obtain the discretised version of the equation (6.2.2) as

$$H(\mathbf{P}_k) = \sum_{j=Nl+1}^{Nl+n} -\mu_j \int_{\Delta S_j} \log|\mathbf{P}_k - \mathbf{q}|_i dq, k = Nl+1, \dots, Nl+n, \quad (6.2.9)$$

where $n = N_2 + N_3 + N_2$ and μ_j is the constant value of μ over the j th subinterval ΔS_j .

In the above equations, the n input data $H(\mathbf{P}_k)$ specified over \bar{S}_u are related to n unknown μ_j specified over S_L . Now, denoting the input data $H(\mathbf{P}_{Nl+1}), H(\mathbf{P}_{Nl+2}), \dots, H(\mathbf{P}_{Nl+n})$ by H_1, H_2, \dots, H_n respectively, and ΔS_{Nl+j} by ΔS_j , $j=1, 2, \dots, n$, we rewrite the equations (6.2.9) as

$$\begin{aligned} H_k &= \sum_{j=1}^n -\mu_j \int_{\Delta S_j} \log|\mathbf{P}_k - \mathbf{q}|_i dq, k = 1, 2, \dots, n, \\ &= \sum_{j=1}^n a_{kj} \mu_j, k = 1, 2, \dots, n, \end{aligned} \quad (6.2.10)$$

$$\text{where } H_k = H(\mathbf{P}_k) \text{ and } a_{kj} = - \int_{\Delta S_j} \log_i |\mathbf{q} - \mathbf{P}_k| dq. \quad (6.2.11)$$

The equations (6.2.10) represent a system of n simultaneous linear algebraic equations in n unknown μ_j over S_L . On finding the μ_j over S_L as solution of the equations (6.2.10), the μ_j is labeled back as μ_{Nl+j} . Subsequently, the μ over \bar{S}_o can be obtained directly from the discretised version of (6.2.3) written as

$$\pi\mu_k = H_k + \sum_{j=Nl+1}^{Nl+n} a_{kj} \mu_j, k = 1, 2, \dots, Nl, (Nl+n+1), (Nl+n+2), \dots, N, \quad (6.2.12)$$

where $\mu_{N+1}, \mu_{N+2}, \dots, \mu_{N+n}$ of (6.2.12) are the $\mu_1, \mu_2, \dots, \mu_n$ respectively of the equation (6.2.10) with their labels retrieved.

For a horizontal continuation boundary S_L , say \bar{S}_L , the down continued field over \bar{S}_L is given by (4.2.7)

$$H(q_j) = \pi\mu(q_j), q_j \in \bar{S}_L, \quad (6.2.13)$$

on finding the μ_j as solution of (6.2.10) for a horizontal S_L extending over a large finite length.

On the basis of the same assumption that the μ is constant over a subinterval, the boundary formula (6.2.4) can be discretised as

$$H_k = \sum_{j=1}^n (a_{kj} + \pi\delta_{kj})\mu_j, k = 1, 2, \dots, N, \quad (6.2.14)$$

where μ_j is the constant value of μ over the j^{th} subinterval and

$$a_{kj} = - \int_{\Delta S_j} \log|q_k - q_j| dq, \quad (6.2.15)$$

q_k defining the nodal point of the piecewise straight subinterval ΔS_k and δ_{kj} defining the Kronecker delta $\delta_{kk} = 1$ and $\delta_{kj} = 0, k \neq j$.

6.2.2 Uniqueness of Solution

It is already shown in Appendix I that the inverse problem formulated by equation (6.2.2) has theoretically a unique solution. For a numerical verification, we are to show that the solution of (6.2.2) agrees with the Dirichlet- μ over the curved boundary S_L (Fig. 3.2.1) to a reasonable accuracy. For this purpose, let us compute the vertical component magnetic field due to a vertically polarised logarithmic line mass extending

from $x=-12$ to $x=12$ lying at depth 3 units below the datum line $\bar{S}(=\bar{S}_o + \bar{S}_u + \bar{S}_o)$, Fig.3.2.1). Vertically downward component field T_z at a point $P(x_k, z_k)$ in a xoz frame with z -axis upward is given by the formula (6.2.8). The true H_k values so computed with $z_k=0$, $z=-3$, $l=0$, $m=-1$ and $\mu=1$ are shown as H_i in column 2 of Table 6.2.1 at some representative node points over the datum line \bar{S} extending from $x=-10.25$ to $x=10.25$.

The continuation boundary $S(=\bar{S}_o + S_L + \bar{S}_o)$, Fig.3.2.1) is now formed by the line segments joining $A(-10.25,0)$ and $B(-8.25,0)$, $C(-3.25,-1)$ and $D(3.25,-1)$, $E(8.25,0)$ and $F(10.25,0)$ with curved parts BC and DE at flanks. AB and EF , each identified as \bar{S}_o over \bar{S} , define the horizontal arms of S and the curved parts BC and EF with straight horizontal part CD between them form the continuation part S_L of S with CD at depth 1 unit below \bar{S} .

Considering the subinterval length $h = 0.5$ over $\bar{S}(=\bar{S}_o + \bar{S}_u + \bar{S}_o)$, Fig.3.2.1), we find $AB(=\bar{S}_o)$ and $EF(=\bar{S}_o)$ contain 4 subintervals each, $\bar{B}\bar{C}$, and \bar{D} , \bar{E} contain 10 subintervals each and \bar{C} , \bar{D} , contains 13 subintervals. It is to be noted here that the N nodal points over \bar{S} are distributed as $N_4 = N_1=4$, $N_2=10$ and $N_3=13$. This makes $N=N_1+2N_2+N_3+N_4 = 41$ and $n=2N_2+N_3=33$.

The N piecewise straight subintervals ΔS_j over S are obtained by projecting the $(N+1)$ end points of the N subintervals $\Delta \bar{S}_j$ of \bar{S} over S . For P_k defining the nodal point of $\Delta \bar{S}_k$, the field value at P_k is denoted by H_k , $k=1,2,\dots,N$. Subsequently, the coefficients a_{kj} of (6.2.10) is considered as J_p of (5.3.10) with a negative sign. The

equations (6.2.10) are then solved for μ_j over S_L by Gauss-Seidal iterative method with convergence condition $\varepsilon=0.000001$. On obtaining the μ_j over S_L , the μ_j over $AB(=\bar{S}_0)$ and $EF(=\bar{S}_0)$ are computed by (6.2.12). The μ_j so obtained are shown as $\mu(I)$ in column 6 of Table 6.2.1 at some representative points over $S(=\bar{S}_0+S_L+\bar{S}_0)$.

Table 6.2.1: Uniqueness of solution in down-continuation of a magnetostatic field to a curved lower boundary.

| Node point x | Input at $\bar{S}(z=0)$ H_t | z -co-ord of $q_j \in S$ z_j | Dirichlet μ over \bar{S} $\bar{\mu}$ | Dirichlet μ over S $\mu(D)$ | Inverse μ over S $\mu(I)$ | Difference $ \mu(D) - \mu(I) $ E |
|-------------------|-------------------------------------|--|--|---|------------------------------------|--|
| -10.0 | 0.0489 | 0.0 | 0.0156 | 0.0159 | 0.0159 | 0.0 |
| -8.5 | 0.1860 | 0.0 | 0.0592 | 0.0598 | 0.0595 | 0.0003 |
| -8.0 | 0.2079 | -0.01 | 0.0662 | 0.0668 | 0.0667 | 0.0001 |
| -3.5 | 0.1974 | -0.99 | 0.0628 | 0.0625 | 0.0618 | 0.0007 |
| -3.0 | 0.1937 | -1.0 | 0.0617 | 0.0608 | 0.0602 | 0.0006 |
| -2.5 | 0.1906 | -1.0 | 0.0607 | 0.0594 | 0.0588 | 0.0006 |
| -0.5 | 0.1838 | -1.0 | 0.0585 | 0.0566 | 0.0560 | 0.0006 |
| 0.0 | 0.1835 | -1.0 | 0.0584 | 0.0565 | 0.0559 | 0.0006 |
| 0.5 | 0.1838 | -1.0 | 0.0585 | 0.0566 | 0.0560 | 0.0006 |
| 2.5 | 0.1906 | -1.0 | 0.0607 | 0.0594 | 0.0588 | 0.0006 |
| 3.0 | 0.1937 | -1.0 | 0.0617 | 0.0608 | 0.0602 | 0.0006 |
| 3.5 | 0.1974 | -0.99 | 0.0628 | 0.0625 | 0.0618 | 0.0007 |
| 8.0 | 0.2079 | -0.01 | 0.0662 | 0.0668 | 0.0667 | 0.0001 |
| 8.5 | 0.1860 | 0.0 | 0.0592 | 0.0598 | 0.0595 | 0.0003 |
| 10.0 | 0.0489 | 0.0 | 0.0156 | 0.0159 | 0.0159 | 0.0 |

[The vertical component magnetic field is due to a vertically polarised logarithmic line mass extending from $x=-12$ to $x=12$ lying at depth 3 units below the datum line \bar{S} defined by $z=0$ in a cartesian ref. frame with z -axis upward.]

The H_k values at the N nodal points q_k of S are then computed by (6.2.8) and the a_{kj} of equations (6.2.14), the discretised version of the Dirichlet problem for the domain B_i bounded below by S , are evaluated analytically with P_k replaced by q_k . The coefficient a_{kj} shown in (6.2.15) is the b_{kj} of (5.3.11) with a negative sign for $j \neq k$ and a_{kk} is the b_{kk} of (5.3.13), the value of it being zero. The equations (6.2.14) are then solved by Gauss-Seidal iterative method with $\varepsilon=0.000001$. The Dirichlet μ_j so obtained are shown as $\mu(D)$ in column 5 of Table 6.2.1 for comparison with $\mu(I)$. It is to be noted here that all the computations in this subsection are carried out in double precision.

For the same setup of the boundaries and the causative mass, as shown in Fig.3.2.1, a similar exercise is carried out for down-continuation of the gravity response from the datum line \bar{S} to the continuation boundary S . In this case, the input data are the gravity response due to the logarithmic line mass extending from $x=-12$ to $x=12$ placed at depth 3 units below \bar{S} . The 2-D gravity response H_k is computed over the datum line \bar{S} by (6.2.7) with universal gravitational constant $G=1$, logarithmic line density $\lambda=1$, $z_k=0$ and $z=-3$. The values so obtained are shown as H_i in column 2 of Table 6.2.2. Subsequently, following the same procedure mentioned above, $\mu(D)$ and $\mu(I)$ are obtained and these are shown in columns 5 and 6 respectively in Table 6.2.2

It is evident from Tables 6.2.1 and 6.2.2 that for both gravimetric and magnetostatic cases, the $\mu(I)$ and $\mu(D)$ values agree closely with each other, providing a numerical verification of the theoretical conclusion that the inverse problem (4.2.3) theoretically has a unique solution since $\mu(D)$ is unique over $S(= \bar{S}_0 + S_L + \bar{S}_0)$.

Table 6.2.2: Uniqueness of solution in down-continuation of a gravimetric field to a curved lower boundary.

| Node point x | Input at $\bar{S} (z=0)$ H_t | z -co-ord of $q_i \in S$ z_j | Dirichlet μ over \bar{S} $\bar{\mu}$ | Dirichlet μ over S $\mu(D)$ | Inverse μ over S $\mu(I)$ | Difference $ \mu(D) - \mu(I) $ E |
|-------------------|--------------------------------------|--|--|---|---------------------------------------|--|
| -10.0 | 1.4219 | 0.0 | 0.4526 | 0.4490 | 0.4487 | 0.0003 |
| -8.5 | 1.8737 | 0.0 | 0.5964 | 0.5902 | 0.5877 | 0.0025 |
| -8.0 | 1.9937 | -0.01 | 0.6346 | 0.6259 | 0.6259 | 0.0 |
| -3.5 | 2.4905 | -0.99 | 0.7928 | 0.7980 | 0.8049 | 0.0069 |
| -3.0 | 2.5099 | -1.0 | 0.7989 | 0.8060 | 0.8128 | 0.0068 |
| -2.5 | 2.5255 | -1.0 | 0.8039 | 0.8121 | 0.8191 | 0.0070 |
| -0.5 | 2.5574 | -1.0 | 0.8141 | 0.8239 | 0.8300 | 0.0061 |
| 0.0 | 2.5587 | -1.0 | 0.8145 | 0.8244 | 0.8305 | 0.0061 |
| 0.5 | 2.5574 | -1.0 | 0.8141 | 0.8239 | 0.8300 | 0.0061 |
| 2.5 | 2.5255 | -1.0 | 0.8039 | 0.8121 | 0.8191 | 0.0070 |
| 3.0 | 2.5099 | -1.0 | 0.7989 | 0.8060 | 0.8128 | 0.0068 |
| 3.5 | 2.4905 | -0.99 | 0.7928 | 0.7980 | 0.8049 | 0.0069 |
| 8.0 | 1.9937 | -0.01 | 0.6346 | 0.6259 | 0.6259 | 0.0 |
| 8.5 | 1.8737 | 0.0 | 0.5964 | 0.5902 | 0.5877 | 0.0025 |
| 10.0 | 1.4219 | 0.0 | 0.4526 | 0.4490 | 0.4487 | 0.0003 |

[The gravity field is due to a logarithmic line mass extending from $x=-12$ to $x=12$ lying at depth 3 units below the datum line \bar{S} defined by $z=0$ in a cartesian ref. frame with z -axis upward.]

6.2.3 Downward Continuation of Erroneous Input Data to a Horizontal and a Flat-Bottom Curved Boundary

Let a finite interval \bar{D} extend from $x=-10.25$ to $x=10.25$ over the datum line \bar{S} defined by $z=0$ in a xoz reference frame with z -axis upward. This interval \bar{D} be divided into $N(=41)$ equal subintervals $\Delta\bar{S}_j$ of length $h=0.5$ units each. Let us now consider a horizontal continuation boundary S_h at a depth $d=1$ vertically below \bar{D} such that S_h also extends from $x=-10.25$ to $x=10.25$ and contains $N(=41)$ equal sub-intervals ΔS_j in it. Subsequently, let us consider a flat bottom curved boundary $S (= \bar{S}_o + S_l + \bar{S}_o)$ such that its flat part extends from $x=-3.25$ to $x=3.25$ coinciding with the central part of S_h as shown in Fig.3.2.1. The curved boundary $S (= \bar{S}_o + S_l + \bar{S}_o)$ is now divided into $N(=N1+N2+N3+N2+N4)$ unequal subintervals ΔS_j such that the projection of ΔS_j on \bar{S} coincides with $\Delta\bar{S}_j$ of \bar{S} , $j=1,2,\dots,N$. In this case, $N1(=4)$ and $N4(=4)$ sub-intervals lie on \bar{S} , $N3(=13)$ subelements coincide with those over the central part of S_h and each of the curved parts of S contains $N2(=10)$ unequal subintervals.

(a) Continuation to Horizontal Boundary

On dividing the boundaries \bar{S} and S_h , each into N piecewise straight subintervals as described above, vertical component magnetic field, H_k , $k=1,2,\dots,N$ is computed at the nodal points (x_k, z_k) of \bar{S} by (6.2.8) with $\mu=1$, $z_k=0$, $z=-3$, $l=0$, $m=-1$, $x_1=-12$ and $x_2=12$. These are then contaminated with random error E , $|E| \leq 1\%$ of the true response for treating them as input data. The input data so obtained are shown as H_i in the column 2 of Table 6.2.3.

It is already mentioned that the horizontal continuation boundary S_h (-10.25, 10.25) is divided into $N(=41)$ equal subintervals. Assuming that the μ is constant over a subinterval, the coefficients a_{kj} of equation (6.2.10) for $q_j \in S_h$ as described in subsection 6.2.2, are evaluated by analytical means and the resulting $n(=N)$ equations are solved for approximate μ_j following the procedure described earlier with $\xi=0.000001$ for less than 1% mean squared error (MSE) in input data, the largest field value being 0.2070 over \bar{S} . On finding the μ over S_h , the continued field H_j over S_h is obtained by (6.2.13). The values so obtained are shown in column 5 of Table 6.2.3 along with the true field H_t in column 4 for comparison.

Subsequently, the gravity values at the nodal points (x_k, z_k) , $k=1, 2, \dots, N$ are computed by formula (6.2.7) with $G=1$, $\lambda=1$, $z_k=0$, $z=-3$, $x_1=-12$ and $x_2=12$. These are contaminated with random error E , $|E| \leq 1\%$ of the true response to treat them as input data. The input data so obtained are shown in column 2 of Table 6.2.4. These are then normalised and the above procedure is followed with $\xi=0.0001$ for 1% MSE in the normalised data to find the continued field over S_h . The field so obtained over S_h are multiplied by the normalising factor $M=2.5674$ to get back the field due to the causative mass. The continued field so obtained are shown in column 5 along with the true values in column 4 of Table 6.2.4 for comparison.

Table 6.2.3: Down-continuation of magnetic data to a horizontal and a flat-bottom curved lower boundary at a shallow depth.

| Node points x | Input over $\bar{S}(z=0)$ H_i | % error in data E_r | True field over S_h (d=1) H_i | Down-continued field at depth d=1(=2h) unit below \bar{S} . | | | |
|------------------|------------------------------------|--------------------------|--------------------------------------|---|-----------|--------------------------------|-----------|
| | | | | over Hrtz S_h \tilde{H} | % Er E | over Crvd S_L \tilde{H} | % Er E |
| -10.0 | 0.0494 | 0.9447 | 0.0495 | -0.1908 | -485.310 | -- | -- |
| -8.5 | 0.1847 | -0.7192 | 0.2934 | 0.3622 | 23.4350 | -- | -- |
| -8.0 | 0.2071 | -0.3841 | 0.3049 | 0.2578 | -15.4450 | -- | -- |
| -3.5 | 0.1976 | 0.1049 | 0.2130 | 0.2101 | -1.3526 | -- | -- |
| -3.0 | 0.1938 | 0.0257 | 0.2072 | 0.2161 | 4.2759 | 0.2052 | -0.9752 |
| -2.5 | 0.1891 | -0.7902 | 0.2025 | 0.1895 | -6.4091 | 0.1978 | -2.3364 |
| -0.5 | 0.1820 | -0.9780 | 0.1927 | 0.1810 | -6.0657 | 0.1886 | -2.1376 |
| 0.0 | 0.1841 | 0.3395 | 0.1923 | 0.1894 | -1.5039 | 0.1914 | -0.4540 |
| 0.5 | 0.1853 | 0.8388 | 0.1927 | 0.2001 | 3.8493 | 0.1934 | 0.3497 |
| 2.5 | 0.1901 | -0.2767 | 0.2025 | 0.1987 | -1.8730 | 0.1992 | -1.6109 |
| 3.0 | 0.1928 | -0.4941 | 0.2072 | 0.2013 | -2.8664 | 0.2030 | -2.0243 |
| 3.5 | 0.1965 | -0.4746 | 0.2130 | 0.2011 | -5.5837 | -- | -- |
| 8.0 | 0.2082 | 0.1256 | 0.3049 | 0.2644 | -13.2670 | -- | -- |
| 8.5 | 0.1873 | 0.6972 | 0.2934 | 0.3728 | 27.0470 | -- | -- |
| 10.0 | 0.0493 | 0.7694 | 0.0495 | -0.1907 | -485.240 | -- | -- |

[The field is due to a vertically polarised logarithmic line mass extending from x=-12 to x=12 lying at depth 3 units below the datum line \bar{S} . The horizontal continuation boundary S_h at depth coincides with the flat part of S_L over the interval (-3.25, 3.25)]

(b) Continuation to Curved lower Boundary

For continuation of magnetic data of column 2 of Table 6.2.3 from the datum line \bar{S} to the curved lower boundary S , the co-efficients a_{kj} of equations (6.2.10) are evaluated by analytical means and an approximate stable μ_j over S_L are obtained by solving the equations with terminating condition $\xi_5=0.000001$. Subsequently, the μ_j over \bar{S}_0 are

obtained by (6.2.12) and the field values over the horizontal part of S_1 are computed by the discretised version (6.2.14) of formula (6.2.1). The results obtained are shown in column 7 of Table 6.2.3 along with the true values in column 4 for comparison. The same exercise is carried out for gravity data and results obtained are shown in column 7 of Table 6.2.4 along with the true values in column 4 for comparison.

From the down-continued field values, obtained over the central part of the horizontal continuation boundary and these obtained over the central flat part of the curved continuation boundary, exhibited in Tables 6.2.3 and 6.2.4, it appears that for a finite length of input data, down-continuation to a curved boundary is having a slight edge over continuation to a horizontal boundary.

(c) Down-continuation of Magnetic Data to Horizontal and Flat-bottom curved Boundary at Deeper Depth

On finding the continued field at a depth $D(=2h)=1$ unit below \bar{S} , the procedure is repeated for the same input magnetic data for S_h and \bar{S}_1 (Fig.3.2.1) at depth $d(=4h)=2$ units below \bar{S} without changing the values of N_1, N_2, N_3 and N_4 . The continued field values obtained over S_h and S are shown in columns 3 and 7 respectively of Table 6.2.5 along with the true values for comparison.

Table 6.2.4: Down continuation of gravity data to a horizontal and a flat-bottom curved lower boundary.

| Node points X | Input over \bar{S} (z=0) H_1 | % error in data E_r | True field over S_h (z=-1) H_1 | Down-continued field at depth d=1(=2h) unit below \bar{S} . | | | |
|------------------|---|-----------------------------|---|--|-----------|---------------------------|-----------|
| | | | | over | | over | |
| | | | | Hrtz S_h \tilde{H} | % Er E | Crvd S_L \tilde{H} | % Er E |
| -10.0 | 1.4353 | 0.9447 | 1.4711 | 3.4141 | 132.0700 | -- | -- |
| -8.5 | 1.8602 | -0.7192 | 2.1066 | 1.9167 | -9.0171 | -- | -- |
| -8.0 | 1.9860 | -0.3841 | 2.2455 | 2.3525 | 4.7651 | -- | -- |
| -3.5 | 2.4931 | 0.1049 | 2.6960 | 2.7463 | 1.8662 | -- | -- |
| -3.0 | 2.5105 | 0.0257 | 2.7106 | 2.7966 | 3.1723 | 2.8884 | 6.5569 |
| -2.5 | 2.5056 | -0.7902 | 2.7223 | 2.6779 | -1.6338 | 2.6675 | -2.0132 |
| -0.5 | 2.5324 | -0.9780 | 2.7459 | 2.6324 | -4.1329 | 2.6406 | -3.8327 |
| 0.0 | 2.5674 | 0.3395 | 2.7468 | 2.8034 | 2.0590 | 2.7866 | 1.4496 |
| 0.5 | 2.5789 | 0.8388 | 2.7459 | 2.8870 | 5.1401 | 2.9067 | 5.8567 |
| 2.5 | 2.5186 | -0.2767 | 2.7223 | 2.7354 | 0.4802 | 2.7211 | -0.0463 |
| 3.0 | 2.4975 | -0.4941 | 2.7106 | 2.6854 | -0.9316 | 2.6980 | -0.4654 |
| 3.5 | 2.4787 | -0.4746 | 2.6960 | 2.6383 | -2.1404 | -- | -- |
| 8.0 | 1.9962 | 0.1256 | 2.2455 | 2.3903 | 6.4487 | -- | -- |
| 8.5 | 1.8867 | 0.6972 | 2.1066 | 2.0371 | -3.3015 | -- | -- |
| 10.0 | 1.4328 | 0.7694 | 1.4711 | 3.7239 | 153.1400 | -- | -- |

[The field is due to a vertically polarised logarithmic line mass extending from $x=-12$ to $x=12$ lying at depth 3 units below the datum line \bar{S} . The horizontal continuation boundary S_h at depth coincides with the flat part of S_L over the interval $(-3.25, 3.25)$]

Table 6.2.5: Down-continuation of vertical field magnetic data to a horizontal and to a flat bottom curved lower boundary with their central parts at depth $d=2$ units below the datum line

| Node over \bar{S} | Down-continued field to horztl boundary S_h placed at depth $d=2$ | | | Down-continued field to curved boundary with its central part CD at depth $d=2$ | | | |
|------------------------|---|----------------|---------|---|---------------|----------------|---------|
| | True field | Contd field | % Error | Depth co-ord | True field | Contd field | % Error |
| X | H_t | H | E | $-z_s$ | H_t | H | E |
| -10.0 | 0.0499 | -0.3549 | -811.49 | 0.0 | 0.0489 | 0.0492 | 0.6855 |
| -8.5 | 0.5154 | 0.4122 | -20.039 | 0.0 | 0.1860 | 0.1831 | -1.5649 |
| -8.0 | 0.4554 | 0.6219 | 36.574 | 0.02 | 0.2094 | 0.2080 | -0.6407 |
| -5.5 | 0.2760 | 0.2420 | -12.319 | 1.18 | 0.2546 | 0.2393 | -6.0362 |
| -5.0 | 0.2587 | 0.2402 | -7.1542 | 1.5 | 0.2495 | 0.2387 | -4.3377 |
| -3.5 | 0.2240 | 0.2461 | 9.8730 | 1.98 | 0.2238 | 0.2228 | -0.4421 |
| -3.0 | 0.2165 | 0.2140 | -1.1535 | 2.0 | 0.2165 | 0.2165 | -0.0062 |
| -2.0 | 0.2058 | 0.1906 | -7.4281 | 2.0 | 0.2058 | 0.2021 | -1.8235 |
| -1.0 | 0.1999 | 0.1892 | -5.3747 | 2.0 | 0.1999 | 0.1981 | -0.9306 |
| 0.0 | 0.1980 | 0.1995 | 0.7564 | 2.0 | 0.1980 | 0.1966 | -0.7330 |
| 1.0 | 0.1999 | 0.1974 | -1.2495 | 2.0 | 0.1999 | 0.1986 | -0.6609 |
| 2.0 | 0.2058 | 0.1965 | -4.5329 | 2.0 | 0.2058 | 0.2053 | -0.2567 |
| 3.0 | 0.2165 | 0.1972 | -8.8998 | 2.0 | 0.2165 | 0.2153 | -0.5320 |
| 3.5 | 0.2240 | 0.2114 | -5.6253 | 1.98 | 0.2238 | 0.2211 | -1.2075 |
| 5.0 | 0.2587 | 0.2387 | -7.7385 | 1.5 | 0.2495 | 0.2377 | -4.7272 |
| 5.5 | 0.2760 | 0.2390 | -13.404 | 1.18 | 0.2546 | 0.2404 | -5.6054 |
| 8.0 | 0.4554 | 0.6866 | 50.771 | 0.02 | 0.2094 | 0.2091 | -0.1381 |
| 8.5 | 0.5154 | 0.4240 | -17.745 | 0.0 | 0.1860 | 0.1857 | -0.1527 |
| 10.0 | 0.0499 | -0.3728 | -847.42 | 0.0 | 0.0489 | 0.0491 | 0.5091 |

[Both the datum line \bar{S} and the horizontal continuation boundary S_h extend from $x=-10.25$ to $x=10.25$, S_h lying at a depth $d=2$ units below \bar{S} defined by $z=0$. The coordinates of some of the node points over \bar{S} and S_h are shown in column 1 and the corresponding z -coordinates of those over S are shown in column 5]

It is evident from Table 6.2.5 that for input data within 1% random error specified over an interval $\bar{D}(-10.25, 10.25)$, the continued field at a depth $d(=2h)=2$ units below it can be obtained within a reasonable error over the flat interval $(-3.25, 3.25)$ of the curved continuation boundary.

Further, it is also evident from Tables 6.2.3 and 6.2.5 that the error in the down-continued field values over the central part of the horizontal boundary increases more rapidly with increase of depth of continuation than that over the central part of the curved continuation boundary. Moreover, it is evident from Table 6.2.5 that when the error over the outer parts of the finite horizontal boundary increases rapidly with encroachment towards the central part, the error remains reasonable all over the curved boundary for all depths of continuation $\leq 4h$, h defining the spacing of data over the datum line.

6.3 Depth-Determination

6.3.1 Choice of Boundary and spacing of data over the datum line

Usual downward continuation of an observed potential field to a horizontal level cannot reach the basement low in a geological basin without encountering the neighbouring basement high. This violates the Dirichlet condition of continuation, i.e., the continued field is a harmonic function above the continuation boundary. This situation can be avoided if the continuation boundary approaches the target in a tapering shape extending below a finite interval with its arms extending along the datum line. On computing the field at the apex of the tapering boundary, as it moves downward along a vertical in steps, the depth to the top of the basement can be obtained from the gradient of the computed field along the vertical.

In downward continuation of an observed potential field, spacing of data over the datum line plays an important role in obtaining a well-behaved set of field values along a vertical. It is shown in subsection 4.2.4 that for h defining the uniform length of subinterval $\Delta \bar{S}_k$ over the datum line \bar{S} and D_s defining the depth of continuation,

$$h \geq \frac{D_s}{4}. \quad (6.3.1)$$

provides a well behaved computed field up to a depth of D_s below \bar{S} .

Further, it is shown in subsection 4.2.5 that for a finite data-length \bar{D} over \bar{S} , the error in the down-continued field $H(z_k)$ along a vertical uniformly increases as depth of the apex z_k of the boundary increases, while the field increasing rapidly near the causative mass. It is also shown in the subsection that the error in the

computed $H(z_k)$ decreases as length of \bar{D} increases. However, it is our working experience that

$$\bar{S}_u \geq 5D_s \tag{6.3.2}$$

\bar{S}_u defining the central part of \bar{S} with S_L directly below it (Fig. 4.2.1), provides the computed field $H(z_k)$ along the axis of S_L with steadily increasing percentage error for $D_k \leq D_s = 4h$, D_k defining the depth of z_k below \bar{S} . Under such a situation, the vertical gradient of the computed field along the vertical shows its first maximum at the top of the causative mass.

6.3.2 Generation of Input Data

Let a vertically polarised logarithmic line-mass of line-density λ be placed at a depth d units below the datum line \bar{S} coinciding with x -axis of a reference frame xoz with z -axis upward. For the line-mass extending from $x=x_1$ to $x=x_2$, lying at a depth d below the datum line \bar{S} , its gravity and downward vertical component magnetic fields at a point $P_k(x_k, z_k)$ are given by (6.2.7) and (6.2.8) respectively.

Assuming $G=1$, $\lambda=1$, $z=-d=-3$, $x_1=-12$, $x_2=12$, $\mu=1$ and assigning $l=0$, $m=-1$ for vertically downward doublets, the gravity and the vertical component magnetic responses of the line mass are computed at the nodal points of the subintervals of \bar{D} (-20.5, 20.5) of \bar{S} by (6.2.7) and (6.2.8) respectively taking $z_k=0$ and x_k running over the nodal points of \bar{D} . The true responses so obtained are shown at some representative points in columns 2 and 5 as $H_l(=\Delta g)$ and $H_l(=T_z)$ respectively in Table 6.3.1. The data contaminated with random error are shown as H_i in columns 3 and 6 in Table 6.3.1 for treating them as input data.

Table 6.3.1: Input gravity and magnetic data over a datum line \bar{S}

| Node over \bar{S} x | Gravity data over \bar{S} | | | Magnetic data over \bar{S} | | |
|-----------------------------|-----------------------------|---------------|---------|------------------------------|---------------|---------|
| | True field | Input data | % Error | True field | Input data | % Error |
| | $H_t(\Delta g)$ | H_i | E | $H_t(T_z)$ | H_i | E |
| -20.0 | 0.2653 | 0.2678 | 0.94 | -0.0786 | -0.0794 | 0.94 |
| -15.0 | 0.6747 | 0.6759 | 0.17 | -0.1301 | -0.1314 | 0.97 |
| -10.0 | 2.0233 | 2.0430 | 0.98 | 0.1985 | 0.1991 | 0.34 |
| -5.0 | 2.5620 | 2.5418 | -0.79 | 0.1777 | 0.1792 | 0.82 |
| -4.0 | 2.5975 | 2.5722 | -0.97 | 0.1700 | 0.1686 | -0.83 |
| -3.0 | 2.6224 | 2.6035 | -0.72 | 0.1641 | 0.1653 | 0.73 |
| -2.0 | 2.6390 | 2.6502 | 0.42 | 0.1600 | 0.1602 | 0.13 |
| -1.0 | 2.6485 | 2.6226 | -0.98 | 0.1576 | 0.1562 | -0.95 |
| 0.0 | 2.6516 | 2.6606 | 0.34 | 0.1569 | 0.1581 | 0.77 |
| 1.0 | 2.6485 | 2.6708 | 0.84 | 0.1576 | 0.1586 | 0.60 |
| 2.0 | 2.6390 | 2.6384 | -0.02 | 0.1600 | 0.1607 | 0.42 |
| 3.0 | 2.6224 | 2.6307 | 0.81 | 0.1641 | 0.1628 | -0.82 |
| 4.0 | 2.5975 | 2.5999 | -0.28 | 0.1700 | 0.1689 | -0.62 |
| 5.0 | 2.5620 | 2.5549 | -0.28 | 0.1777 | 0.1770 | -0.40 |
| 10.0 | 2.0233 | 2.0399 | 0.82 | 0.1985 | 0.1991 | 0.30 |
| 15.0 | 0.6747 | 0.6778 | 0.45 | -0.1301 | -0.1299 | -0.11 |
| 20.0 | 0.2653 | 0.2673 | 0.77 | -0.0786 | -0.0786 | -0.02 |

(Gravity and vertical component magnetic fields are due to a vertically polarized logarithmic line mass extending from $x=-12$ to $x=12$ lying at a depth 3 units below \bar{S} defined by $z=0$ in a xoz reference frame with z -axis upward)

6.3.3 Down-Continuation of Erroneous Potential Field to a Tapered Parabolic boundary

Considering the continuation or search-depth $D_s=4$, the normalised gravity data over the interval \bar{D} (-13.5, 13.5) of \bar{S} are sampled following (6.3.1) at a regular spacing $h=1$ and these are assigned at the nodal points of the subintervals $\Delta\bar{S}_i$ of \bar{D} . This subdivision yields $N=27$ data over \bar{D} with the central one at $x=0$. Following the scheme of distribution of data over \bar{S} , as shown in Fig.4.2.1, $N_1=2$ data over \bar{S}_0 to the left of \bar{S}_u , $N_4=2$ over \bar{S}_0 to the right of \bar{S}_u , and n

$=[N2(=10)+N3(=3)+N2(=10)]=23$ over \bar{S}_u are assigned. The values of $N2$ and $N3$ so chosen automatically satisfies the condition (6.3.2) for all choice of $h \leq D_s / h$.

Considering the first configuration $S_{L(1)}$ of S_L (Fig. 4.2.1) with its apex z_1 at depth $d=\Delta z=0.5$ below \bar{S} at the vertical $x=0$, equations (6.2.10) in $n(=23)$ unknown μ_j are solved for stable approximate μ_j allowing a mis-match of 1% mean squared error (MSE) between the reproduced field and the input data over \bar{S}_u by setting $\xi=0.0001$ for a preassumed 1% maximum average error in the normalised input data. On finding the approximate μ_j over $S_{L(1)}$, the μ_j over \bar{S}_o are obtained by (6.2.12). On obtaining the μ_j over $S(=\bar{S}_o+S_L+\bar{S}_o)$, Fig.4.2.1) for data specified over the interval $\bar{D}(-13.5, 13.5)$ of \bar{S} , the down-continued field $H(z_1)$ at the apex $z_k=z_1$ at depth $d_1=\Delta z=0.5$ below \bar{S} is computed by (6.2.14), the discretised version of (6.2.1). The value so obtained is multiplied by the normalising factor M of the data over \bar{D} to find the down-continued field value of the original field.

In the next step, keeping \bar{S}_u and the input data unchanged over \bar{D} , S_L is extended downward with its apex z_2 on $x=0$ at a depth $d=2\Delta z(=1)$ below \bar{S} . The procedure described above is followed to compute $H(z_2)$. The procedure of extending of S_L downward with its apex z_k moving in steps of Δz along the vertical at $x=0$ and subsequent computation of $H(z_k)$ is continued till z_k attains a depth $d \geq D_s$ below \bar{S} . The $H(z_k)$ values so obtained along the vertical are shown in column 3 of Table 6.3.2 along with the true values for comparison. Similar procedure is followed for the input data specified over the interval $\bar{D}(-20.5, 20.5)$ at a spacing of $h=1$ over \bar{S} keeping \bar{S}_u

fixed in position with $n=23$, and $N1=N4=10$ at same spacing $h=1$ over \bar{S}_0 on both sides of \bar{S}_u . The $H(z_k)$ values so obtained at steps of $\Delta z=0.5$ along the vertical at $x=0$ are shown in column 5 in Table 6.3.2.

Following the same procedure, the erroneous vertical component magnetic data H_i , shown in column 6 of Table 6.3.1, are considered over the intervals $\bar{D}(-13.5, 13.5)$ and $\bar{D}(-20.5, 20.5)$ at a spacing $h=1$ over \bar{S} , for down-continuation of the field along the vertical at $x=0$. The results obtained are shown in Table 6.3.3 along with the true values for comparison.

Table 6.3.2: Down-continued gravity field along a vertical through mid-point of \bar{D} of datum line \bar{S} .

| Depth of z_k | True field H_i | Down-continued field for data-length | | | |
|----------------|------------------|--------------------------------------|---------|------------------------|---------|
| | | $\bar{D}(-13.5, 13.5)$ | | $\bar{D}(-20.5, 20.5)$ | |
| | | $H(z_k)$ | % Error | $H(z_k)$ | % Error |
| 0.5 | 2.7308 | 2.6240 | -3.91 | 2.6316 | -3.63 |
| 1.0 | 2.8112 | 2.7520 | -2.11 | 2.7554 | -1.98 |
| 1.5 | 2.8929 | 2.8416 | -1.77 | 2.8457 | -1.63 |
| 2.0 | 2.9753 | 2.9286 | -1.57 | 2.9334 | -1.40 |
| 2.5 | 3.0583 | 3.0157 | 1.39 | 3.0186 | 1.29 |
| 3.0 | -- | 3.1616 | -- | 3.1708 | -- |
| 3.5 | -- | 3.2538 | -- | 3.2405 | -- |
| 4.0 | -- | 3.3408 | -- | 3.3488 | -- |
| 4.5 | -- | 3.4227 | -- | 3.4288 | -- |
| 5.0 | -- | 3.5021 | -- | 3.5062 | -- |

[The field is reproduced at the apex z_k of the parabolic part of the down-continuation boundary as it extends downward with its ends fixed at the datum line and apex moving downward in steps along the vertical at $x=0$.]

Table 6.3.3: Down-continued magnetic field along a vertical through mid-point of \bar{D} of datum line \bar{S} .

| Depth of z_k | True field H_t | Down-continued field for data-length | | | |
|----------------------|------------------------|--------------------------------------|---------|------------------------|---------|
| | | $D(-13.5, 13.5)$ | | $\bar{D}(-20.5, 20.5)$ | |
| | | $H(z_k)$ | % Error | $H(z_k)$ | % Error |
| 0.5 | 0.1597 | 0.190 | 18.97 | 0.163 | 2.06 |
| 1.0 | 0.1622 | 0.197 | 21.45 | 0.169 | 4.19 |
| 1.5 | 0.1641 | 0.204 | 24.31 | 0.175 | 6.64 |
| 2.0 | 0.1655 | 0.211 | 27.49 | 0.180 | 8.76 |
| 2.5 | 0.1664 | 0.206 | 23.79 | 0.186 | 11.77 |
| 3.0 | -- | 0.211 | -- | 0.191 | -- |
| 3.5 | -- | 0.217 | -- | 0.197 | -- |
| 4.0 | -- | 0.223 | -- | 0.184 | -- |
| 4.5 | -- | 0.230 | -- | 0.188 | -- |
| 5.0 | -- | 0.237 | -- | 0.192 | -- |

[The field is reproduced at the apex z_k of the parabolic part of the down-continuation boundary as it extends downward with its ends fixed at the datum line and apex moving downward in steps along the vertical at $x=0$.]

It is evident from Tables 6.3.2 and 6.3.3 that for the input data specified over an interval \bar{D} , the error in the down-continued field along the axis of S_L steadily increases with depth as expected in subsection 4.2.5 for a negative μ_m . The error in the computed $H(z_k)$ however decreases at a fixed depth of z_k when the data interval \bar{D} increases in length, as expected in subsection 4.2.5. Further, for a fixed input data-length, the error in $H(z_k)$ for the magnetostatic cases increases at a much faster rate than that in the gravimetric case as expected in subsection 4.2.5. It is to be noted here that the average percentage error in input data over $\bar{S}_u(-5.5, 5.5)$ is negative for the gravimetric case and it is positive for the magnetostatic case as can be seen in Table 6.3.1. Hence, the % error in the reproduced $H(z_k)$ for these set of model data starts with a negative value for the gravimetric case and with a positive value for the magnetostatic case.

6.3.4 Depth-Determination from Down-continued Field-values

It is evident from the $H(z_k)$ columns in Tables 6.3.2 and 6.3.3 that contrary to expectation, all the $H(z_k)$ profiles smoothly go past the causative mass with increasing values without exhibiting a visible change in them at the causative mass. A distinct change in property of the field on crossing the target lies suppressed for smoothening of boundary μ obtained by introducing an extra term λ that appears in the diagonal vector of the system of linear algebraic equations (5.4.12) to ensure convergence of the solution.

Considering the down-continued gravity and magnetic values $H(z_k)$ of Tables 6.3.2 and 6.3.3 respectively, obtained from data specified over $\bar{D}(-13.5, 13.5)$, the vertical gradient $\nabla_z H$ of $H(z_k)$ profiles are computed by formula (4.2.10) along with η , the normalised variation in $\nabla_z H$ relative to the first (or shallowest) gradient value $\nabla_z H_1$, by (4.2.11). The details of computation are shown in Table 6.3.4 and 6.3.5, for gravity and magnetic fields respectively.

It is evident from Tables 6.3.2 and 6.3.3 that even when the computed $H(z_k)$ values are with large error and the error increasing with depth of z_k , as expected, the vertical gradient of $H(z_k)$ shows its first maximum at the top of the causative mass at depth $d=|z|=3$ units below the datum line \bar{S} . Subsequently, gradients of $H(z_k)$ values obtained from input data of $\bar{D}(-20.5, 20.5)$ are computed. The down-continued $H(z_k)$ values and η values so obtained from gravity and magnetic data are shown in columns 2&3 and 4&5 respectively in Table 6.3.6. In this case also depth to the causative mass is shown at depth $d=3$.

It is evident from Tables 6.3.4, 6.3.5 and 6.3.6 that for both the input data intervals $\bar{D}(-13.5, 13.5)$ and $\bar{D}(-20.5, 20.5)$, the first maximum of the vertical gradients of $H(z_k)$ occurs at the top of the causative mass. Hence, a input data interval $\bar{D} > \bar{S}_0$ with $(2N_2+N_3)$ data, is expected to lead to correct depth to the causative mass, as expected in subsection 4.2.5, for the mass lying at depth $d \leq 4h$, h defining the spacing of data over \bar{D} .

Table 6.3.4: Depth-determination by down-continuation of gravity data along a vertical for data specified over the interval $\bar{D}(-13.5,13.5)$ of \bar{S} at a regular interval $h=1$.

| Depth of z_k | Continued field | | 1 st | 2 nd | 3 rd | Grad | Normalised variation η |
|----------------|-----------------|-------------------------|--------------------|--------------------|--------------------|----------------|-----------------------------|
| | True H_t | Reproduced $H(z_k)=f_k$ | Diff. $\Delta_1 f$ | Diff. $\Delta_2 f$ | Diff. $\Delta_3 f$ | f $\Delta_z f$ | |
| 0.5 | 2.7308 | 2.6240 | | | | | |
| 1.0 | 2.8112 | 2.7520 | 0.1280 | | | | |
| 1.5 | 2.8929 | 2.8416 | 0.0896 | -0.0384 | | 0.1702 | 0.000 |
| 2.0 | 2.9753 | 2.9286 | 0.0870 | -0.0026 | 0.0358 | 0.1639 | -0.010 |
| 2.5 | 3.0583 | 3.0157 | 0.0871 | 0.0001 | 0.0027 | 0.2420 | 0.878 |
| 3.0 | -- | 3.1616 | 0.1459 | 0.0588 | 0.0587 | 1.0487 | 1.000 |
| 3.5 | -- | 3.2538 | 0.0922 | -0.0537 | -0.1125 | 0.1710 | -0.026 |
| 4.0 | -- | 3.3408 | 0.0870 | -0.0052 | 0.0485 | | |
| 4.5 | -- | 3.4227 | 0.0819 | -0.0051 | 0.0001 | | |

[Down-continued field $H(z_k)$ is obtained along the vertical $x=0$ from input data shown in column 3 of Table 1 specified over $\bar{D}(-13.5,13.5)$. $\Delta_i f$ stands for the i^{th} order difference of f in the horizontal difference Table, $\nabla_z f$ stands for downward vertical gradient of f and η stands for normalised relative variation in $\nabla_z f$.]

Table 6.3.5: Depth-determination by down-continuation of magnetic data along a vertical for data specified over the interval $\bar{D}(-13.5,13.5)$ of \bar{S} at a regular interval $h=1$.

| Depth Of z_k | Continued field | | 1 st | 2 nd | 3 rd | Grad | Normalised variation η |
|----------------------|-----------------|----------------------------|-----------------------|-----------------------|-----------------------|---------------------|-----------------------------------|
| | True H_t | Reproduced $H(z_k)=f_k$ | Diff. $\Delta_1 f$ | Diff. $\Delta_2 f$ | Diff. $\Delta_3 f$ | f $\Delta_1 f$ | |
| 0.5 | 0.1597 | 0.190 | | | | | |
| 1.0 | 0.1622 | 0.197 | 0.007 | | | | |
| 1.5 | 0.1641 | 0.204 | 0.007 | 0.0 | | 0.0160 | 0.0 |
| 2.0 | 0.1655 | 0.211 | 0.007 | 0.0 | 0.0 | -0.0003 | -0.736 |
| 2.5 | 0.1664 | 0.206 | -0.005 | -0.012 | -0.012 | -0.0020 | -0.801 |
| 3.0 | -- | 0.211 | 0.005 | 0.010 | 0.022 | 0.0130◀ | -0.099◀ |
| 3.5 | -- | 0.217 | 0.006 | 0.001 | -0.009 | 0.0120 | -0.138 |
| 4.0 | -- | 0.223 | 0.006 | 0.0 | -0.001 | | |
| 4.5 | -- | 0.230 | 0.007 | 0.001 | 0.001 | | |

[Down-continued field $H(z_k)$ is obtained along the vertical $x=0$ from input data shown in column 4 of Table 1 specified over $\bar{D}(-13.5,13.5)$. $\Delta_i f$ stands for the i^{th} order difference of f in the horizontal difference Table, $\nabla_z f$ stands for downward vertical gradient of f and η stands for normalised relative variation in $\nabla_z f$.]

Table 6.3.6: Computation of depth to the causative mass from gravity and magnetic data specified over $\bar{D}(-20.5,20.5)$ of \bar{S} by down-continuation along the vertical at $x=0$.

| Depth of z_k | Gravity field along $x=0$ $H(z_k)$ | Relative vertical gradient η | Magnetic field along $x=0$ $H(z_k)$ | Relative vertical gradient η |
|----------------------|--|--|---|--|
| 0.5 | 2.632 | | 0.163 | |
| 1.0 | 2.755 | | 0.169 | |
| 1.5 | 2.846 | 0.000 | 0.175 | 0.000 |
| 2.0 | 2.933 | -0.129 | 0.180 | -0.008 |
| 2.5 | 3.019 | 0.878 | 0.186 | -0.108 |
| 3.0 | 3.171 | 1.000◀ | 0.191 | 0.099◀ |
| 3.5 | 3.241 | -0.072 | 0.197 | -0.938 |
| 4.0 | 3.349 | -0.107 | 0.184 | -1.000 |
| 4.5 | 3.429 | | 0.188 | |
| 5.0 | 3.506 | | 0.192 | |

[The first maximum of the vertical gradient of the down-continued gravity and magnetic field values along $x=0$ occurs at $z_k=3$, the actual depth of the source below the datum line \bar{S} .]

6.3.5 General Remarks on Down-Continuation and Depth-Determination

- (i) Formulation of problem of down-continuation to a horizontal half-space boundary and that to a curved continuation boundary with a flat central part, are both built up on sound theoretical basis. However, for data specified over a finite datum length, it appears that the later provides a better down-continued field over its flat part than that provided by the former over the same interval coinciding with it.
- (ii) Numerical analysis on down-continuation of erroneous data with error E , $|E| \leq 1\%$ of the true response, is carried out in this work. It is observed that the error in the continued field increases to about 2% in general when the field is continued to a level $2h$ below the datum line, h defining the spacing of data over the datum line.
- (iii) Since the parabolic continuation boundary approaches the top of the causative mass taking a tapering shape as depth increases, the approach is expected to provide a reasonable point to point depth to the top of the undulated basement in a geological basin.
- (iv) For a causative mass lying at a depth $d \geq D_s$, the search depth, below the datum line \bar{S} , the vertical gradient of the continued field $H(z_k)$ will not exhibit its first maximum at a depth shallower than D_s . To determine the depth in such a case, D_s is to be increased and accordingly, the spacing h of data over \bar{S} is to be refixed as $h=D_s/4$. Further, the technique in general produces the depth within a maximum error $E_{\max} < \Delta z$, the step size of z_k along the vertical. However, the result can be improved by considering a smaller value of Δz .

- (v) The observed ground magnetic data are with more than 1% error in them in general. The error in the data can be reduced by up-continuation of them to a higher level. Presence of unacceptable error in data will be revealed either in non-convergence of solution or in yielding of unacceptable depth to the subsurface causative mass.
- (vi) Profile magnetic data in 2D with normal corrections, can be treated as isolated for its use in determination of depth to the causative mass by use of the down-continuation technique described in the work. This provides as easy approach in finding depth to the basement in a geological basin from observed magnetic data.

CHAPTER VII

APPLICATION TO FIELD DATA

7.1 Identification of EW trending faults and determination of sedimentary thickness in Shillong-Mawlong area by analysis of magnetic data

7.1.1 Introduction

On June 12, 1897 Shillong, the capital of Meghalaya, was violently rocked by the great Assam Earthquake of magnitude 8.1 in Richter scale. The main cause of the quake remained unknown for over a century. Most scientists previously believed that this quake was caused by a rupture on the Himalayan thrust fault that dipping to the north and propagating all along beneath Bhutan.

At the turn of the century, Captain Bond discovered an 8 ft uplift of the Shillong plateau while working for the Survey of India (SoI) to remeasure the triangular points established by the original survey of the Plateau in 1862. His superiors dismissed his results, says Prof. Bilham (Geology news, 2001).

In the early 20th century, Richard Oldham concluded that continuing movement of the Shillong Plateau following the Assam event caused errors in the original data and recommended a retriangulation in the northern portion of the plateau. He later wrote about the Assam earthquake in extraordinary detail and went on to discover the core of the earth (Billham and England 2001).

Finally, Bilham and England (2001) analyzed Bond's data and found that the northern edge of the Shillong plateau rose violently by more than 11m following the rupture of a buried 110 km long reverse fault, dipping steeply away from the Himalaya and penetrating 9 to 45km beneath the surface. They dubbed it 'Oldham fault'. They also inferred that there must exist a reverse fault at the southern edge of the plateau dipping northwards that acted in concert with the Oldham fault to wedge the Shillong Plateau uniformly upward without tilting it (Geology news 2001).

The reverse fault at South of Shillong coincides with the exposed Dauki fault which is clearly visible at the southern edge of the plateau. However, the northern Oldham fault does not show any outcrops in the Nongpoh-Barapani area (Bilham and England, 2001) which is mostly covered by Proterozoic Shillong group of sediments. The Shillong plateau with a high elevation and positive Bouguer gravity (~20-40 mGal) does not have a crustal root in the mantle and the crust underneath is thinner ≈ 35 km, (Mitra et. al., 2005). It must therefore be supported by dynamics along two reverse faults, the south bounding Dauki fault and the north bounding Oldham fault, as opined by Mitra et. al. (2005). But there is no direct visual evidence of the existence of the Oldham fault. The paper addresses the question by interpreting magnetic data available for the area.

Nandy and Dasgupta (1986) used satellite images to delineate a number of buried lineaments beneath the Alluvium in northeast India. The NE-SW Tyrsad-Barapani lineament/shear is clearly discernible on the imagery, but the Oldham fault, if it exists, between Barapani and Nongpoh under the cover of Proterozoic sediments, finds no mention in Nandy (2001).

Magnetic traverses from Guwahati to Shillong along National Highways NH37 (extending from Guwahati to Jorabat) and NH40 (extending from Jorabat to Shillong via Nongpoh, Umsning and Barapani) were laid out by Jawahar and Ramaiah (1991). Without incorporating topographic and crooked-line correction to data, they considered a vertical field profile passing through Nongpoh, Barapani and Shillong as if the data were acquired on a horizontal line. A qualitative interpretation of data showed high fluctuation of magnetic anomaly over Nongpoh on the exposed granite and a negative anomaly over the Nongpoh-Shillong area, covered by sediment. In their work, no attempt was made to identify any buried feature across NH40 in Nongpoh-Shillong area.

Recently, the Geological Survey of India (GSI) carried out close-grid gravity-magnetic (GM) surveys in certain parts in Meghalaya. GM maps of Umroi-Shillong, a southern portion of the study area, were presented by Pathak et. al. (2003). The maps clearly indicate an alignment of faults in the area. No such survey however was carried out in the Barapani-Nongpoh area.

In the year 1977, an Aeromagnetic survey of the area had been conducted by National Geophysical Research Institute (NGRI) for the North East Council (NEC) at two different altitudes; the eastern and western blocks at 4600ft and the central block at 7000ft aMSL with a flight line spacing of 2km. A contour map of the magnetic anomaly was prepared for each individual block and these were composited to present an aeromagnetic map of the Plateau. A qualitative analysis of the map was carried out by Rama Rao (1999) showing EW lineaments generally in the central part of the plateau, but none through the Nongpoh-Barapani EW sector.

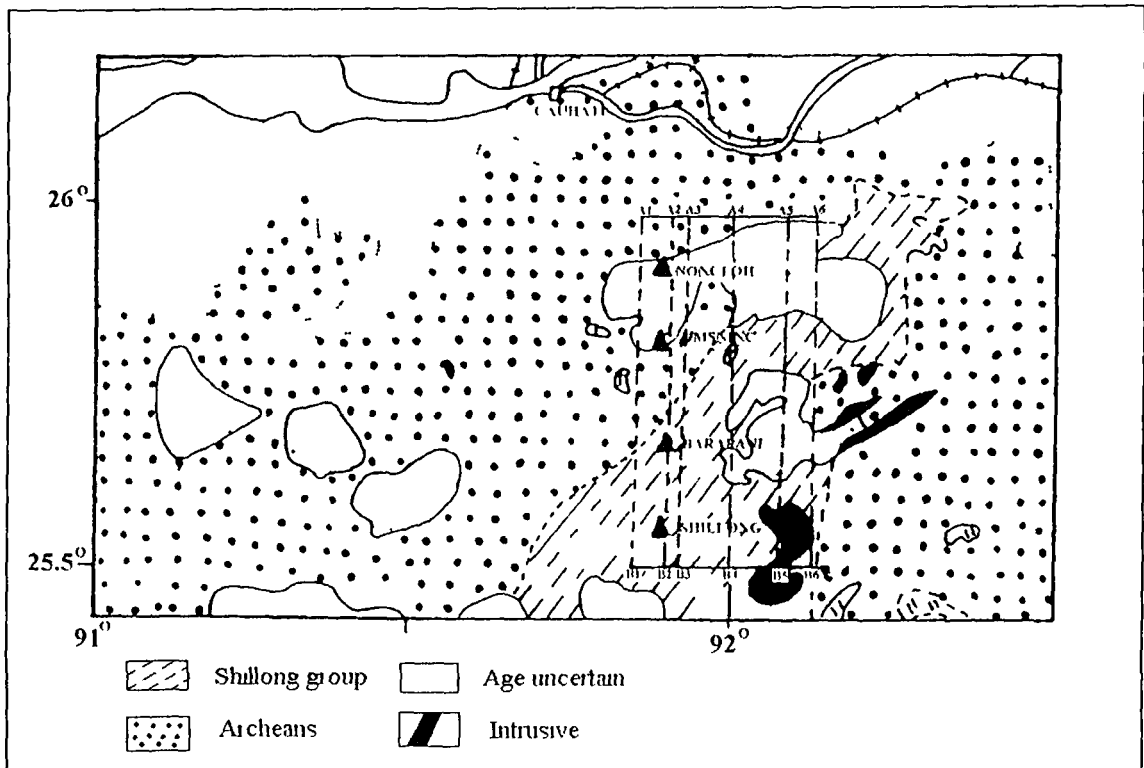
In this work, we attempt to examine the existence of the Oldham fault by quantitative analysis of aeromagnetic data. An attempt has also been made to reexamine the ground magnetic data of Jawahar and Ramaiah (1991).

7.1.2. Geology and topography of the study area

The Shillong plateau is a granite massif with a prominent NE-SW trending wide patch of Proterozoic Shillong group of sediments with a few exposed intrusives at its eastern edge. The study area, namely the Shillong-Nongpoh-Mawlong, bounded by latitudes $25^{\circ}30'$ and $26^{\circ}N$ and longitudes $91^{\circ}50'$ and $92^{\circ}7'30''$ E (Toposheets Nos. 78O/13, 78O/14, 83C/1, 83C/2), lies mainly in the Proterozoics. Nongpoh, north of Shillong, lies at the western edge of the Proterozoic patch, Umsning and Barapani lie at its central part (Fig. 7.1.1) and Mawlong sits on exposed granites, north of the patch.

The topographic height gradually increases towards the south as we move from Nongpoh (500m approx.) to Shillong and attains a maximum of 1964 m (Shillong peak) ~ 6km south of Shillong. The height generally varies from 500 to 1300m aMSL in the E-W sector, bounded by the latitudes of Nongpoh and Barapani. The National Highway NH40 with a zigzag course passes through Nongpoh, between Guwahati and Shillong and apparently traverses the predicted Oldham fault somewhere between Nongpoh and Barapani (Bilham and England 2001).

Fig 7.1.1 Geological map of Shillong-Nongpoh area and NS lines over it
Scale 1:10,000,000



7.1.3. Analysis of Aeromagnetic Data

(a) Qualitative Analysis

The area under study is covered by aeromagnetic survey with flight-line spacing of 2km at flight level 7000ft (21336m) AMSL. A copy of the magnetic map on 1:250,000 scale in 10nT contour interval and its parts in 1:50,000 scale are now available at NEC, Shillong, were obtained for a quantitative analysis. However, in the absence of the associated report, it is assumed that the data had a probable error of 1nT. A magnetic map of the study area read from 1:50,000 maps is reproduced in Fig 7.1.2

Fig.7.1.2: Aeromagnetic Map of Nongpoh-Shillong area showing lines of 2-D magnetic profiles under consideration.

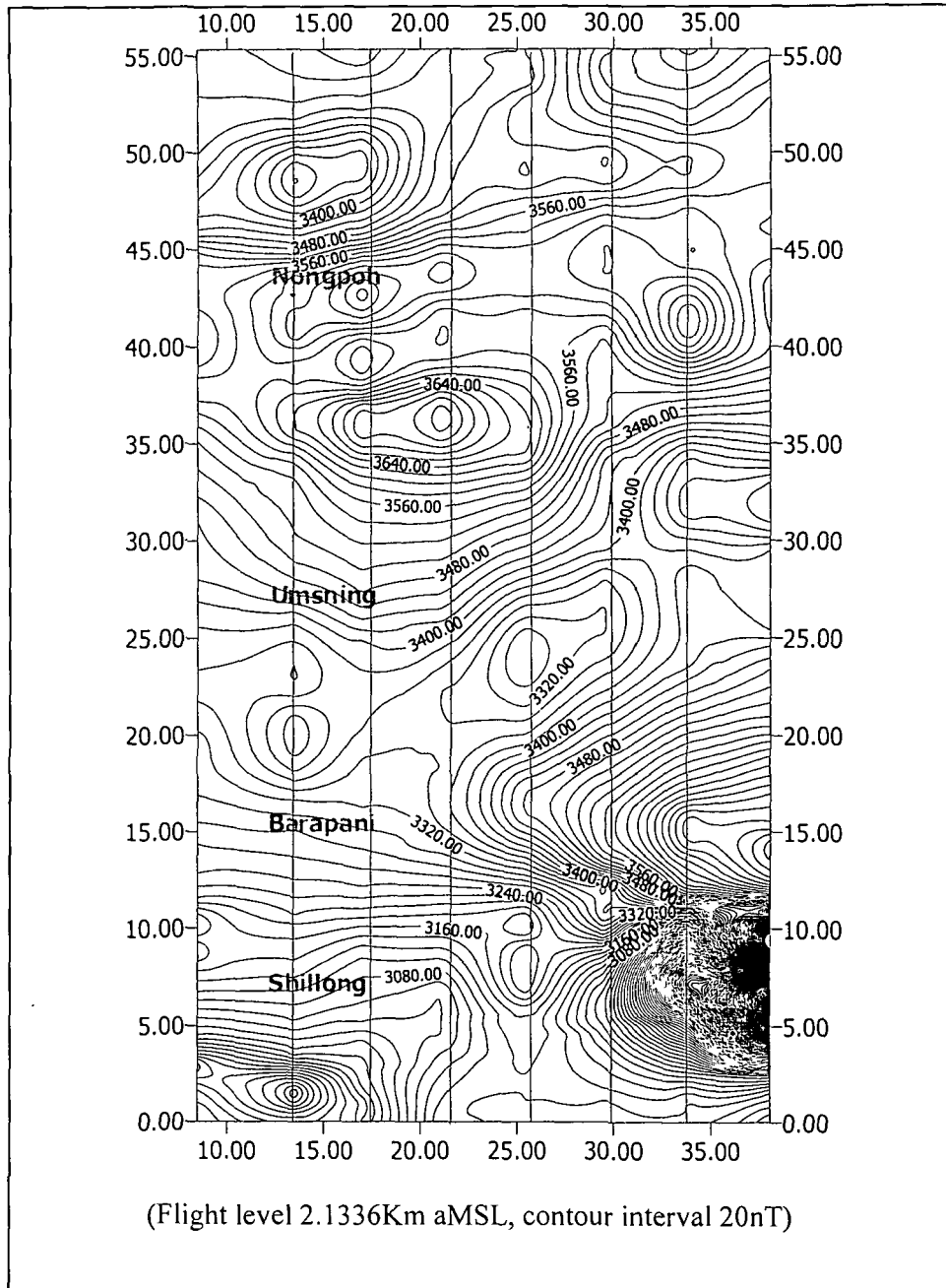


Fig. 7.1.2 clearly reflects the response of the exposed granite of Nongpoh-Mawlong corridor at its north, that of the intrusives at the southeast corner and the response of NE-SW trending Barapani lineament/shear in its central part. It further shows E-W magnetic lineaments immediately north of Shillong and NEW trending lineament immediately south of the Nongpoh-Mawlong corridor. No EW lineament could be traced in the area bounded by the latitudes of Nongpoh and Barapani.

(b) Quantitative Analysis

To carry out a quantitative analysis of the aeromagnetic data, six NS lines were drawn between latitudes 26°N and 25.5°N so that the magnetic field anomaly along each of them could be approximately regarded as a two-dimensional one. The lines are identified as A1-B1, A2-B2, A3-B3, A4-B4, A5-B5, A6-B6 in Fig. 7.1.1. The line A1-B1 extends along longitude $91^{\circ}50'\text{E}$ and A6-B6 extends along longitude $92^{\circ}7.5'\text{E}$. The line A2-B2, shown in Fig. 7.1.1, passes near Nongpoh, Umsning, Barapani and Shillong and A6-B6 defines the eastern boundary of the area under study. Topographic height along A2-B2, read from the contour map of Toposheets, is shown in Fig. 7.1.7 and that along A6-B6, in Fig. 7.1.8. It is evident from Fig. 7.1.7 that the topographic height along A2-B2 varies from 500 to 1100m over the EW Nongpoh-Barapani sector and rises sharply in the Barapani-Shillong sector beyond Barapani attaining 1964m over a distance of about 9km. The height along A6-B6 varies from 750 to 1100m over the EW sector and rises to approx. 1500m south of Barapani.

Assuming that the effect of remanent magnetic elements, if present, is negligibly small, the downward vertical component magnetic field T_z is computed along each line using the formula $T_z = T \sin i$, where T_z is the vertical field, T the total field and i

the inclination of the Earth's magnetic field at the point under consideration. (Murthy, 1998). The inclination angle i varies from 37.33° to 36°N as we move from latitudes 26°N (north of Nongpoh) to 25.5°N (south of Shillong). The normalised versions of T_z obtained along the line A2-B2 and A6-B6 are shown in Figs. 7.1.3 and 7.1.4 respectively.

(i) Gradients of Vertical magnetic profile and Identification of Approximate Fault-trace Points

Thin plates represent the simplest model of step faults in two-dimensions. For a 35° angle of polarisation, all the points, maximum of T_z , inflexion of its horizontal gradient T_{zx} and the minimum of its vertical gradient T_{zz} , form a cluster in the vicinity of the fault-trace point. (Fig. 1, Appendix III)

To model the approximate location of a basement fault from observed magnetic data; we computed the gradients of T_z numerically. It has been pointed out by Hammer (1979) that computed gradients of an observed potential field are highly sensitive to errors in the input data. However, stable and reliable horizontal and vertical gradients of a gravity or magnetic profile can be computed from field data at $z=2h$ level above the datum line $z=0$ by the source technique of Laskar (1999), where h defines the uniform spacing of data over the datum line. In this case the error in the computed horizontal gradient T_{zx} appears almost within the uncertainty of input data, whilst the error in the vertical gradient T_{zz} is slightly enhanced, without any shift in the locations of the extrema of T_{zz} (Laskar et.al 1996). Hence, horizontal and vertical gradients of the vertical field were computed following Laskar (1999). Computed gradients T_{zx} and T_{zz} of the vertical field T_z at up-continued level along A2-B2 and A6-B6 are shown in Figs. 7.1.3 and 7.1.4 respectively.

Fig.7.1.3: Vertical Component field and its horizontal and vertical gradients defining approx. location of basement faults along A2-B2.

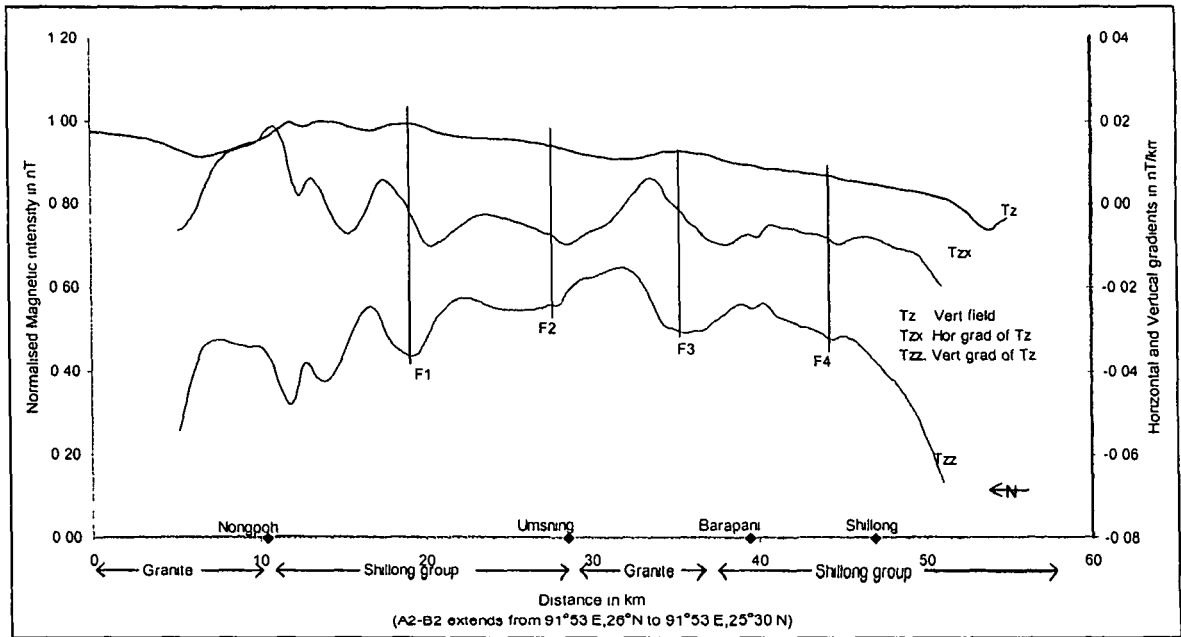
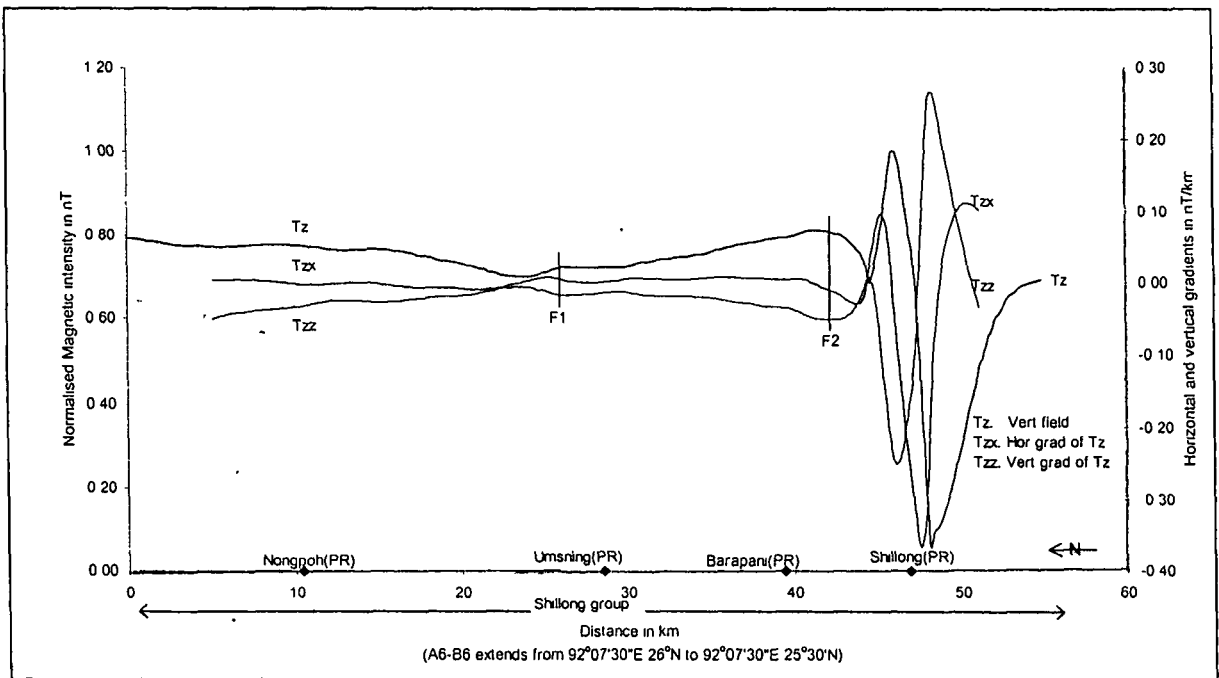


Fig.7.1.4: Vertical Component field and its horizontal and vertical gradients defining approx. location of basement faults along A6-B6



Following the criteria for identifying the approximate location of a fault from gradient analysis of the vertical field discussed earlier, possible locations of the faults across the NS lines have been noted. The T_z profile and its gradients along A2-B2 and A6-B6 are shown in Figs. 7.1.3 and 7.1.4 respectively. Four possible faults lying across A2-B2 over the EW sector are identified and designated as F_1 , F_2 , F_3 and F_4 (Fig. 7.1.3). Fault F_1 lies south of the Umsaw reserve forest (RF), at a distance of about 7km north of Umsning, F_2 lies at around Umsning at the southern margin of the Proterozoic basin bounded to the south by an intruding patch of exposed granite (Fig.7.1.1), F_3 lies about 3km north of Barapani and F_4 lies about 6km south of Barapani. On examining the T_z , T_{zx} and T_{zz} profiles of A6-B6, we find that the northern half of the T_z profile is almost flat and two possible faults F_1 and F_2 lie across the southern part of A6-B6. Fault F_1 lies about 4km north of Umsning and F_2 about 4km south of Barapani.

The flat, smooth behaviour of the magnetic profile indicates that either the basement is flat or, with small topographic variation, it lies at a greater depth. As such, to pick up the variation, if any, at the basement below the northern portion of A6-B6, the observed magnetic profile need to be continued downward to a level below the flight altitude.

On examination of the geological map (Fig.7.1.1) and the Sol toposheets, we find that the flight line clearance varies approximately from 834m to 1634m over the EW sector bounded by the Nongpoh and Barapani latitudes. The topography rises sharply south of Barapani and it attains a maximum height of 1964m over a distance of about 9km south of Barapani. As such, for a reliable continued field along a NS line over the EW sector, the field is to be continued downward to a curved lower boundary, as

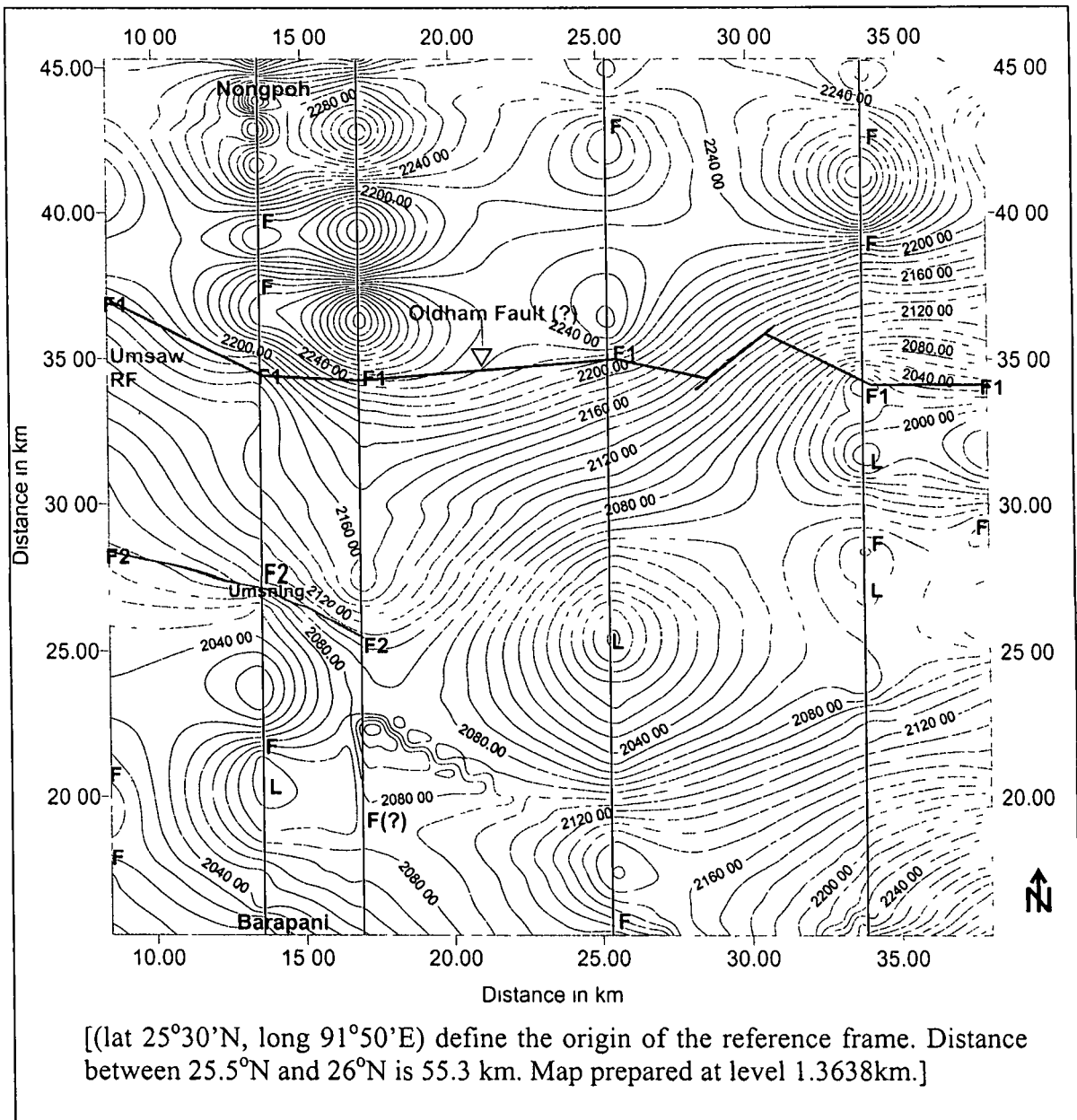
shown in Fig. 7.1.8, with its flat part lying above the EW sector at a depth 750m below the flight level.

(ii) Downward Continuation of Profile Magnetic Data and Preparation of Magnetic Map at a lower level

It is evident from the topographic variation of the area under study that the T_z -profiles can be continued downward to a level 1.3836km aMSL (750m below the flight level) over the E-W sector mentioned above, on a curved lower boundary ABCDEF (Fig. 7.1.7) without violating the Dirichlet condition that T_z remains a harmonic function in the upper half-space domain bounded below by the continuation boundary. Formulation of the problem is presented in subsection 4.2.1 and model studies is carried out in subsection 6.2. It may be mentioned here that for the input data within 1% random error spaced at a regular interval $h(=0.5\text{m})$ over the datum line, the field can be continued downward within 2% error, in general, to a level which is 1 unit ($=2h$) below it.

To prepare a map of the magnetic field at a lower level, the vertical component profiles were continued downward taking into consideration the full-length data extending from latitudes $25^{\circ}30'N$ to $26^{\circ}N$. The down-continued field obtained along A6-B6 profile is shown at the top of Fig. 7.1.8. The down-continued field so obtained along the lines at the lower level are contoured by SURFER-32 at intervals of 10nT. The map so prepared is shown in Fig.7.1.5. The approximate fault trace points identified earlier along the NS profiles by gradient analysis were transferred to the new map shown as F.

Fig. 7.1.5: Contour map of vertical component magnetic field at level above EW central sector (Contour interval =10nT)



It is evident from Fig.7.1.5 that all the faults identified earlier by the gradient analysis of profile data, visibly appear in the new map without much change in their locations. Further, a new fault location across A6-B6 distinctly appears at a latitude about 8km north of Umsing. This fault did not appear in the gradient analysis along the line at the flight level.

Fig. 7.1.6: Regional Magnetic profile along Guwahati-Shillong highway and its harmonic components

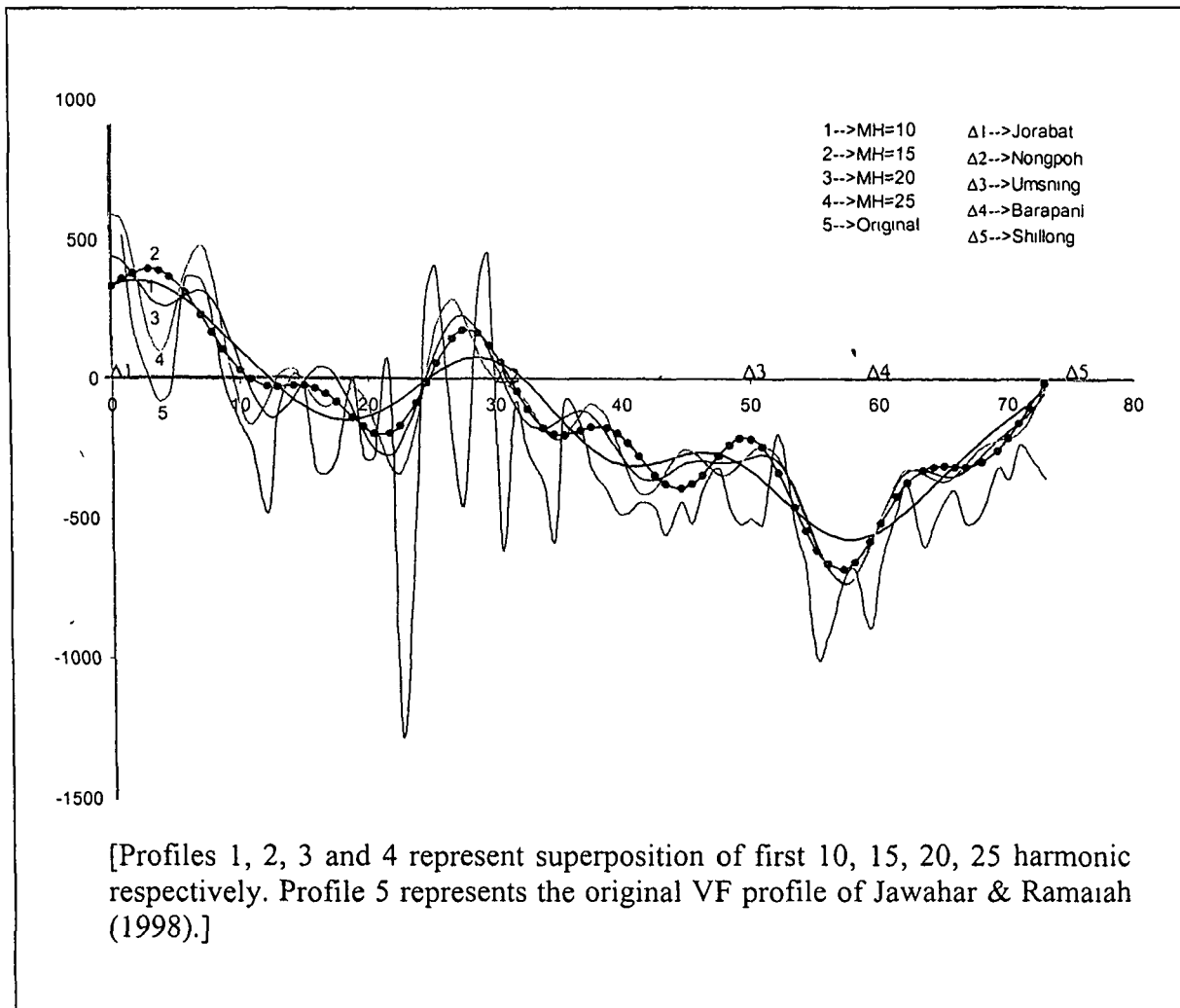


Fig. 7.1.7: Flight level, Continuation boundary, ground and basement topographic profiles along A2-B2

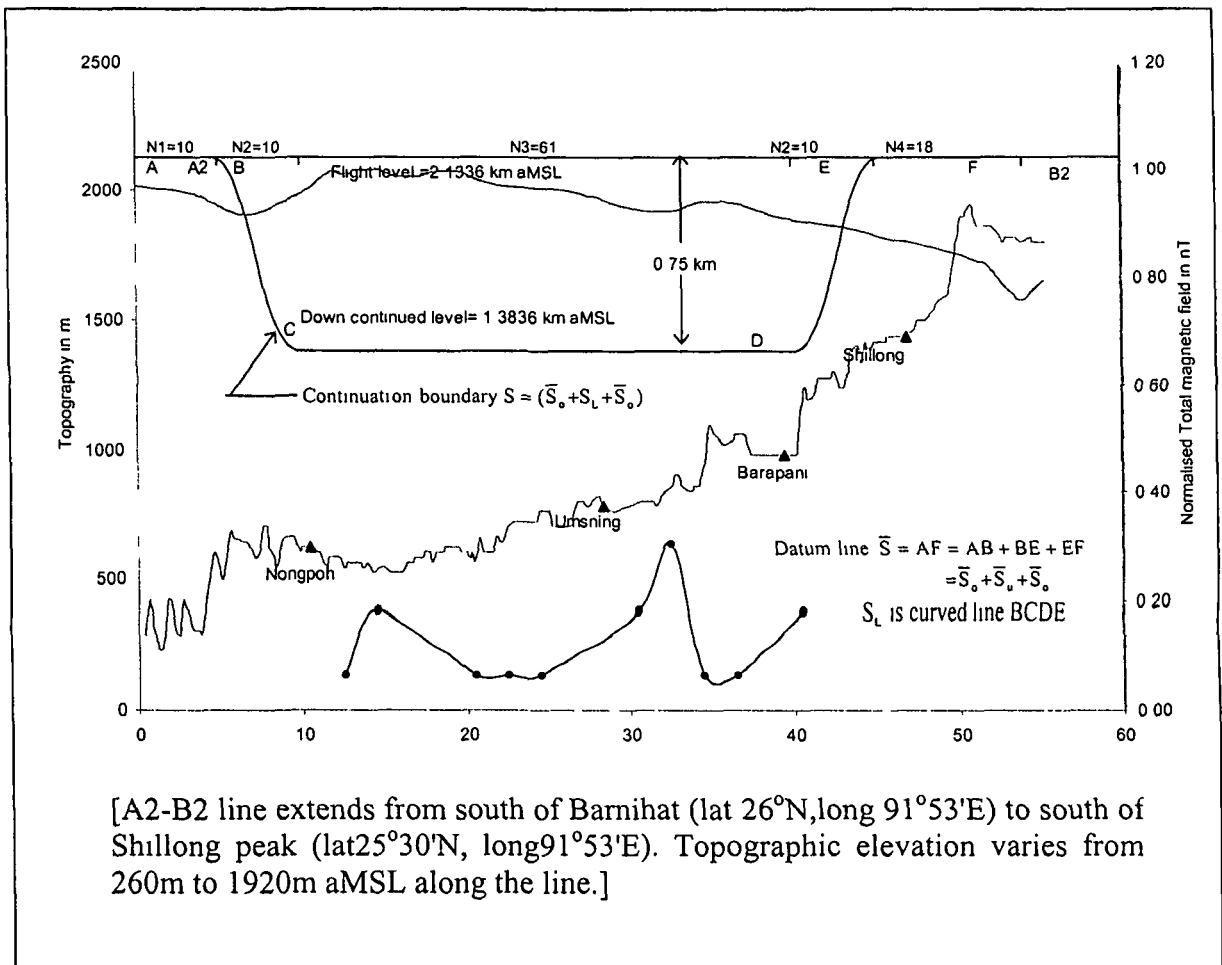
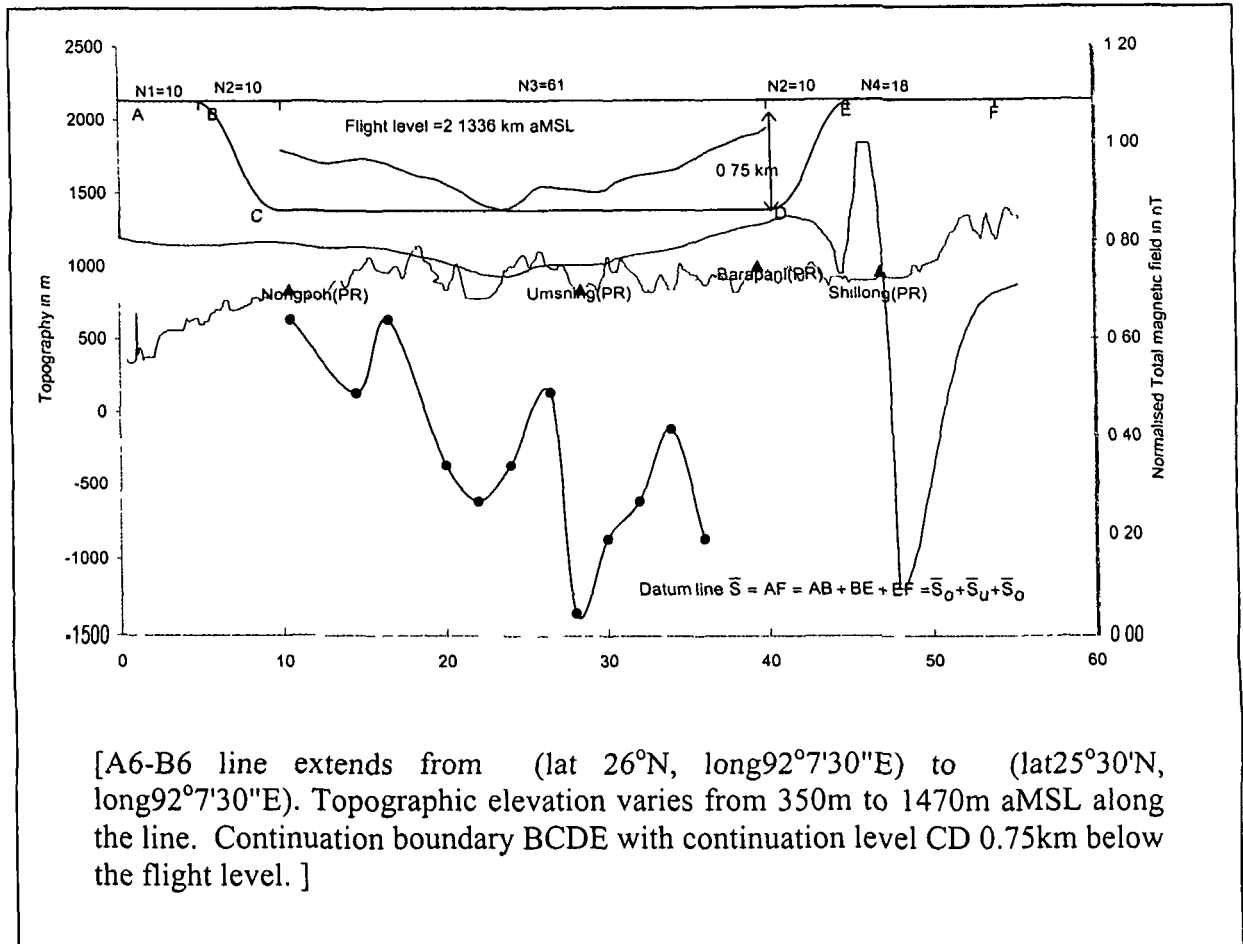


Fig.7.1 8: Normalised Total field, Topography and basement profile along A6-B6



(c) Alignment of EW Trending Faults in Nongpoh- Barapani sector

The down-continued magnetic map (Fig. 7.1.5) shows a series of lows aligned in a NE-SW trending corridor at the central part of the Nongpoh-Barapani sector. This coincides with the Barapani shear identified by Nandy (2001).

On joining the approximate fault trace-points, shown as F_1 on each of the NS lines in Fig. 7.1.5, we note that a nearly E-W trending fault begins to appear north of the Umsaw reserve forest (91°50'E longitude) continuing eastwards up to the end of the study area, taking a northward shift in between the NS lines 4 and 5 where it

encounters a NE-SW trending fault of the Barapani shear. In the western part, it lies about 7km north of Umsning and follows the up-stream course of the west flowing tributary of the Umsaw River. In the eastern part it shows a SEW trend on crossing the Barapani shear. The analysis also reveals the existence of a second fault at Umsning, defined by the trace points F_2 marked on the first 3 NS lines, that extends in the SEW direction and joins the Barapani shear about 5km east of Umsning.

7.1.4 A Comparative Study of Throw of the Faults

On acquiring vertical component magnetic data along the zigzag and undulated Guwahati-Shillong road with a spacing of 1km, Jawahar and Ramaiah (1991) presented a vertical field profile extending from Jorabat to Shillong passing through Nongpoh, Umsning and Barapani. The data were not corrected for topographic and crooked line corrections as mentioned earlier. The profile is therefore unsuitable for the study of small throw faults. However, since the basement lies at a shallow depth along the NS line (Fig. 7.1.1) that passes through Nongpoh and Shillong, the data acquired by Jawahar and Ramaiah (1991) may be expected to contain at least a weak signature of faults, if any, even though it be masked by errors.

To extract this information, the profile data were decomposed into different harmonics using the finite Fourier Series. Superposition of the first 10,15,20 and 25 harmonics are presented along with the original data in Fig. 7.1.6. We observe that the 3rd and 4th profiles show their maxima at around Umsning and also at a point about 6km north of Umsning indicating the possible existence of faults at these locations. On examination of trace 2, which is obtained by a combination of the first 15 harmonics, we observe that the maximum at around Umsning persists whilst the other

maximum north of Umsning, disappears. This indicates that for a shallow basement, the fault north of Umsning is of much smaller throw than that near Umsning.

7.1.5 Sedimentary thickness in the Shillong-Nongpoh-Mawlong Area

The Proterozoic Shillong group of sediments directly overlies the basement in the area (Das 1990, Karim et. al. 2003). Once the depth to the basement below the flight level is known, the sedimentary thickness can be determined from a knowledge of the topographic height of the ground surface.

To find the depth to the basement, we use the DEPTHDC software (Laskar & Singh 1993) for computing point to point depth to the basement along a 2-D profile. The theoretical basis and working principles of DEPTHDC are outlined in Subsection 4.2.3.

Two vertical field profiles A2-B2 and A6-B6, shown in Fig. 7.1.3 and 7.1.4 respectively, were analyzed to determine depth to the basement underneath. The profiles are given at the flight level 2134m aMSL. Flight line clearance varies approximately from 1030 to 1634m along A2-B2 and approximately from 1030 to 1384 along A6-B6 over the EW sector bounded by the latitudes of Nongpoh and Barapani.

Since the maximum flight-line clearance along A2-B2 is 1634m and that along A6-B6 is 1384 over the sector, the search-depth for the basement top can be initially taken as being 2km for the apex z_k of S_L moving downward along a vertical in $\Delta z=0.25$ km steps (see Fig.4.2.1). Depending on the search-depth, the data spacing along the datum line \bar{S} at flight level becomes $h=0.5$ km. (See Subsection 4.2.4)

Depths to the basement along A2-B2 and A6-B6 were obtained at points every 2km apart. The basement is encountered almost at every point along A2-B2 but only at a few points along A6-B6 at the northern margin of the basin. The depth profile, so obtained along A2-B2 thus shown at the bottom of Fig.7.1.7. Subsequently, the program was run for a 4km search depth along A6-B6 with $h=1\text{km}$ and $\Delta z=0.5\text{km}$. These were then further refined by taking $\Delta z=0.25\text{km}$. The depth profile so obtained, is shown at the bottom of Fig.7.1.8 along with the normalised total field and down-continued T_z profiles on its upper part.

It is evident from Fig.7.1.7 that the maximum possible thickness of sediment is about 300m between Nongpoh and Umsning and a fault of small throw clearly appears in the basement profile about 7km north of Umsning. Further, an apparently incorrect depth appears at the exposed narrow NE trending granite patch, south of Umsning showing that the computed depth to the top of the granite lies about 200m below the actual. This happens because the response at the flight level, at about 1.5km above the exposed patch, is devoid of the high frequency response of the granite patch. The software therefore yielded a smooth version of the top of the basement showing it at about 200m below the actual over the exposed patch of granite south of Umsning. Further, from Fig.7.1.8, we find that the basement is more undulated in the central part of A6-B6 with depths varying from 3.416 to 2.066 km below the flight level than that found along A2-B2. A maximum of about 2.5km thick sediment overlies the basement along A6-B6.

It can also be inferred from the above exercise that the Shillong group of sediments are probably non-magnetic in nature since the analysis did not indicate the presence of a magnetic causative at the ground surface over the EW sector.

7.1.6 Discussion

- (i) Bilham and England (2001) predicted that the Oldham fault with a small throw extends east-west over a distance of about 110km passing through the study area somewhere between Nongpoh and Barapani and it penetrates to a depth of about 9 to 45km, dipping away from the Himalayas. The present study indicates the possible existence of two EW trending faults in the study area. The first one, an EW trending fault, extends over the entire EW sector of the study area located at 7km north of Umsning and the second one, a SEW trending fault, extends over a distance about 10km starting from west of Umsning and ending at around the Barapani shear. The former has a small throw as evident from the harmonic analysis of the ground magnetic profile along A2-B2 and also from the basement profiles computed along A2-B2 and A6-B6. The trend, length and throw all appear to be closely matching with the Oldham fault (Bilham and England, 2001), although its depth extent and dip angle remain to be verified by other geophysical means.
- (ii) The method used here for locating an approximate fault-trace using the simplest fault model, appears to work well for field data. It is evident from Fig. 7.1.5 that the possible existence of faults identified by gradient analysis also appear in the contour map of down-continued data. Furthermore, they corroborate the basement profiles obtained along A2-B2 and A6-B6 lines in the area.
- (iii) The technique of down-continuation of data from the datum line to a horizontal line below it, could have been used by limiting the data-length over the EW Nongpoh-Barapani sector at the flight level. Excluding the end values, unacceptable for any practical purpose, however would have restricted reliable field values only to the central part of the EW sector. The present approach

provides reliable field values over the entire NS-span of the EW sector taking into account the contribution of data specified over the entire data-length from north of Nongpoh to south of Shillong.

- (iv) The ground gravity-magnetic (GM) survey, carried out by Pathak et.al (2003), in the southern part of the area suggests that close grid GM data with proper corrections may possibly provide sharper indications of faults in the area.
- (v) The basement profile obtained from magnetic data, in a shear zone in particular, needs further verification from gravity data. The exercise could not be carried out for non-availability of gravity data.
- (vi) Upward or downward continuation of a potential field from boundary data is governed by the theory of reproduction of a harmonic function from boundary data. Implementation of total field as boundary data leads to generation of an unknown harmonic function, in general, above or below the boundary. As such, in this work, vertical component magnetic field is constructed from total field for its upward or downward continuation from the boundary.

7.1.7. Conclusion

The possible existence of a long EW trending continuous fault of small throw in the northern half of the Shillong-Nongpoh-Mawlong area of Meghalaya appears to be required by the analysis of available magnetic data. Appearing somewhere west of the Umsaw reserve forest, it follows the upstream course of a west flowing tributary of the river Umsaw, crosses the Barapani shear and continues past the eastern boundary of the study area in the SEW direction. This corresponds rather well with the Oldham fault predicted by Bilham and England (2001). The shillong group of sediments appears to be non-magnetic in nature, its thickness varying from 200 to 300m in Nongpoh-Umsning area, and about 2.5km thick in the eastern part of the study area.

CHAPTER VIII

CONCLUSION

A half-space problem in potential theory is treated as a particular case of a closed domain problem with a part of the boundary at infinity. Derivation of a half-space problem by Green's formula is straightforward. For a closed domain problem expressed in simple or double layer boundary density, consideration of the order of the density at infinity leads to its conversion to a half-space problem.

On up-continuation of a two dimensional harmonic function H , an anomalous gravity field or a component magnetic field with asymptotic behaviour $H = O(r^{-n}), n \geq 1, r \rightarrow \infty$, from boundary data, it is shown that for the data specified over a half-space boundary, the field in the upper half-space domain B_1 can be reproduced as potential of a simple as well as a double layer boundary density. It is also shown that the field can be reproduced in B_1 by Green's formula without finding Green's function for the boundary.

In down continuation of a two-dimensional potential field from a finite datum line it is shown that down-continuation to a curved boundary with a flat central part, its arms coinciding with the datum line, provides a better numerical result over the flat central part than that provided over the same flat part by down-continuation to a horizontal boundary coinciding with it. The technique so developed helps in providing a better coverage in down-continuation of aeromagnetic data acquired over a narrow valley bounded by steeply rising high granitic hills at its boundary.

On depth-determination by down-continuation of a 2-D potential field towards its source, it is expected that down-continuation to a concave boundary with its arms extending along the datum line and the apex moving downward in steps along a vertical giving the boundary a tapering shape as depth increases, will lead to determination of point to point depth to an undulated basement in a geological basin when continuation to a horizontal boundary theoretically fails to achieve it.

An analysis is carried out to determine the spacing of data over the datum line for achieving a reliable continued field upto a depth D_s along a vertical. It is shown that the data-spacing $h = D_s/4$ provides a reliable continued field at the apex of the concave boundary as it moves downward along the vertical. Further, in down-continuation of data from a finite datum line, it is shown that the error in the continued field computed along the vertical steadily increases with depth. As such, this does not affect the position of the first maximum of the vertical gradient of the field along the vertical, the depth of the first maximum of the vertical gradient defining the depth to the top of the subsurface causative mass.

In application to field data, isolation of a magnetic anomaly is not required for determination of depth to the basement from it. The data read from a map or profile data prepared with normal correction acquired along a line, can be treated as isolated for its use in depth determination.

On successful testing of the techniques on model data, these are applied to aeromagnetic data of Umium valley of Shillong-Nongpoh area, bounded at south by a steeply rising hill of Meghalaya. The analysis identifies EW trending basement faults un-identified in the exposed geology of the area and predicts existence of 2 to 2.5 thick sedimentary cover, possibly non-magnetic in nature.

APPENDIX I

UNIQUENESS OF SOLUTION OF THE INVERSE PROBLEM

For a two-dimensional harmonic function H with asymptotic behaviour $H = O(r^{-n})$, $n \geq 1$, $r \rightarrow \infty$ defined in the upper half-space domain B_i bounded below by a half-space boundary $S(= \bar{S}_0 + S_L + \bar{S}_0$, Fig.3.2.1), given H over S , there exists a double layer boundary density μ over S that reproduces the field H in B_i (Laskar 1984) as

$$H(\mathbf{P}) = - \int_S \log_i |\mathbf{q} - \mathbf{P}| \mu(\mathbf{q}) d\mathbf{q}, \mathbf{P} \in B_i. \quad (i)$$

As $\mathbf{P} \rightarrow \mathbf{p} \in S$, following Jaswon and Symm (1977), the formula (i) yields the boundary relation between H and μ as

$$H(\mathbf{p}) = \pi \mu(\mathbf{p}) - \int_S \log_i |\mathbf{q} - \mathbf{p}| \mu(\mathbf{q}) d\mathbf{q}, \mathbf{p} \in S. \quad (ii)$$

Given H over S , the equation (ii) formulates a Dirichlet problem in μ for the upper half-space domain B_i in terms of H specified over S . That the equation has a unique μ over S , can be shown considering B_i as an interior domain enclosed by $\partial B = S + S_{uR}$, S_{uR} being a semicircle of radius R with ends over S (Fig. 3.2.1). Since the interior Dirichlet problem in μ represented by

$$H(\mathbf{p}) = \pi \mu(\mathbf{p}) - \int_{S+S_{uR}} \log_i |\mathbf{q} - \mathbf{p}| \mu(\mathbf{q}) d\mathbf{q}, \mathbf{p} \in \partial B,$$

has a unique solution (Jaswon and Symm, 1977) and $\mu = O(H)$, $r \rightarrow \infty$, shown in Subsection 2.4.3, we find the integrand over S_{uR} vanishes as $R \rightarrow \infty$ and the above equation takes the form of equation (ii) with a unique μ over S . This μ reproduces the field H on and above S as its potential.

Let us now assume that the field H be specified over a horizontal half-space boundary $\bar{S}(= \bar{S}_o + \bar{S}_u + \bar{S}_o, \text{Fig.3.2.1})$ and the curved continuation boundary S , having a central concave part S_L with its ends common to those of \bar{S}_u , extend to infinity along \bar{S}_o on both sides of \bar{S}_u . Now for $P \in \bar{S}_u$, excluding its end points, the half-space formula (i) yields

$$\begin{aligned} H(P) &= - \left[\int_{S_L} \log_i |\mathbf{q} - \mathbf{P}| \mu(\mathbf{q}) d\mathbf{q} + \int_{\bar{S}_o} \log_i |\mathbf{q} - \mathbf{P}| \mu(\mathbf{q}) d\mathbf{q} \right] \\ &= - \int_{S_L} \log_i |\mathbf{q} - \mathbf{P}| \mu(\mathbf{q}) d\mathbf{q}, \quad \mathbf{P} \in \bar{S}_u, \end{aligned} \quad (\text{iii})$$

the integral over \bar{S}_o having no contribution to H at $\mathbf{P} \in \bar{S}_u$. This is evident from the fact that $\log_i |\mathbf{q} - \mathbf{P}| = 0$ for $\mathbf{P}, \mathbf{q} \in \bar{S}$ and $\mathbf{P} \neq \mathbf{q}$. Once the μ over S_L is obtained as solution of the equation (iii), μ over \bar{S}_o is given by (ii) rewritten as

$$\begin{aligned} \pi\mu(P) &= H(P) + \int_{S_L + \bar{S}_o} \log_i |\mathbf{q} - \mathbf{P}| \mu(\mathbf{q}) d\mathbf{q}, \quad \mathbf{P} \in \bar{S}_o, \\ &= H(P) + \int_{S_L} \log_i |\mathbf{q} - \mathbf{P}| \mu(\mathbf{q}) d\mathbf{q}, \quad \mathbf{P} \in \bar{S}_o, \end{aligned} \quad (\text{iv})$$

the integral over \bar{S}_o being zero.

Let us now assume that given H over $\bar{S}(= \bar{S}_o + \bar{S}_u + \bar{S}_o)$, the equation (iii) i.e.

$$H(P) = - \int_{S_L} \log_i |\mathbf{q} - \mathbf{P}| \mu(\mathbf{q}) d\mathbf{q}, \quad \mathbf{P} \in \bar{S}_u \quad (\text{v})$$

has a $\bar{\mu}$ over S_L as its solution. Once the $\bar{\mu}$ over S_L is known, the $\bar{\mu}$ over \bar{S}_o can be obtained from (iv)

$$\pi\bar{\mu}(\mathbf{p}) = H(\mathbf{p}) + \int_{S_i} \log|\mathbf{q} - \mathbf{p}| \bar{\mu}(\mathbf{q}) d\mathbf{q}, \mathbf{p} \in \bar{S}_0 \quad (\text{vi})$$

This $\bar{\mu}$ belonging to S reproduce the H in B_i , including the boundary \bar{S} . If \bar{H} be the potential in B_i due to $\bar{\mu}$ over S ($=\bar{S}_0 + S_L + \bar{S}_0$, Fig.3.2.1) we find, following the above conclusion

$$\bar{H}(\mathbf{P}) = H(\mathbf{P}), \mathbf{P} \in \bar{S}. \quad (\text{vii})$$

Now let us construct a harmonic function δH in B_i as

$$\delta H(\mathbf{P}) = - \int_S \log|\mathbf{q} - \mathbf{P}| \delta\mu(\mathbf{q}) d\mathbf{q}, \mathbf{P} \in B_i \quad (\text{viii})$$

where $\delta H(\mathbf{P}) = H(\mathbf{P}) - \bar{H}(\mathbf{P})$, $\mathbf{P} \in B_i$ and $\delta\mu(\mathbf{q}) = \mu(\mathbf{q}) - \bar{\mu}(\mathbf{q})$, $\mathbf{q} \in S$. Since $H = \bar{H}$ over \bar{S} , we obtain

$$0 = H(\mathbf{P}) - \bar{H}(\mathbf{P}) = - \int_S \log|\mathbf{q} - \mathbf{P}| \delta\mu(\mathbf{q}) d\mathbf{q}, \mathbf{P} \in \bar{S} \quad (\text{ix})$$

Since $\delta H(\mathbf{P}) = 0$ over the half-space boundary \bar{S} it must be zero at infinity. This means, $\delta H = 0$ in upper half-space domain \bar{B} bounded below by \bar{S} . This leads to

$$\delta H'_i(\mathbf{P}) = H'_i(\mathbf{P}) - \bar{H}'_i(\mathbf{P}) = 0, \mathbf{P} \in \bar{S} \quad (\text{x})$$

Since H and \bar{H} are potentials due to μ and $\bar{\mu}$ respectively, both belonging to the boundary S , H and \bar{H} must satisfy Laplace's equation in the upper half-space domain B_i bounded below by S and at an interior point $\mathbf{P}(x_0, z_0)$ of \bar{S}_0 , both H and \bar{H} and their respective normal derivatives H'_i and \bar{H}'_i are analytic functions. Hence, considering the origin of reference frame at \mathbf{P} , by (ix) and (x), we obtain

$$H(x_0) = \bar{H}(x_0) = H_0(x_0) \text{ say,}$$

$$\text{and } H'_i(x_0) = \bar{H}'_i(x_0) = H_1(x_0) \text{ say,}$$

where H_0 and H_1 are two different analytic functions on the portion of \bar{S}_u containing \mathbf{P} . Now following Cauchy-Kowalevsky existence theorem (Kellogg, 1929, p.245), we conclude in the present case that there exists a two dimensional neighbourhood N of \mathbf{P} and a function $U(x,z)$ which is harmonic in N and which assumes on the portion of \bar{S}_u in N the same values as the function $H_0(x)$ and whose normal derivative assumes on the same portion of \bar{S}_u the values $H_1(x)$. There is only one such function. Here we would like to mention that unlike other existence theorems Cauchy-Kowalevsky theorem asserts continuation of U across the portion of \bar{S}_u containing \mathbf{P} . This means, $H = \bar{H} = U$ in two dimensional neighbourhood of the portion of \bar{S}_u containing \mathbf{P} . This conclusion on H and \bar{H} remains true over all other portions of \bar{S}_u and as such it leads to

$$H(\mathbf{P}) = \bar{H}(\mathbf{P}), \mathbf{P} \in S_{int}, \quad (xi)$$

where S_{int} is a half-space boundary with its central part immediately below \bar{S}_u and arms coinciding with \bar{S}_o of \bar{S} .

On repeated application of the above procedure to subsequent lower boundaries S_{int} , we arrive at

$$H(\mathbf{P}) = \bar{H}(\mathbf{P}), \mathbf{P} \in S$$

$$\text{Or } \delta H(\mathbf{P}) = H(\mathbf{P}) - \bar{H}(\mathbf{P}) = 0, \mathbf{P} \in S. \quad (xii)$$

This implies,

$$0 = \delta H(\mathbf{p}) = \pi \delta \mu(\mathbf{p}) - \int_S \log_i |\mathbf{q} - \mathbf{p}| \delta \mu(\mathbf{q}) d\mathbf{q}, \mathbf{p} \in S. \quad (xiii)$$

This equation is identical to the homogeneous component of (ii) with μ replaced by $\delta\mu$. Considering the equation in B_1 enclosed by $S + S_u$, $R \rightarrow \infty$, it can be shown following Jaswon and Symm (1977) that the equation (xiii) has no non-trivial solution. This leads to the conclusion that

$$\delta\mu(\mathbf{q}) = \mu(\mathbf{q}) - \bar{\mu}(\mathbf{q}) = 0, \mathbf{q} \in S$$

or $\bar{\mu}(\mathbf{q}) = \mu(\mathbf{q}), \mathbf{q} \in S.$ (xiv)

Since μ is unique over S , being a solution of a half-space Dirichlet problem expressed by equation (ii) for H specified over S , the solution $\bar{\mu}$ of equation (v) over S_L and consequently the $\bar{\mu}$ over $S (= \bar{S}_0 + S_L + \bar{S}_0)$ is unique and it is identical to the Dirichlet μ over S .

APPENDIX II

DENSITY INTEGRAL OVER THE HALF-SPACE BOUNDARY

In upward continuation of a two-dimensional potential field H with asymptotic behaviour $H=O(r^{-n})$, $n \geq 1$, $r \rightarrow \infty$, from a half-space curved boundary $S(=\bar{S}_o + S_l + \bar{S}_o$, Fig.4.2.1), given H over S , following Laskar (1984), H in the upper half space domain B_l , bounded below by S , can be reproduced as a double layer potential

$$H(\mathbf{P}) = - \int_S \log |\mathbf{q} - \mathbf{P}| \mu(\mathbf{q}) d\mathbf{q}, \mathbf{P} \in B_l. \quad (i)$$

It is evident from (i) that as $|\mathbf{P}| \rightarrow \infty$,

$$H(\mathbf{P}) = O(|\mathbf{P}|^{-1}) \int_S \mu(\mathbf{q}) d\mathbf{q}. \quad (ii)$$

For the gravimetric case, H vanishes asymptotically in $O(|\mathbf{P}|^{-1})$ as $|\mathbf{P}| \rightarrow \infty$ and as such, (iv) yields

$$\int_S \mu(\mathbf{q}) d\mathbf{q} = O(1), \quad (iii)$$

a constant, not equal to zero, necessarily. This holds for a horizontal boundary S , say $\bar{S} (= \bar{S}_o + \bar{S}_u + \bar{S}_o$, Fig.4.2.1), a particular case of S ,

$$\int_{\bar{S}} \bar{\mu}(\mathbf{q}) d\mathbf{q} = O(1), \quad (iv)$$

where $\bar{\mu}(\mathbf{q})$ is the density over \bar{S} .

For the magnetostatic case, H vanishes asymptotically in $O(|\mathbf{P}|^{-2})$ as $|\mathbf{P}| \rightarrow \infty$ and as such, (ii) yields

$$\int_S \mu(\mathbf{q}) d\mathbf{q} = 0 \quad (v)$$

For a horizontal S , say \bar{S} ,

$$\int_{\bar{S}} \bar{\mu}(q) dq = 0, \quad (\text{vi})$$

where, as before, $\bar{\mu}(q)$ is the density over \bar{S} .

Now, considering the integrals (iii), (iv), (v), (vi) we rewrite the integral properties of μ as

$$\int_{\bar{S}_o} \mu(q) dq + \int_{S_1} \mu(q) dq = \int_{\bar{S}_o} \bar{\mu}(q) dq + \int_{\bar{S}_u} \bar{\mu}(q) dq, \quad (\text{vii})$$

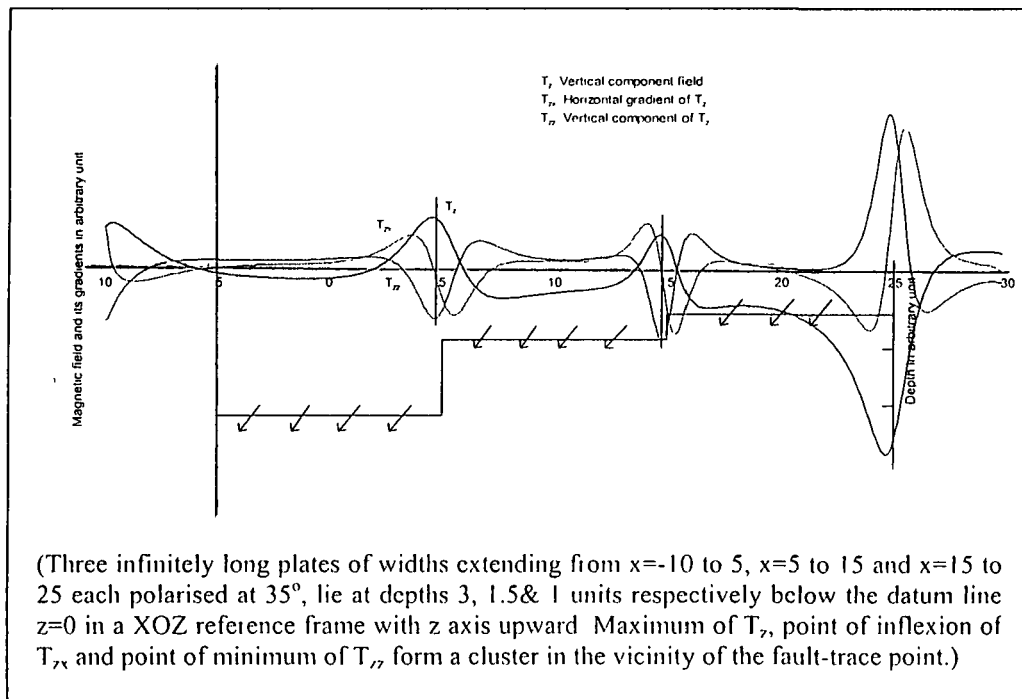
valid for both gravimetric as well as magnetostatic case with \bar{S}_o extending to infinity at both ends of \bar{S}_u .

APPENDIX III

MAGNETIC RESPONSE OF THIN PLATES FORMING A STEP-FAULT

Let three infinitely long thin plates of width AB, CD and EF, each extending from $-\infty$ to $+\infty$ in the direction of y-axis of a Cartesian reference frame with z-axis upward, be placed at depths h_1 , h_2 and h_3 respectively below the (x,y) plane such that the plates form a step-fault, its strike pointing in the direction of y-axis. Let the plates be uniformly polarised by downward doublets of strength μ per unit area and let the doublets be inclined at an angle θ with the x-axis, as shown in Fig.1. The plates so arranged produce two-dimensional magnetic field T_z in (x,z) plane as shown in Fig. 1.

Fig. 1: Vertical component magnetic response and its gradients of step-faults approximation to basement in a geological basin



(i) Magnetic Response of a Single Plate

For $q(x,z)$ defining a point on the line ΛB with Λ and B defined by (x_1,z) and (x_2,z) respectively in the vertical plane $y=0$, the magnetostatic potential due to the plate at a point $P(X,Z)$ is

$$W(\mathbf{P}) = - \int_{\Lambda B} \log_n |\mathbf{q} - \mathbf{P}| \mu(\mathbf{q}) dq \quad (i)$$

where \mathbf{P}, \mathbf{q} define the position vectors of the field point P and the source point q respectively, dq is the arc element at q , $|\mathbf{q} - \mathbf{P}|$ is the distance r between P and q , $\log_n |\mathbf{q} - \mathbf{P}|$ defines the derivative of $\log |\mathbf{q} - \mathbf{P}|$ at the point q keeping P fixed in the direction \hat{n} , \hat{n} defining the direction of the doublet of strength μ at q . On further simplification, the equation (i) becomes

$$\begin{aligned} W(X,Z) &= - \int_{\Lambda B} |\mathbf{q} - \mathbf{P}|^{-2} (\mathbf{q} - \mathbf{P}) \cdot \hat{n} \mu(\mathbf{q}) dq \\ &= - \int_{x=\Lambda}^{x=B} \frac{(x-X)l + (z-Z)m}{(x-X)^2 + (z-Z)^2} \mu(x) dx, \end{aligned} \quad (ii)$$

where l, m are the direction cosines of \hat{n} .

Now, the downward vertical component field T_z at P is,

$$T_z(X,Z) = \frac{\partial W(X,Z)}{\partial Z} = \left[\frac{(z-Z)l - (x-X)m}{(x-X)^2 + (z-Z)^2} \right]_{x=x_1}^{x=x_2} \quad (iii)$$

(ii) Vertical Component Magnetic field due to the Plates forming Step-Faults

Three infinitely long thin plates AB, CD and EF of widths extending from x_1 to x_2 , x_2 to x_3 and x_3 to x_4 respectively lying at depths h_1, h_2 and h_3 respectively below the (x,y) plane. They provide the simplest possible configuration of a step-fault below the ground plane $z=0$. Superposition of T_z response of each plate computed by (iii) provides the T_z response of the faults at $(X,0)$ on the datum line. Using the T_z values

calculated for an angle of inclination $i=\theta=35^\circ\text{N}$ on the datum line, its horizontal gradient T_{zx} and vertical gradient T_{zz} are computed at level $z=2h$, by the numerical formulae given by Laskar (1999), $z=0$ defining the datum line and $h(=0.125)$ defining the spacing of data over $z=0$. The T_z , T_{zx} and T_{zz} so obtained are shown in Fig. 1. It is evident from Fig. 1 that the point of maximum of T_z , point of inflexion of T_{zx} and the point of minimum of T_{zz} form a cluster near the fault trace point.

REFERENCE

- Bard, Y., 1970, Comparison gradient methods for solution of non-linear parameters estimation problems. *SIAM. J. Numer. Anal.* 7(1), 157 – 186.
- Bhattacharyya, B.K. and Chan, K.C., 1977, Reduction of magnetic and gravity data on an arbitrary surface acquired in a region of high topographic relief, *Geophys.*, 42, 1411 – 1430.
- Bilham, R. and England, P., 2001, Plateau pop-up during the great 1897 Assam earthquake, *Nature (Lond)*, **410**, 806-809.
- Courtillot, V.E., Ducruix, J. and Le Muel, J.L., 1973, Le Prolongement d'un champ de potential dun contour quelconque sur un contour horizontal: Une application de la methode de Backus et Gilbert, *Ann. Geophys.*, 29, 361 – 366.
- Das, M.K., 1990, Meghalaya regional Geology, an Overview, *Records of Geological Survey of India*, V.123, part 4, GSI, Shillong.
- Geology News, April 12, 2001, Mystery of Assam Earthquake (1897) Solved, *Geological Society News*.
- Gibson, R.I., 2005, Primer on Gravity and Magnetism: online at <http://www.gravmag.com/gmprimr.html>
- Glasko, G., Mudretsova, E.A. and Strakhov, V.N., 1987, Inverse problems gravimetry and magnetometry, (edited by A.N. Tikhonov and A.V. Goncharsky) *mathematics and Mechanics series*, MIR Publishers, Moscow.
- Hamel, G., 1949, *Integralgleichungen*, Springer-Verlag, Berlin.
- Hammer, S. 1979, Relative precision of vertical and horizontal gravity gradients measured by gravimeter; *Geophysics*, v.44, p.99 – 101.
- Hammer, S. and Anzoleaga, R., 1975, Exploring for stratigraphic traps with gravity-gradients, *Geophysics*, V.42, P.265-288.

- Hess, J. L. and Smith, A.M.O., 1967, Calculation of potential flow about arbitrary bodies in "Progress in Aeronautical Sciences", v. 8 (D.Kuchemann ed.), Pergamon Press, London.
- Himmelblau, D.M., 1972, Applied non-linear programming. McGraw hill, New York.
- Jaswon, M.A., 1963, Integral equation methods in potential theory, I. Proc. Roy. Soc(A), 275, 23-32.
- Jaswon, M.A. and Symm, G.T., 1977, Integral equation methods in potential theory and elastostatics, Academic Press, London.
- Jawahar G. and Ramaiah K. Raghu, 1991, Gravity and Magnetic Observations along Guwahati-Shillong-Silchar-Lunglei Road, Records of the Geological Survey of India, Vol. 124, Part-4, GSI, Shillong.
- Karim, M.A., Choudhury, J., Kumar, A. and Khonglah, M.A., 2003, Specialised thematic mapping in parts of Tyrsad- Barapani shear zone East Khasi Hills and Ri Bhoi Districts, Meghalaya with special emphasis on the Basement-Shillong group relationship, Records of The Geological survey of India, Vol. 135, Part 4, GSI, Shillong.
- Kellogg, O.D., 1929, Foundations of potential theory, Frederick Ungar Publishing Co., New York
- Laskar, S.K., 1984, Upward continuation of two-dimensional gravity and magnetic data from an irregular terrain. The Bulletin of ONGC, 21, 75 – 82.
- Laskar, S.K., and Singh, T.P., 1993, Some special software for interpretation of gravity magnetic data, KDMIPE, ONGC, Dehradun.
- Laskar, S.K., 1994, Gravity-magnetic data interpretation: Theory and Practice, (a hand written Manuscript), Consultancy report, KDMIPE, ONGC, Dehradun.

- Laskar, S.K., Verma, D.P., Kumar, R. and Burman, M.M., 1996, Identification of top of basalt, faults and pinchouts from gravity-magnetic data acquired along Manekpura-Karsenpura line in Mansa area, Gujrat, ONGC Bulletin v.33, No.2 (December'96), p.45 – 66.
- Laskar S.K. 1999, Computation of gradients of a potential field from observed boundary data, J. Geophysics, India 20(2), 83 – 87.
- Laskar, S.K., 2000, A note on uniqueness of depth determination from observed potential field data, journal of Geophysics, Vol. XXI, No.1, pp 37-40.
- Laskar, S.K. and Bhattacharyya, A.K., 2002, Final report on continuation of potential field data acquired in an irregular terrain and determination of point to point depth to the basement in a sub-Himalayan basin, A DST report, Earth Science Section, Technology Bhawan, New Delhi.
- Marquardt, D.N., 1963, An algorithm for least squares estimation of non-linear parameters, J. Soc. Appl. Math. 11, 431 – 441.
- Mendel, J.M., 1983, Optimal seismic deconvolution: An estimated based approach, Academic Press, New York.
- Mitra S., Priestley K., Bhattacharyya A.K., Gaur V.K., 2005, Crustal Structure and earthquake Focal Depths Beneath Northeastern India and the Southern Tibet, Geophysical Journal International, Vol.160, Issue 1.
- Murthy, I.V.R., 1998, Gravity and Magnetic Interpretation in Exploration Geophysics, Geological Society of India, Bangalore.
- Nandy D.R. and Das Gupta S., 1986, Application of Remote sensing in regional geological studies- a case study in Northeastern part of India: Proc.Int.Sem. on Photometry and remote sensing for developing countries; Vol.1, pp.T.4-P./6.1-T.4-P/6.4.

- Nandy D.R., 2001, Geodynamics of Northeastern India and the Adjoining Region, acb Publications, Kolkata.
- Pathak B., Banik B.L., Singh A.K., Lyngdoh A.C., Syiem S.M., Thongney R., Ranjan R. and Srivastava A.K., 2003, Active Fault Mapping for Neotectonic and Palaeoseismic Studies in East Khasi Hills, Meghalaya and Kamrup District, Assam, Records of the Geological Survey of India, Vol. 135, Part-4.
- Peters, L.J., 1949, The direct approach to magnetic data interpretation and its practical application, *Geophysics*, 4, 13 – 23.
- Rama Rao J.V., 1999, Geological and Structural Inferences of Shillong Massif from Aeromagnetic data, *Jour. of Geophysics*, Vol.XX, No.1, pp 21 to 24.
- Roy, A., 1962, Ambiguity in geophysical interpretation, *geophysics*, 4, 184 –194.
- Roy, A., 1966, Downward continuation and its application to electromagnetic data interpretation, *Geophysics*, 31, 167 – 184.
- Scarborough, J.B., 1966, Numerical Mathematical Analysis, Mohan Pritam, Oxford and IBM Publishing Co., New Delhi.
- Strakhov, V. N., 1963, Reduction of the problem of analytic continuation in a horizontal layer to that of the solution of convolution type integral equations of the first kind with rapidly decreasing kernals, *Bull (Izvestiya). Acad. USSR. Geophysics series*, v.8, p.733-739 (English).
- Strakhov, V. N., 1967, The solution of incorrectly posed magnetometric and gravimetric problems expressed by convolution type integral equations, I, *Izv. Physics of Solid Earth*, No.4, 228 – 355 (English).
- Tikhonov, A.N. and Goncharsky, A.V., 1987, Ill-posed problems in natural Sciences (ed), Mathematics and Mechanics series, MIR Publication, Moscow.
- Volterra, V., 1959, Theory of Functionals and of Integral and Integro-Differential Equations, Dover, New York.